Alma Mater Studiorum – Università di Bologna

DOTTORATO DI RICERCA IN SCIENZE DELLA TERRA

Ciclo XXII

Settore scientifico-disciplinare di afferenza: GEO 02

TITOLO TESI

Thermochronologic and geodynamic evolution of the Pontides: Sakarya terrane (Karakaya Complex) and İstanbul terrane, Turkey.

Presentata da: Dr.ssa Ilaria Federici

Coordinatore Dottorato

Prof. Roberto Barbieri

Relatore

Prof. Massimiliano Zattin

Esame finale anno 2010

ACKNOWLEDGEMENTS

I thank Professors Massimiliano Zattin and William Cavazza of Department of Earth and Geoenvironmental Sciences of the University of Bologna, for their support and suggestions during all the course of this study.

I am grateful to Professor Aral Okay of the Eurasia Institute of Earth Sciences, Istanbul Technical University (Turkey) for his helpfulness during the field trip in Turkey and for his comments and suggestions during the review of the manuscripts that are part of this thesis.

I am greatly in debt to Dr. Olivier Beyssac of the Institut de Minéralogie et de Physique des Milieux Condensés CNRS-Paris (France), for the kind hospitality in his lab, for all the time spent on my training and for his comments to the manuscript.

I am also very grateful to Dr.ssa Sveva Corrado of Department of Geological Sciences of University of "Roma Tre" for the hospitality in her lab and mainly for her precious comments and ideas during the draft of the manuscript.

I express my gratitude to Dr Francesco Dellisanti of Department of Earth and Geoenvironmental Sciences of the University of Bologna, for his fruitful discussions that enriched my knowledge of clay minerals analysis and for his contribution to the manuscript.

I deeply appreciate Professor Gian Gaspare Zuffa of Department of Earth and Geoenvironmental Sciences of the University of Bologna, and Dr Fabio Tateo of the Department of Geosciences of University of Padua for their careful review of the thesis.

A friendly tanks goes to Selvihan Goktak that accompanied me during the field trip in Turkey.

I am very grateful to my family and friends that support and encourage me during all the course of this study. Finally, last but not least, a special thanks goes to Riccardo.

CONTENTS

ABSTRACT

An integrated array of analytical methods -including clay mineralogy, vitrinite reflectance, Raman spectroscopy on carbonaceous material, and apatite fission-track analysis- was employed to constrain the thermal and thermochronological evolution of selected portions of the Pontides of northern Turkey.

(1) A multimethod investigation was applied for the first time to characterise the thermal history of the Karakaya Complex, a Permo-Triassic subduction-accretion complex cropping out throughout the Sakarya Zone. The results indicate two different thermal regimes: the Lower Karakaya Complex (Nilüfer Unit) -mostly made of metabasite and marble- suffered peak temperatures of 300-500°C (greenschist facies); the Upper Karakaya Complex (Hodul and the Orhanlar Units) –mostly made of greywacke and arkose- yielded heterogeneous peak temperatures (125-376°C), possibly the result of different degree of involvement of the units in the complex dynamic processes of the accretionary wedge. Contrary to common belief, the results of this study indicate that the entire Karakaya Complex suffered metamorphic conditions. Moreover, a good degree of correlation among the results of these methods demonstrate that Raman spectroscopy on carbonaceous material can be applied successfully to temperature ranges of 200-330°C, thus extending the application of this method from higher grade metamorphic contexts to lower grade metamorphic conditions.

(2) Apatite fission-track analysis was applied to the Sakarya and the İstanbul Zones in order to constrain the exhumation history and timing of amalgamation of these two exotic terranes. AFT ages from the İstanbul and Sakarya terranes recorded three distinct episodes of exhumation related to the complex tectonic evolution of the Pontides. (i) Paleocene - early Eocene ages (62.3-50.3 Ma) reflect the closure of the İzmir-Ankara ocean and the ensuing collision between the Sakarya terrane and the Anatolide-Tauride Block. (ii) Late Eocene - earliest Oligocene (43.5-32.3 Ma) ages reflect renewed tectonic activity along the İzmir-Ankara. (iii) Late Oligocene- Early Miocene ages reflect the onset and development of the northern Aegean extension. The consistency of

AFT ages, both north and south of the tectonic contact between the İstanbul and Sakarya terranes, suggest that such terranes were amalgamated in pre-Cenozoic times.

(3) Fission-track analysis was also applied to rock samples from the Marmara region, in an attempt to constrain the inception and development of the North Anatolian Fault system in the region. The results agree with those from the central Pontides. The youngest AFT ages (Late Oligocene - early Miocene) were recorded in the western portion of the Marmara Sea region and reflect the onset and development of northern Aegean extension. Fission-track data from the eastern Marmara Sea region indicate rapid Early Eocene exhumation induced by the development of the İzmir-Ankara orogenic wedge. Thermochronological data along the trace of the Ganos Fault –a segment of the North Anatolian Fault system- indicate the presence of a tectonic discontinuity active by Late Oligocene time, i.e. well before the arrival of the North Anatolian Fault system in the area. The integration of thermochronologic data with preexisting structural data point to the existence of a system of major E-W-trending structural discontinuities active at least from the Late Oligocene. In the Early Pliocene, inception of the present-day North Anatolian Fault system in the Marmara region occurred by reactivation of these older tectonic structures.

RIASSUNTO

Una serie di metodologie analitiche (mineralogia delle argille, riflettenza della vitrinite, spettroscopia Raman sulla materia organica, analisi delle tracce di fissione in apatite) è stata applicata per determinare l'evoluzione termica e termocronologica di alcuni vasti settori delle Pontidi (Turchia settentrionale).

(1) Per la prima volta è stato utilizzato un metodo integrato dei parametri temperatura- dipendenti per la caratterizzazione termica del Complesso di Karakaya, un complesso di subduzione-accrezione permo-triassico, che affiora estesamente in tutta la Zona di Sakarya. I risultati ottenuti hanno messo in evidenza due diverse storie termiche per tale complesso. La porzione inferiore del Complesso (Unità di Nilüfer) – costituita prevalentemente da metabasiti e marmi- è caratterizzata da un intervallo di temperature massime compreso tra 300-500°C, indicando condizioni metamorfiche nel campo degli scisti verdi. La porzione superiore del Complesso (Unità di Hodul e Orhanlar) – costituita prevalentemente da grovacche e arcose- ha registrato un intervallo di temperature massime molto ampio (120-376°C) dovuto al diverso grado di coinvolgimento delle unità nei complessi processi dinamici del prisma di accrezione. I risultati di questo studio indicano che anche tutta la porzione superiore del Complesso di Karakaya ha subito condizioni metamorfiche, contrariamente a quanto riportato in letteratura. Le tre metodologie applicate (mineralogia delle argille, riflettenza della vitrinite, spettroscopia Raman sulla materia organica) hanno mostrato un buon grado di correlazione, permettendo così di applicare la spettroscopia Raman sulla materia organica anche a temperature comprese tra 200°C e 330°C. L'applicazione di tale metodo a condizioni di basso grado metamorfico risulta quindi molto promettente.

(2) Le analisi termocronologiche (studio delle tracce di fissione in apatiti) sono state applicate alle Zone di İstanbul e di Sakarya, al fine di ricostruire la storia di esumazione e vincolare la tempistica dell'amalgamazione di questi due terreni esotici. I dati termocronologici provenienti dalle Zone di İstanbul e di Sakarya hanno registrato tre distinti episodi di esumazione legati alla complessa evoluzione delle Pontidi. (i) Le età di esumazione del Paleocene-Eocene inferiore (62.3-50.3 Ma) sono associate alla

chiusura dell'oceano İzmir-Ankara e alla risultante collisione tra la Zona di Sakarya a nord e il blocco anatolide-tauride a sud. (ii) Le età eocenico superiori - oligocenico inferiori (43.5-32.3 Ma) sono collegate ad una successiva fase deformativa lungo la sutura İzmir-Ankara, come anche indicato da deformazione e iati sedimentari nei bacini interni. (iii) Un terzo gruppo coerente di età (Oligocene superiore – Miocene inferiore) nella parte più occidentale dell'area di studio testimonia l'inizio dell'estensione egea. L'uniformità delle età di esumazione riscontrate in entrambe le zone (İstanbul e Sakarya) indica che la collisione tra questi due frammenti continentali è avvenuta durante il Mesozoico, cioè prima degli eventi deformativi registrati dalle tracce di fissione.

(3) L'analisi delle tracce di fissione è stato applicato anche a campioni provenienti dalla regione del Mare di Marmara, per caratterizzare l'evoluzione del ramo occidentale della Faglia Nord-Anatolica. I risultati sono in accordo con quelli provenienti dalle Pontidi centrali. Nei settori più occidentali si riscontrano le età di esumazione più recenti legate all'estensione egea; mentre i settori più orientali registrano una rapida esumazione nell'Eocene inferiore derivante dalla strutturazione dell'orogene di İzmir-Ankara. I dati ottenuti lungo la Faglia di Ganos – un segmento del sistema di faglia nord-anatolico- mettono in evidenza la presenza di una discontinuità tettonica attiva già dall'Oligocene superiore, ben prima della nucleazione della Faglia Nord-Anatolica ad est. L'integrazione dei dati termocronologici con quelli strutturali pre-esistenti su tutta la regione del Mare di Marmara suggerisce l'esistenza di un sistema di discontinuità tettoniche orientate E-O attive almeno dall'Oligocene superiore, lungo le quali, a partire dal Pliocene inferiore, si è impostato l'attuale sistema di faglia nord-anatolico.

CHAPTER 1

1.1 Introduction

Turkey occupies a crucial position in the geodynamic evolution of the Tethyan domain and particularly in the Eastern Mediterranean region. The present-day geological setting of Turkey (Fig. 1) is the result of complex geodynamic processes that involved the Tethyan domain during Paleozoic and Mesozoic time. Turkey is made of numerous continental fragments (also called terranes) that during the evolution of the Paleotethys and Neotethys rifted off from either sides of these two oceanic domains and eventually collided with the opposite continental margins (e.g. Okay & Tüysüz 1999; Stampfli & Hochard 2009). The final amalgamation of these terranes occurred in Late Tertiary time when the Arabian plate collided with the Eurasian plate (Okay & Tüysüz 1999).

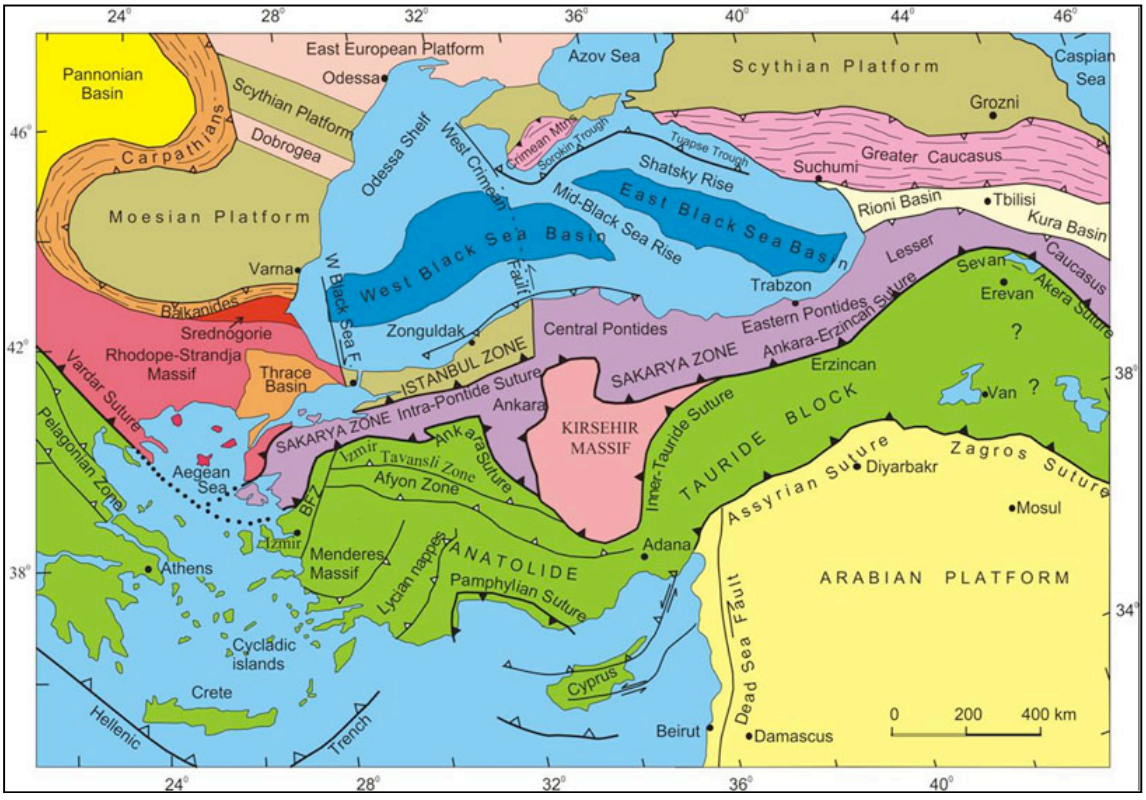

Figura 1. Simplified tectonic map of Turkey and surrounding region. Modified from Okay and Tüysüz (1999).

Geologically, Turkey can be divided into three main tectonic units: the Pontides, the Anatolide-Tauride Block and the Arabian platform (Okay 2008). The Pontides (Fig. 1), that comprise the Strandja Massif, the İstanbul and the Sakarya Zones (or terranes), show Laurasian stratigraphic affinities whereas the Anatolide –Tauride Block and the Arabian platform are tectonically and stratigraphically related to Gondwana (Şengör & Yılmaz 1981; Okay *et al.* 1996; Okay & Tüysüz 1999).

This dissertation is focused on different aspects of the geological evolution of the Pontides of northern Turkey.

The Pontides, a composite orogene stretching >1,500 km from eastern Bulgaria to the Lesser Caucasus, from late Paleozoic to Recent times, have suffered the cumulative effects of a complex structural history, including the Variscan (Carboniferous), Cimmerian (Triassic), and Alpine (Late Cretaceous-Paleocene) orogenies (Yılmaz *et al.* 1997; Tüysüz 1999) as well as Aegean extension and significant strike-slip deformation associated with the North Anatolian Fault system (for a review, see Stephenson *et al.* 2004).

In this complex geodynamic setting, a multidisciplinary methods has been applied to investigate the thermochronological and geodynamic evolution of selected elements of the Pontides. In details the main goals of the dissertation may be summarised as follow:

(i) the thermal evolution of the Karakaya Complex, a Permo-Triassic Paleotethyan subduction-accretion complex cropping out throughout the Sakarya terrane (Chapter 2);

(ii) the exhumation history of the İstanbul and Sakarya exotic terranes (Chapter 3);

(iii) the tectonic evolution of the western North Anatolian Fault in the Marmara Sea region (Chapter 4).

i) The Karakaya Complex is the tectonostratigraphic term used to designate the strongly deformed Permo-Triassic rock units in the Sakarya terrane of northern Anatolia (Figure 2). This complex developed during Permo-Triassic northward subduction of the Paleotethys along the southern margin of Eurasia (Tekeli 1981; Pickett and Robertson 1996; Okay 2000; Stampfli & Borel 2004).

The Karakaya Complex was studied by many authors since 1975 when Bingöl *et al.* defined for the first time this complex. In the following years many interpretations about the origin and the stratigraphy of the Karakaya Complex were made (Tekeli 1981;

Akyürek & Soysal 1983; Akyürek *et al.* 1984; Şengör *et al.* 1984; Koçyiğit 1987; Kaya *et al.* 1989; Okay *et al.* 1991; Altıner & Koçyiğit 1993; Pickett & Robertson 1996; Y. Yılmaz *et al.* 1997; Göncüoğlu *et al.* 2000). Up to now two geodynamic models are still in competition to explain the evolution of the Karakaya Complex and more in general to explain the evolution of this complex in the western Tethyan (Paleo-Tethyan) domain: the rift model (Bingöl *et al.* 1975) and the subduction-accretion one (Tekeli 1981), each of them with many different variations (Y. Yılmaz 1981; Şengör & Yılmaz 1981; Şengör 1984; Şengör *et al.* 1984 Koçyiğit 1987; Genç & Yılmaz 1995; Göncüoğlu *et al.* 2000; Pickett *et al.* 1995; Pickett & Robertson 1996; Okay 2000).

Generally two tectono-stratigraphic units were defined in the Karakaya Complex: the first one, made up of metabasites, phyllites and marble, and the second one, made up of highly deformed clastic and volcaniclastic rocks which generally are considered non metamorphosed or slightly metamorphosed (e.g. Pickett 1994)

In this contribution I have used, for the first time, an integrated analytical methods for determination of organic and inorganic temperature-dependent parameters to characterise the thermal structure and evolution of the Karakaya Complex.

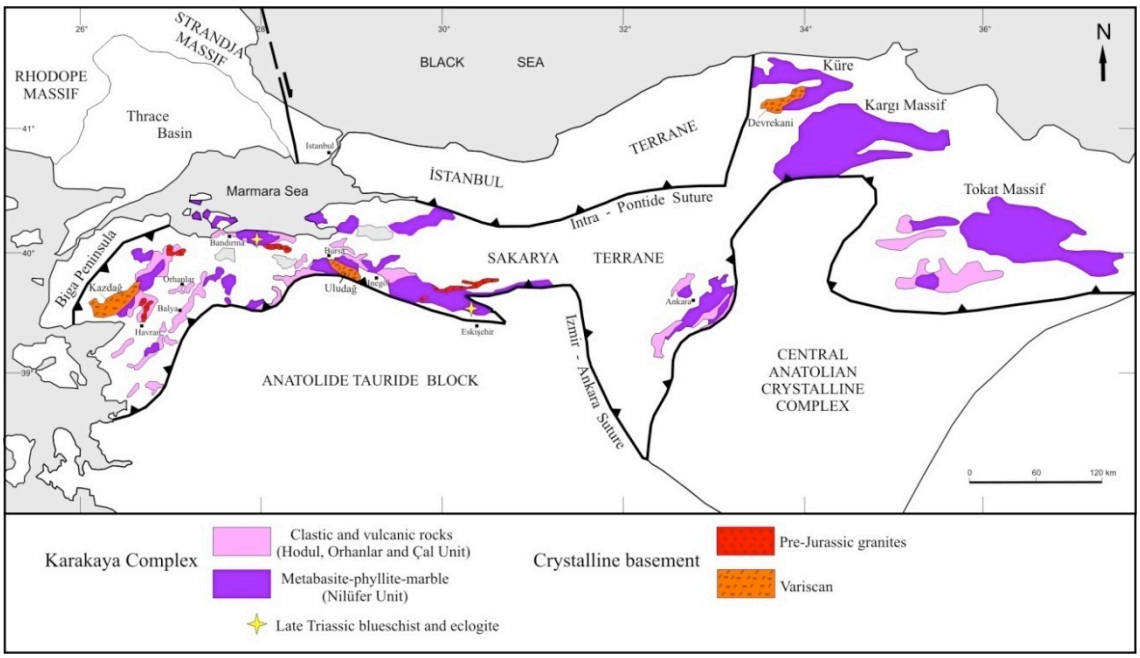

Figura 2. Outcrops of the Karakaya Complex. Modified from Okay & Göncüoğlu (2004).

More in detail, these methods include clay mineral parameters, such as the Kübler Index and the percentage of illite in I-S mixed layers, vitrinite reflectance (Ro%) and Raman spectroscopy on carbonaceous material (RSCM).

Clay mineral parameters and vitrinite reflectance are traditionally used to constrain thermal conditions from diagenesis (Corrado *et al.* 2005; Aldega *et al.* 2007a, b) to epizone (Ferreiro Mählmann 2001; Rantitsch *et al.* 2005; Potel *et al.* 2006; Judik *et al.* 2008); on the other hand, Raman spectroscopy (RSCM) was applied to provide reliable estimates of peak metamorphic temperatures in the range 330°-650°C (Beyssac *et al.* 2002a,b, 2003, 2004, 2007; Rantitsch *et al.* 2004). More recent studies focussed on lower temperature ranges (Lahfid 2008), and now a good qualitative approach is also available to estimate temperature <330°C (Lahfid 2008). In this work I have applied the Raman spectroscopy on carbonaceous material also to low grade metamorphic conditions (200-330°C) to test the reliability of this technique in this temperature range.

ii) The Intra-Pontide suture is the boundary between the İstanbul and the Sakarya terranes. This boundary is considered by Okay and Tüysüz (1999) the result of the progressive closure of an Intra-Pontide ocean during the Senonian. In contrast, according to Şengör and Yılmaz (1985), the Intra-Pontide suture formed in the early Eocene after an orthogonal opening between İstanbul and Sakarya terranes during the Liassic. Stampfli and Hochard (2009) support a middle Jurassic collision between İstanbul and Sakarya terranes. Akbayram *et al.* (2009) favour a Cenomanian collision.

In this geological context apatite fission-track (AFT) analysis has been used to constrain the exhumation history of the İstanbul and Sakarya terranes.
Fission-track dating is a powerful tool to infer the time of uplift and exhumation of the rocks and to give a measure of their motion toward the Earth's surface. The large number of samples collected from both terranes (İstanbul and Sakarya) isolate three discrete episodes of exhumation related to the complex tectonic evolution of the Pontides. These results have significant bearings on paleogeographic-paleotectonic reconstructions of the eastern Mediterranean region.

iii) The Neogene tectonics in the Marmara region is the result of interaction between the Aegean extension regime and the westward escape of the Anatolian microplate guided by the North Anatolian Fault (NAF) (Fig. 3). In the Aegean region, the rigid westward translation of the Anatolian microplate combined with back-arc spreading behind the Aegean Trench gave way to distributed north-south extension along E-W–trending normal faults. This extension resulted in the formation of E-W trending grabens, which

are the most prominent neotectonic feature of western Anatolia (Bozkurt, 2001). The same structural trend is observed in the Marmara Sea region, where the NAF developed as a complex fault system.

Following the work of Zattin *et al.* (2005) that deals with the activity of the NAF in the southwestern Thrace Basin, new apatite fission-track (AFT) data, have been integrated with (U-Th)/He ages and preexisting structural data (Aksoy, 1998; Okay *et al.,* 2008) to characterise the tectonic evolution of the western segment of the North Anatolian Fault (NAF) in the Marmara Sea region.

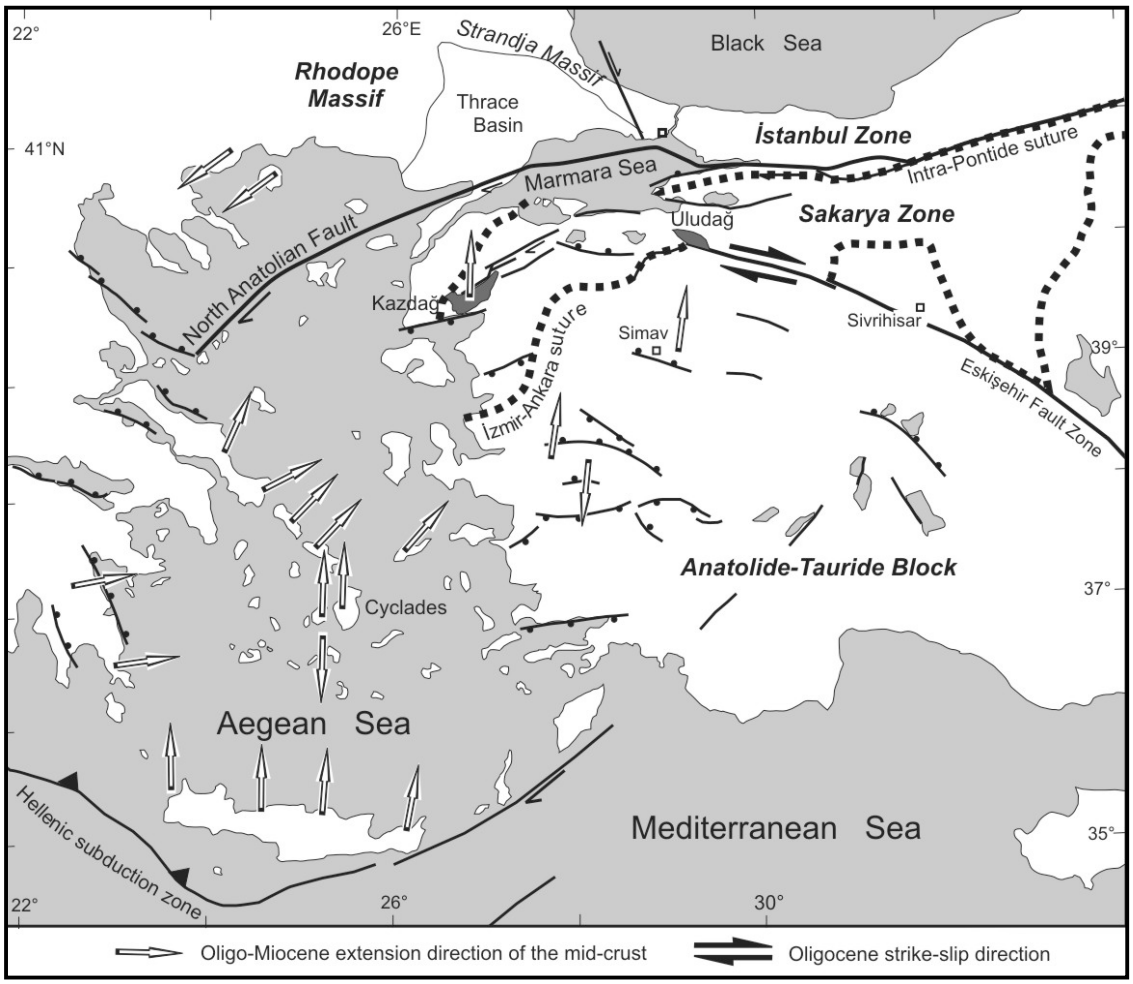

Figura 3. Simplified tectonic map of the Marmara region showing the North Anatolian Fault system. Modified from Okay *et al*., 2008.

Due to the different objectives dealt with in this study, associated with the vast dimensions of the study area, this dissertation is written as a collection of three papers (Chapter 2, 3, and 4) focused on the single goals outlined above. In the final chapter (Chapter 5) the main results are summarized and integrated in a broader geodynamic context.

1.2 Methodology

To investigate the thermal and thermochronological evolution of selected elements of the Pontides I have used a multidisciplinary approach including clay mineralogy, vitrinite reflectance and Raman spectroscopy on carbonaceous material for the thermal characterization of the Karakaya Complex, and apatite fission track analysis to constrain the exhumation history of the İstanbul and the Sakarya terranes, and the tectonic evolution of the western segment of the North Anatolian Fault (NAF) in the Marmara Sea region.

Because of the complicated nature of the Karakaya Complex such a multidisciplinary (integrated) approach has more chance to give a coherent result than the use of a single one.

In the sections below a concise description of these methodologies are given.

1.2.1 Clay mineralogy

Prograde clay mineral transformations in a sedimentary basins are primarily a response to burial and varying degrees of tectonic fabric development at temperatures below 300°C. Some transformations produce predictable patterns of change in mineral assemblage that can be used to characterised the conditions of diagenesis and very low grade-metamorphism in basins (Merriman, 2005). These patterns involve the smectite-illite-to-muscovite transformation that is part of a more extended series of reactions in 2:1 dioctahedral clay minerals. The series of reactions: *smectite → mixed-layer illite/smectite (I/S) →illite → muscovite* is characterised by a progressive increase in crystal thickness (illite "crystallinity") and decrease in defect densities, lattice strain and compositional variability as illite-muscovite becomes better ordered (Peacor, 1992)

The most common method now used for determining grade in metapelitic sequences is the Kübler Index of illite "crystallinity", which measures changes in the shape of the first basal reflection of dioctahedral illite-muscovite at an X-ray diffraction (XRD) spacing of approximately 10 Å. This method is a good tool to determine the thermal maturity in sediments in a range between the deep diagenetic zone to the epizone (Merriman & Peacor, 1999). Another important measurement is the quantification of mixed-layer illite/smectite (I/S). Measurement of proportions and degree of ordering in the smectite-/I/S-illite reaction series is the most widely used indicator of reaction progress in the diagenetic zone (Merriman, 2005).

Progress in the trioctahedral 2:1 reaction series can be also monitored using the Árkai Index of chlorite "crystallinity" (Árkai 1991; Guggenheim *et al.* 2002).

1.2.2. Vitrinite Reflectance

Vitrinite Reflectance is the most widely used indicator of thermal maturity in sedimentary rocks containing organic particles. Vitrinite is a maceral family of humic coals derived from the decay of ligno-cellulose parts of higher plants (Durand *et al.,* 1987). With increasing temperature and pressure within the Earth's crust, irreversible chemical reactions take place within the vitrinite structure. This process, termed maturation or coalification, include chemical transformation such as decarboxylation, dehydroxylation, demethylation, aromatization, and finally polycondensation of aromatic lamellae (Mukhopadhyay, 1994). The major physical manifestation of the maturation process is the increase in the reflectance of vitrinite. The reflectance of vitrinite is defined as the proportion of normal incident light reflected by a plane polished surface of vitrinite, which changes according to the level of maturation (Mukhopadhyay, 1994). This thermal maturity indicator is an effective method for estimating the maximum temperatures experienced from sedimentary rocks in the diagenetic zone.

1.2.3 Raman Spectroscopy on carbonaceous material

The Raman Spectroscopy on Carbonaceous Material (RSCM) is a new geothermometer and can be applied to metasedimentary rocks to indicate the peak of the metamorphic condition.

During diagenesis and metamorphism, carbonaceous material present in the initial sedimentary rock progressively transforms into graphite (graphitization). The corresponding progressive evolution of degree of organization of the carbonaceous material is considered to be a reliable indicator of metamorphic grade, especially of temperature (Beyssac *et al.*, 2002a).

Because of the irreversible character of graphitization, the carbonaceous material structure is not sensitive to retrograde metamorphism and therefore primarily depends

on the maximum temperature reached during metamorphism, whatever the retrograde history of the sample (Beyssac *et al.*,2002b). It also has been observed that samples collected from neighbouring outcrops with clearly different strain have the same degree of graphitization, indicating that deformation does not significantly affect the structural organization of the carbonaceous material (Beyssac *et al.*,2002b).

Now this technique is successfully applied in the range of high grade metamorphism (T between 350°C to 650°C) (Beyssac *et al.* 2002a,b, 2003, 2004, 2007; Rantitsch *et al.* 2004). Recently, Lahfid (PhD thesis 2008) focused his study to lower the range of temperature investigation. And now there is a good qualitative approach to estimate temperature values from Raman analysis. In this work I have applied the Raman spectroscopy on carbonaceous material also to low grade metamorphic conditions (200-330°C) to contribute to lower the temperature range of this new methodology.

1.2.4. Correlation of methodologies

Such multi-method investigation shows a good degree of correlation among the obtained results (widely described in chapter 2). Reliability of data is therefore increased because each methodology investigates different parameters, organic and inorganic, and each in a different range of temperature. Moreover these results demonstrate that Raman spectroscopy on carbonaceous material can be applied successfully to temperature ranges of 200-350°C, thus extending the application of this method from higher grade metamorphic contexts (Bollinger *et al.* 2004; Beyssac *et al.* 2007; Gabalda *et al.* 2009) to lower grade metamorphic conditions.

1.2.5. Fission tracks in apatite

Thermochronology is a technique that permits the extraction of information about the thermal history of rocks. Because temperature increases with depth in the Earth's lithosphere, this temperature information can be translated into structural information, thermochronological data contain a record of the depth below the surface at which rocks

resided for a given time. This methodology is able to constrain quantitatively the time of rock exhumation towards the surface (Braun *et al.*, 2006).

Fission track dating method is based on the spontaneous fission of ^{238}U which cause a structural damage in the crystal lattice. This technique is no different from other isotopic dating methods based on the decay of a naturally radioactive parent to a stable daughter atom. In the fission track method it is the spontaneous fission tracks instead of daughter isotopes that are measured as a product of the decay of ^{238}U (Wagner & Van Den Haute, 1992).

Experimental study on minerals (Fleischer *et al.,* 1965) showed that temperature is the most important parameter that influence the stability of fission tracks in minerals. The damage zone comprising a fission track in the crystal lattice is not stable and tend to be repaired with the increase of temperature by a process called *annealing*. This process is gradual and the temperature range at which tracks density and their length decrease is known as *Partial Annealing Zone (PAZ)* (Wagner & Van Den Haute, 1992). In fission track dating, the cooling range in the PAZ have to be "adapted" in a single temperature value, to which the age has to be referred; this temperature value is defined by Dodson (1973) as the *closure temperature(T_c).* Wagner and Reimer (1972) suggest that the closure temperature correspond to a temperature within the PAZ, where about 50% of the tracks are stable.

For apatite the PAZ spam from about 60°C to 120°C and the T_c is about 110°C ± 10°C

Apatite fission track analysis is a powerful tool to determine the time of deformation and the crustal depth at which it took place.

CHAPTER 2

This chapter consists of the manuscript titled “Thermal evolution of the Permo-Triassic Karakaya subduction-accretion complex from the Biga Peninsula to the Tokat Massif (Anatolia)” by Ilaria Federici, William Cavazza, Aral I. Okay, Olivier Beyssac, Massimiliano Zattin, Sveva Corrado and Francesco Dellisanti. The manuscript was submitted to the “Turkish Journal of Earth Sciences” on October 27th, 2009.

Thermal evolution of the Permo-Triassic Karakaya subduction-accretion complex from the Biga Peninsula to the Tokat Massif (Anatolia)

ILARIA FEDERICI[1], WILLIAM CAVAZZA[1], ARAL I. OKAY[2], OLIVIER BEYSSAC[3], MASSIMILIANO ZATTIN[4], SVEVA CORRADO[5] & FRANCESCO DELLISANTI[1]

[1]Department of Earth and Geoenvironmental Sciences, University of Bologna (Italy) (i.federici@unibo.it)

[2]Eurasia Institute of Earth Sciences, Istanbul Technical University (Turkey)

[3]IMPMC, UMR 7590 CNRS-Paris 6-Paris 7-IPGP, Paris (France)

[4]Department of Geosciences, University of Padua (Italy)

[5]Department of Geological Sciences, University Rome3, (Italy)

Abstract

The results of the combined application of a series of analytical methods (clay mineralogy, vitrinite reflectance, Raman microspectroscopy) placed tight constraints on the thermal evolution of the Karakaya Complex of northern Anatolia, a mostly Permo-Triassic subduction-accretion complex resulting from the progressive closure of the Paleotethys. The thermal evolution of the Karakaya Complex is the result of Permian-Triassic subduction-accretion processes, and was not significantly affected by later Alpine-age tectonism, as shown by Liassic shallow-water siliciclastic and carbonate deposits unconformably overlying the Karakaya Complex which did not undergo any significant

burial. The Lower Karakaya Complex –made of metabasite and subordinate marble and phyllite- experienced maximum temperatures ranging from 340 to 497°C, in agreement with independently determined thermobarometric reconstructions. The entire Upper Karakaya Complex –previously considered either unmetamorphosed or slightly metamorphosed - was affected by zeolite to lower greenschist facies metamorphism (120-376°C). The coherent results of this study show that Raman microspectroscopy has great potential for the determination of relatively low paleotemperatures (200-350°C).

Key Words: vitrinite reflectance, clay mineralogy, Raman microspectroscopy, metamorphism, Pontides

Introduction

Karakaya Complex is the tectonostratigraphic term used to designate the strongly deformed Permo-Triassic rock units in the Sakarya terrane (Sakarya Composite Terrane of Göncüoğlu et al. 1997; also known as Sakarya Zone) of northern Anatolia (Figure 1). This complex developed during Permo-Triassic northward subduction of the Paleotethys along the southern margin of Eurasia (Tekeli 1981; Pickett and Robertson 1996; Okay 2000; Stampfli & Borel 2004).

Although the pre-Jurassic rocks of the Sakarya terrane have been described and mapped by several authors in previous years, the comprehensive term Karakaya Formation was first defined by Bingöl et al. (1975), who supported an intracontinental rift origin for

this unit. Conversely, Tekeli (1981) proposed a subduction-accretion origin. The Karakaya Formation was renamed Karakaya Complex by Şengör et al. (1984). Several other studies have dealt with the Karakaya Complex (e.g. Akyürek & Soysal 1983; Akyürek et al. 1984; Koçyiğit 1987; Kaya et al. 1989; Okay et al. 1991; Altıner & Koçyiğit 1993; Pickett & Robertson 1996; Göncüoğlu et al. 2000, 2004; Okay & Altıner 2004, Yılmaz & Yılmaz 2004) yet the same two geodynamic interpretations are still in competition: the rift model and the subduction-accretion one, each with several different variations (Yılmaz 1981; Şengör & Yılmaz 1981; Şengör 1984; Şengör et al. 1984 Koçyiğit 1987; Genç & Yılmaz 1995; Göncüoğlu et al. 2000; Pickett et al. 1995; Pickett & Robertson 1996, 2004; Okay 2000).

There is general agreement that the Karakaya Complex is restricted to the Sakarya terrane of the Pontides and is absent in the rest of the Pontides and in the Anatolide-Tauride Block (Okay & Göncüoğlu 2004) (Figures 1, 3). Two tectonostratigraphic units were defined in the Karakaya Complex: the first one made of metabasite, phyllite and marble, the second one made of highly deformed epiclastic and volcaniclastic rocks considered unmetamorphosed or slightly metamorphosed (e.g. Pickett 1994). Following Okay & Göncüoğlu (2004), the terms Lower and Upper Karakaya Complex are used here for the metabasite series and the clastic series, respectively.

In this contribution we determine in the Lower and Upper Karakaya Complex (i) clay mineral metamorphism by XRD diffraction-derived parameters such as the Kübler Index and the percentage of illite in I-S mixed layers, and (ii) organic metamorphism by means of vitrinite reflectance data and Raman spectroscopy on carbonaceous material (RSCM). These temperature-dependant parameters have been successfully applied to constrain the thermal structures of high crustal levels of better known regions where very low- to low-grade metamorphic rocks are exposed (e.g. Beyssac et al. 2004; Potel et al.

2006; Judik et al. 2008). Clay mineral parameters such as the Kübler Index and the percentage of illite in I-S mixed layers coupled with vitrinite reflectance are traditionally used to constrain thermal conditions from diagenesis to epizone (Ferreiro Mählmann 2001; Rantitsch et al. 2005; Potel et al. 2006), and their correlations have been widely explored both in diagenetic (Corrado et al., 2005; Aldega et al. 2007a, b) and metamorphic conditions (Potel et al. 2006). Raman spectroscopy has been applied widely to provide reliable estimates of peak metamorphic temperatures between 350° and 650°C (Beyssac et al. 2002, 2003, 2004, 2007; Rantitsch et al. 2004); a pilot study focused on temperature below 350°C (Lahfid 2008).

Geological setting

The study area is located in the Sakarya terrane, an east-west-trending continental block about 1,500 km long and 120 km wide (Figure 1). To the northwest the Sakarya terrane is in tectonic contact with the İstanbul terrane by means of the Intra-Pontide suture, and to the north it is bounded by the Black Sea. The contact with the Anatolide-Tauride Block to the south is marked by the Izmir-Ankara-Erzincan suture. Outcrops of the Permo-Triassic, highly deformed, low-grade metamorphic rocks of the Karakaya Complex characterize the Sakarya terrane over a distance of ca. 1,100 km from the Biga Peninsula to the Lesser Caucasus. The Sakarya terrane, together with the İstanbul and Strandja terranes, has Laurasian affinity (Okay & Tüysüz 1999) with Paleozoic and Mesozoic stratigraphies different from the Anatolide-Tauride Block to the south. These terranes were amalgamated into a single continental unit during the latest Cretaceous-Paleocene continental collision (Şengör & Yılmaz 1981; Okay & Tüysüz 1999).

The Karakaya Complex is subdivided in a low-grade metamorphic series [Lower Karakaya Complex (LKC), also known as Nilüfer Unit] and a clastic series [Upper Karakaya Complex (UKC)] made of highly deformed epiclastic and volcaniclastic rocks (Hodul, Orhanlar and Çal Units) (Figure 2).

The LKC consists of highly deformed and metamorphosed metabasite, phyllite and marble, with minor amounts of metachert, metagabbro and serpentinite (Okay & Göncüoğlu 2004). Rocks of the LKC are generally foliated, isoclinally folded and cut by a large number of shear zones. The original thickness is difficult to estimate but the structural thickness exceeds 5 km (Okay & Göncüoğlu 2004). Conodonts from marble interbedded with the metabasite gave an Early Triassic age from the type locality of the LKC south of Bursa and a Middle Triassic age from the Biga peninsula (Kaya & Mostler 1992; Kozur et al. 2000).

The LKC is metamorphosed in greenschist facies, with a common mineral paragenesis of actinolite/barroisite + albite + chlorite + epidote in the metabasite (Okay & Moniè 1997; Okay 2000; Okay et al. 2002). Locally metamorphism reaches albite-epidote amphibolite, blueschist, and eclogite facies (Okay & Moniè 1997; Okay et al. 2002; Okay & Göncüoğlu 2004). The blueschist and eclogite facies rocks form tectonic slices within the predominantly greenschist facies rocks. Ar-Ar isotopic ages from phengite and amphibole from an eclogite lens enclosed into the greenschist facies east of Bandırma (Okay & Monié 1997) and from blueschist and high-pressure greenschist facies metabasite north of Eskişehir (Okay et al. 2002) yielded very similar Late Triassic (205-203 Ma) ages. The LKC of the eastern Pontides yielded early Permian (263-260 Ma) Ar-Ar and Rb-Sr ages (Topuz et al. 2004a, b).

The relationship between the LKC and the epiclastic and volcaniclastic rocks of the UKC are almost everywhere tectonic. The UKC consists of three tectonostratigraphic units

made of highly deformed epiclastic and volcaniclastic rocks (Figure 2). The highly deformed nature of these units make their identification and correlation across the Sakarya terrane problematic (Okay & Göncüoğlu 2004). However, there is a general agreement –at least in the western outcrop area- on the fact that the UKC includes a thick series of quartzo-feldspathic sandstone-shale (Hodul Unit) with a continental granitic source, and a greywacke-shale sequence (Orhanlar Unit). The UKC also comprises a series of basalt, debris flows and grain flows with Upper Permian limestone clasts (Çal Unit) (Okay et al. 1991; Pickett & Robertson 1996; Okay & Göncüoğlu 2004). In this paper, we extend tentatively this stratigraphic subdivision to our entire study area. Outside of their type localities in the area of the Biga peninsula, the terms Hodul Unit and Orhanlar Unit as used in this study refer generically to arkosic sandstones and graywackes, respectively, belonging to the upper structural levels of the Karakaya Complex (for a description, see below). Currently, a rigorous tectonostratigraphic correlation throughout the entire outcrop area of the Karakaya Complex is hampered by the high degree of structural complexity combined with the scarcity of detailed regional studies.

From west to east, the **Hodul Unit** crops out from the Biga Peninsula to the region north of Eskişehir, and consists of arkosic sandstones with intercalation of shales and siltstones, which pass upward into debris flows with blocks of basalt and Carboniferous and Permian limestone (Okay et al. 1991; Leven & Okay 1996). Arkosic sandstone ranges from coarse-grained, thickly bedded proximal facies with pebbles of granite to finer-grained distal turbidites. The arkosic sandstone succession is attributed to the Norian, mainly based on a few occurrences of *Halobia* sp. (Kaya et al. 1986; Wiedmann et al. 1992; Leven & Okay 1996; Okay & Altiner 2004). The presence of Ladinian limestone blocks in the Bursa area (Wiedmann et al. 1992) may indicate a longer time span for the Hodul Unit.

The Hodul Unit is strongly deformed with anastomosing shear zones and boudinage obscuring original bedding at all scales, from outcrop to thin section. The estimated total thickness of this unit is >2 km (Okay 2000), a more precise determination being hampered by the high degree of deformation. The Hodul Unit is unconformably overlain by fairly undeformed shallow-water Liassic sandstone and siltstone (Bayırköy Formation, Fig. 2).

The bulk of the **Orhanlar Unit** (>80%) is made up of yellowish green, yellowish brown, highly fractured and generally altered greywacke that rarely shows recognizable bedding (Okay et al. 1991). These rocks are composed of very poorly sorted angular quartz, plagioclase, opaque minerals, black metachert, red radiolarian chert, basalt and phyllite clasts set in an argillaceous matrix. In the locality type near the Orhanlar village, the greywacke series contains small (<1m) olistoliths of dark Lower Carboniferous (Visean and Serpukhovian) limestone and is overlain by undeformed Liassic sandstones and siltstones (Leven & Okay 1996). The Orhanlar Unit shows strong layer-parallel extension that has destroyed much of the original bedding. However, its thickness ranges probably from a few hundred meters to over 1 km. Okay et al. (1991) describe the origin of the Orhanlar as related to an accretionary complex.

The **Çal Unit** (Figure 2) consists mainly of grain and debris flows with basalt and Upper Permian limestone clasts. The siliciclastic mass flows are interbedded with basaltic lava flows, calciturbidites, pelagic limestone, shale, greywacke and rare radiolarian chert (Okay et al. 1991; Pickett & Robertson 1996). A typical feature of this unit is the presence of fossiliferous Upper Permian limestone blocks and olistoliths ranging in size from a few centimeters to one kilometer. The debris-flow deposits are distinguished from those of the Hodul Unit by the abundant presence of spilitized basic volcanic rocks (Sayıt & Göncüoğlu 2009). The Çal Unit is also strongly deformed, and hence the stratigraphic relationships of this unit, if any, with the other units of the UKC are obscure.

The tectonic evolution of the Karakaya Complex is still matter of debate. In the rift model proposed by Bingöl et al. (1975) and then developed by Şengör & Yılmaz (1981), Şengör et al. (1984), Şengör (1984), Genç & Yılmaz (1995), and Göncüoğlu (2000), the Karakaya Complex was deposited in a Late Permian rift, which developed in a small marginal basin and closed in the Late Triassic by southward subduction. Initially Bingöl et al. (1975) assumed that the Karakaya rift was purely intracontinental, but the presence of oceanic crustal lithologies in the Karakaya Complex led to the suggestion that the Karakaya rift developed into a oceanic marginal basin (Şengör & Yılmaz 1981). In this model, it is assumed that the Karakaya marginal basin opened on the northern margin of the Anatolide-Tauride Block above the southward subducting Palaeotethys ocean and that the Permian and Carboniferous limestone blocks are derived from uplifted rift shoulders.

The subduction-accretion model was firstly proposed by Tekeli (1981) and then developed by Pickett et al. (1995), Pickett & Robertson (1996), and Okay (2000). This model assumes that the Karakaya Complex was formed during the Late Permian-Triassic by northward subduction-accretion of the Paleotethys under the active Laurasian margin. The units of the Karakaya Complex were formed either during the steady-state subduction of oceanic crust or during subduction of oceanic seamounts (Pickett & Robertson 2004) or oceanic plateau (Okay 2000).

Sampling

Samples were collected from suitable rock types over a distance of about 800 km from the Biga peninsula to the Tokat Massif (Figures 1, 3). Samples from the Biga Peninsula, Bandırma, and Bursa are from the type areas of the Karakaya Complex. The remaining samples come from the Ankara area, the Tokat Massif, and the Kargı Massif, where the

lithological assemblage has been correlated to the Karakaya Complex of Biga, Bandırma, and Bursa (Yılmaz & Yılmaz 2004; Okay 2000; Okay & Göncüoğlu, 2004; Pickett & Robertson 2004).

Twenty samples for clay mineralogy analysis were collected mainly from clay and silt layers of the Hodul and Orhanlar Units of the UKC. Only two samples were taken from the phyllite of the LKC. Twelve samples for vitrinite reflectance analysis were collected in the same localities mainly from the arenaceous and pelitic beds of the Hodul and Orhanlar Units. Seventeen samples were collected in the same localities for Raman spectroscopy (RSCM) from both the Upper (Hodul and Orhanlar Units) and Lower Karakaya Complex. The results of these analyses are reported in Tables 1 and 2.

Methods

Clay mineralogy

Mineralogical composition of the bulk rock and clay fraction was carried out by powder X ray diffraction (XRD) using a Philips PW 1710 diffractometer (CuKα radiation, 40kV/30 mA power supply, graphite secondary monochromator, 1° divergence and scatter slits, 0.1 mm receiving slit, 0.02° 2q step size, counting time of 2 s/step).

Clay mineralogy was determined on <2mm grain-size fraction by XRD. Following the recommendations by Kisch (1991), the <2mm fraction was obtained by differential settling after disintegration by shaking in demineralized water and ultrasonic disaggregation for up to 15 minutes. Both air-dried and ethylene glycol solvated samples (50°C overnight) were analyzed by XRD. Smeared oriented mounts were prepared for each sample taking into account that the amount of clay on the glass slide was at least 3mg/cm^2 (Lezzerini et al. 1995). Mineralogical parameters were determined via processing of the

XRD patterns by WINFIT program (Krumm 1996) using an asymmetrical Pearson VII function (Stern et al. 1991; Warr & Rice 1994). The semiquantitative modal composition of the clay fraction was calculated using the method by Biscaye (1965) slightly modified to take into account the occurrence of mixed layer illite-smectite (I-S) and chlorite-smectite (C-S).

The very low-grade metamorphism was estimated on air-dried samples by using the illite Kübler Index (KI) obtained by measuring the full-width-at-half-maximum-height (D°2q) on the (001) illite diffraction peak at about 10 Å (Kübler 1967; Guggenheim et al. 2002). KI data were calibrated against the CIS scale (Warr & Rice 1994) using the following regression equation: $KI_{(CIS)} = 1.09\ KI_{(Bologna)} + 0.02$ ($R^2 = 0.96$) (Dellisanti et al. 2008). Chlorite crystallinity was determined on air-dried samples using the Árkai Index (AI) (Árkai 1991) obtained measuring the full-width-at-half-maximum-height (D°2q) on the (002) chlorite diffraction peak at about 7 Å (Árkai 1991; Guggenheim et al. 2002). AI data were calibrated using the equation: $AI_{(CIS)} = 1.13\ AI_{(Bologna)} - 0.02$ ($R^2 = 0.84$) (Dellisanti et al. 2008). The occurrence of mixed layers I-S and C-S was determined on glycolated samples applying the NEWMOD computer modelling (Reynolds 1985; Moore & Reynolds 1997).

Vitrinite Reflectance (Ro%)

Whole-rock samples were mounted on epoxy resin and polished according to standard procedures described in Bustin et al. (1990). Random reflectance (Ro%) was measured under oil immersion, with a Zeiss Axioplan microscope in reflected monochromatic non-polarized light. For each sample, an average of 20 measurements were taken on vitrinite fragments >5μm and only slightly fractured. Mean reflectance and standard deviation values were then calculated.

Raman Spectroscopy on Carbonaceous Material (RSCM)

RSCM thermometry is based on the quantitative study of the degree of graphitization of carbonaceous material (CM) which is a reliable indicator of metamorphic *T*. Because of the irreversible character of graphitization, CM structure is not sensitive to the retrograde path during exhumation of rocks and depends on the maximum *T* reached during metamorphism (Beyssac et al., 2002). *T* can be determined in the range 330-650°C with a precision of ± 50 °C due to uncertainties on petrologic data used for the calibration. Relative uncertainties on *T* are however much smaller, probably around 10-15 °C (Beyssac et al. 2004).

Raman spectra were obtained using a Renishaw InVIA Reflex microspectrometer (Ecole Normale Superieure, Paris). We used a 514 nm Spectra Physics argon laser in circular polarization. The laser was focused on the sample by a DMLM Leica microscope with a 100× objective (NA=0.90). The laser power at the sample surface was set at 1 mW. Rayleigh diffusion was eliminated by edge filters, and the entrance slit was closed down to 10-15 µm to achieve nearly confocal configuration. The signal was finally dispersed using a 1800 gr/mm grating and analyzed by a Peltier cooled RENCAM CCD detector. Before each session, the spectrometer was calibrated with a silicon standard. Because Raman spectroscopy of CM can be affected by several analytical mismatches, we followed closely the analytical and fitting procedures described by Beyssac et al. (2002, 2003). Measurements were taken on polished thin sections cut perpendicularly to the main fabrics (S_0, S_1) and CM was systematically analyzed below a transparent adjacent mineral, generally quartz. 10-15 spectra were recorded for each sample in the extended scanning mode (1000-2000 cm^{-1}) with acquisition times from 30 to 60 s. Spectra were then processed using the Peakfit software (Beyssac et al. 2003).

Lahfid (2008) investigated the applicability of RSCM thermometry at lower temperatures, based on a qualitative comparison with reference spectra from the Glarus Alps of Switzerland. Although elaboration of the definitive version of the quantitative calibration is still in progress, we used a qualitative comparison with the reference spectra to determine temperature values in low-grade rocks.

Results

Clay mineralogy

Mineralogical data of clay fraction are reported in Table 1 and Figure 3. The <2μm fraction is dominated by illite and chlorite, with subordinate mixed layer illite-smectite (I-S) and chlorite-smectite (C-S) present only in a few samples. Overall, the Hodul Unit is characterized by the predominance of illite with respect to chlorite whereas the Orhanlar Unit has similar percentages of illite and chlorite. The LKC (Nilüfer Unit) has a mineralogical composition similar to the Orhanlar Unit with a slight enrichment in illite content.

The illite Kübler index (KI) is used to evaluate the metamorphic grade. KI values of 0.42 and 0.25 (D°2q) are considered as lower and higher boundaries of the anchizone (Merriman & Frey 1999; Merriman 2005; Kübler 1967), whereas the value of 0.30 (D°2q) is defined as the boundary between lower and upper anchizone. The Árkai index is correlated with the Kübler index, and the values of 0.33 and 0.26 are established as deep diagenetic zone - anchizone and anchizone – epizone boundaries, respectively (Árkai 1991).

KI values in analyzed samples range between 0.95 and 0.19, i.e. from deep diagenesis to epizone (Merriman & Frey 1999). In the Biga Peninsula KI data from the

pelitic layers of the Hodul Unit range from 0.95 to 0.86 (D°2q), indicating deep diagenetic conditions (samples IF24 and IF 19; Table 1, Figure 3). These data agree with the presence of highly ordered mixed layers illite-smectite (I-S) with illite content of about 80% and 90% respectively (Table 1) due to an incomplete illitization reaction. KI values from the Hodul Unit in the Bandırma area range narrowly between 0.26 and 0.19, indicating high anchizone/epizone conditions.

Samples from the Bursa area belong to the Hodul Unit to the NE and to the Orhanlar Unit SW of the city (Table 1). The Hodul Unit experienced deep diagenetic conditions (sample IF7; KI = 0.92; 85% illite in I-S) whereas the Orhanlar Unit yielded contrasting results, ranging from deep diagenetic conditions (sample IF 39; KI = 0.52; 95% illite in I-S) to high anchizone – epizone (IF36 and IF37; KI = 0.23 and 0.26, respectively). In the Inegöl area about 60 km SE of Bursa sample TU224 from a pelitic horizon of the Hodul Unit yielded a KI value of 0.31, at the boundary between low and high anchizone (Table 1).

Southwest of Ankara high anchizone conditions prevail in the Orhanlar Unit (TU 229 and TU231; KI = 0.27 and 0.26) whereas east of Ankara the same unit suffered only deep diagenetic conditions (TU233 and TU235; KI = 0.50) (Figure 3). For both the Bursa and the Ankara regions, there is general agreement between KI values and Árkai Index (AI) values from samples of the Orhanlar Unit (Table 1).

In the Tokat Massif KI values from the Orhanlar Unit and the LKC range from 0.32 to 0.27 (TU 237, TU 241, TU242) indicating the boundary between low and high anchizone for both units. KI data agree with Árkai Index (AI) data (Table 1).

In the Kargı Massif one sample (TU244) was collected from the LKC. The KI value of 0.31 indicates the boundary between low and high anchizone. Again KI and Árkai Index (AI) are in agreement.

Vitrinite Reflectance (Ro%)

Kerogen is generally abundant, heterogeneous, and mainly made of poorly preserved macerals. When recognizable, macerals mainly belong to the vitrinite and inertinite groups. Where vitrinite is present, the lower Ro% measurements are representative of indigenous woody fragments and are characterized by a gaussian distribution, whereas the higher Ro% values show a less regular distribution and are mostly made up of altered or recycled fragments. Pyrite, either finely dispersed or in small globular aggregates, is generally present around vitrinite fragments. Overall, Ro% mean values cover a wide range between 0.74 and 3.85%, i.e. from the mid-mature stage of hydrocarbon generation in the deep diagenetic zone to high (i.e. deep) anchizone.

In more detail, in the Biga peninsula (Figure 3) Ro% data from the arkosic sandstones of the Hodul Unit (IF23, IF17, IF20) cluster between 0.74 and 0.97% (Table 1), indicating the beginning of the deep diagenetic zone. Pelites from the same unit (IF24, IF19) yielded higher Ro% values of 1.37 and 1.98. Ro% frequency distribution of sample IF 24 is strongly unimodal and indicates a probably indigenous population of vitrinite fragments; conversely the frequency distribution of sample IF19 is rather scattered and indicates considerable reworking. In summary, the Hodul Unit experienced a thermal evolution from middle to very mature stages of hydrocarbon generation (oil and wet gas) in deep diagenetic conditions. The only sample taken from the Orhanlar Unit in the Biga

peninsula (IF13) yielded an Ro% value of 1.03, in general agreement with the samples from the Hodul Unit within the same area.

In the Bandırma area reliable Ro% data were obtained only from sample IF33 (Hodul Unit) with values indicating anchizone conditions (Ro%=3.3).

Northeast of Bursa sample IF7 from the pelites of the Hodul Unit is characterized by abundant reworked material; nevertheless the Ro% value of the possible indigenous population is 1.17%, indicating the deep diagenetic zone. Southwest of Bursa two samples from the greywackes of the Orhanlar Unit were analyzed (Table 1). IF39 has a mean Ro% of about 1.7% in the deep diagenetic zone for a possible indigenous population, but with abundant reworked vitrinite fragments. IF 36 yielded much higher values (mean Ro of about 3.1%) correlatable with the middle anchizone.

In the Tokat area, Ro% data from greywackes of the Orhanlar Unit range between 3.6% and 3.8%, indicating high anchizone conditions.

Raman spectroscopy on carbonaceous material (RSCM)

Raman spectroscopy-derived temperatures of analyzed samples range between 270°C and 497°C. Samples which yielded temperatures <350°C and >350°C are listed in Tables 1 and 2, respectively. Representative Raman spectra and corresponding RSCM temperatures for samples with temperatures >350°C are shown in Figure 4.

Samples from the Hodul Unit in the Bandırma area (IF28, IF29, IF31, IF33, IF34) (Figure 3) recorded temperatures <300°C. As mentioned earlier, in this case temperature estimates are based on a semiquantitative approach and the result is a homogeneous value

of 270°C±30°C for all samples. These values suggest that in this area the Hodul Unit has undergone very low-grade metamorphic conditions.

In the Bursa area, samples 7249, 7370, 7369 were taken from the LKC phyllite and marble. Sample 7369 yielded a temperature of 405°C whereas for samples 7249 and 7370 temperature estimates reach 340°C±30°C.

In the area south of Inegöl and North of Eskişehir, peak metamorphic temperatures are 376°C (TU224 from the Hodul Unit) and 497°C (TU226 from a marble layer of the LKC) respectively.

RSCM data from the Orhanlar Unit in the Ankara area show an increase in temperatures from northeast (TU233 and TU235; <230°C and 270°C±30°C, respectively) to southwest (TU229; 372°C).

In the Tokat Massif two samples were collected. South of the massif, sample TU237 from the Orhanlar Unit yielded a temperature of 270°C±30°C; in the northern part of the massif sample TU243 from the LKC yielded temperature of 459°C.

Discussion

The results of this research, integrated with preexisting petrological data (Genç & Yılmaz 1995; Okay & Monié 1997; Yılmaz et al. 1997; Yılmaz & Yılmaz 2004; Okay et al. 2002, 2006), provide a comprehensive thermal characterization of the Karakaya Complex of northern Anatolia. In Figure 5 the paleotemperatures obtained from clay mineralogy, vitrinite reflectance, and Raman microspectroscopy are summarized. Overall, two main thermal conditions could be recognized: a deep diagenetic condition in the Biga peninsula to the west and a much higher thermal condition -from low anchizone to epizone- to the

east. Some of the samples taken southwest of Bursa and northeast of Ankara seem to contradict this general pattern.

Okay (1991, fig.13) depicts the Orhanlar Unit in the Biga peninsula regionally thrust over the Hodul Unit. A later (probably late Tertiary) near vertical fault downdropped the Orhanlar Unit and juxtaposed it to the Hodul Unit. We found no substantial difference between hangingwall and footwall thermal maturity indicating that their thermal signature has been acquired in an almost homogeneous shallow environment (deep diagenetic environment; 4-5 km of depth) in a range of 125°-140°C, probably after both thrusting and later high-angle faulting. The lack of a well developed cleavage in the mudstones indicates a negligible illite recrystallization during diagenetic processes, confirming low burial depths and temperatures. Apatite fission-track data acquired on the same units (Cavazza et al. 2009) indicate temperatures higher than 125°C (total resetting).

In the Bandırma area (Figure 3), Ro, KI, and RSCM data from the Hodul Unit indicate anchizone-epizone conditions suggesting that the thermal signature was acquired in a much deeper environment (8-9 Km) with respect to the same unit in the Biga peninsula (Figure 5). In this locality, the Hodul Unit tectonically overlies the LKC (Nilüfer Unit). Okay & Monié (1997) described for the LKC in this area a >5 km thick succession, mainly made of metabasite metamorphosed in greenschist facies with actinolite or barroisite + albite + epidote + chlorite + titanite. Within the metabasite, a tectonic lens of eclogite occurs and its mineral paragenesis indicates high pressure-low temperature metamorphism, whereas the metabasite show no evidence of high pressure metamorphism. Geochronological data ($^{40}Ar/^{39}Ar$) from the eclogite gave an age for the metamorphic peak between 208 and 203 Ma (Triassic-Jurassic boundary) (Okay & Monié 1997). The radiometric age is consistent with stratigraphic data as Liassic deposits unconformably overlain the metamorphic rocks.

Northeast of Bursa vitrinite reflectance and clay mineralogy data from the Hodul Unit (Figures 3 and 5) indicate deep diagenetic conditions suggesting a thermal path with no substantial differences from that of the same unit in the Biga peninsula. Southwest of Bursa the LKC is characterized by high-pressure greenschist facies metamorphism with a mineral assemblage of actinolite/barroisite + epidote + chlorite + albite + leucoxene; within the green metabasite there is an epidote blueschist band with mineral assemblage of quartz + sodic amphibole + epidote + albite (Okay 2004). As there is no evidence for polymetamorphism in these rocks, it could be the result of cogenetic metamorphism in the P-T region of transition between blueschist and greenschist facies (Okay 2004). Kisch et al. (2006) provides mean b_0 data of 9.039 Å from the same unit and suggests a metamorphic condition characterized by intermediate to high pressure in a convergent basin setting with low geothermal gradient (Merriman 2005). RSCM and b_0 data are in agreement with petrological data described by Okay (2004) indicating a low-grade metamorphic condition for the LKC in this area. Our data provide further constraints as RSCM temperatures from the phyllite and marble of the LKC range between 340°C±30°C and 405°C (Table 1).

In the same area the Orhanlar Unit underwent peak temperatures from deep diagenesis to high anchizone/epizone (Figure 5), corresponding to a burial depth from 5-6 to 9-10 km. The progressive change in thermal conditions is confirmed by a different development of microfabric and bulk mineralogy of mudstones samples (Kisch 1987; Merriman & Frey 1999). Mudstones in diagenetic conditions show a bedding-parallel fabric, whereas high anchizone and epizone conditions are characterized by slaty cleavage and increased illite-muscovite/quartz ratios due to recrystallization of strongly oriented illite and muscovite (Norris & Rupke 1986). These estimates are in agreement with temperatures obtained by RSCM (340°C±30°C).

Moving to the east, KI data from the Hodul Unit in the Inegöl area (Figure 3) indicate the boundary between low and high anchizone. Temperature obtained by RSCM (376°C) recorded a slightly higher thermal condition but compatible with the KI value. In this area, the arkosic sandstone of the Hodul Unit is thrust over the LKC (Genç & Yılmaz 1995). A wedge shaped tectonic slice of metaophiolite, consisting of metamorphosed serpentinite, gabbro and basalt, is also present in this area (Genç & Yılmaz 1995).

In the area north of Eskişehir, eclogite and blueschist facies rocks occur as a thrust sheet within the greenschist facies of the LKC. The common blueschist facies mineral assemblage in the metabasite is sodic-amphibole epidote + albite + chlorite + phengite ± garnet. Eclogite paragenesis of garnet + sodic pyroxene + sodic-calcic amphibole + epidote has been found only in one locality (Okay et al. 2002). P-T conditions of the epidote-blueschist facies metamorphism are estimated at 450±50°C and 11-12 kbar, whereas the very low Na contents of calcic amphiboles in the greenschist facies metabasites indicate pressure <4 kbar (Okay et al. 2002). RSCM data (497°C) from a marble layer within the metabasites of the LKC are in agreement with petrological data. Again, phengite, sodic amphibole, and barroisite $^{40}Ar/^{39}Ar$ ages from metabasite range between 215-205 Ma and indicate Late Triassic high pressure metamorphism, similarly to what was found in the Bandırma eclogite (Okay et al. 2002).

In the Ankara region, samples from the Orhanlar Unit record two somehow different thermal evolutions (Figure 3 and 5). KI and RSCM data from samples TU 229 and TU 231 indicate paleotemperatures typical of the high anchizone and the top of the epizone. On the other hand, KI data from samples TU233 and TU235 indicate only deep diagenetic conditions. The different thermal paths observed in the Ankara region could derive from tectonic deformation. In fact, samples indicating high anchizone and epizone conditions show a closely spaced slaty cleavage due to recrystallization and orientation of

platy mineral, mostly illite-muscovite, as a consequence of the progressive burial at temperatures of about 200-300°C. By contrast, the samples with higher KI value show a spaced scaly cleavage typical of tectonic shear. Shear strain can induce lattice defects in the illite structure leading to estimate higher KI values (Árkai et al. 2002; Abad et al. 2003) and consequently to apparent lower thermal conditions. Thus, the samples could have had the same thermal history but different subsequent tectonic evolution, as also shown by the higher RSCM temperatures obtained from the tectonically deformed samples.

In the Tokat Massif, the LKC was affected by regional metamorphism in greenschist facies as the mineral paragenesis suggests pressures of 3 to 6 kbar and temperatures of 300-500°C (Rojay & Göncüoğlu 1997; Yılmaz et al. 1997; Yılmaz & Yılmaz 2004). Our RSCM paleotemperature determinations (380-459°C) from the LKC fit well with the preexisting thermobarometric reconstructions (Figures 3 and 5). KI, Ro, and RSCM paleotemperature determinations from the Orhanlar Unit indicate homogeneous thermal conditions at about 270-300°C.

In the Kargı Massif, our results from the LKC (Figure 3 & 5) are in agreement with the low-grade regional metamorphism in high pressure greenschist facies shown by Okay et al. (2006).

In summary, moving eastward (Figure 5) the Hodul Unit recorded peak thermal conditions from diagenesis (Biga peninsula) to anchizone and epizone (Bandırma and Inegöl). This increase in thermal conditions is interrupted northeast of Bursa, where the Hodul Unit records only deep diagenetic conditions. Similar geographic trends are present in the Orhanlar Unit. In fact, data from organic and inorganic parameters for this unit range from deep diagenetic condition in the Biga peninsula to anchizone and epizone around Bursa, Ankara, and in the Tokat Massif. This coherent geographic trend is somehow interrupted in the Ankara region, where deep diagenetic and low anchizone conditions

were recorded. Data from the LKC are fully concordant with those preexisting thermobarometric reconstructions and peak temperatures determined during this study are everywhere higher than those from the Upper Karakaya Complex. KI data indicate high anchizone conditions and RSCM temperatures (ranging between 340±30°C to 497°C) along with petrological data indicate greenschist facies metamorphism. The highest peak temperature metamorphism detected here is from Bursa, Eskişehir and in the Tokat Massif areas.

The integrated dataset (clay mineralogy, vitrinite reflectance, Raman microspectroscopy) obtained during this study is in agreement with clay mineralogy data recently obtained from the Karakaya Complex by Tetiker et al. (2009a, b). For example, Tetiker et al. (2009b, Fig. 12) report KI values from the UKC in the area between Edremit and Bursa ranging from 0.85 and 0.30. Our average KI value from the same region is 0.62 ± 0.33, if we exclude the results obtained from samples taken around Bandırma –an area not sampled by Tetiker at al. (2009b). Similarly, KI values obtained by Tetiker at al. (2009b, Fig. 6) from the Tokat Massif cluster at 0.15-0.30 for the LKC and 0.25-0.40 for the UKC, again in agreement with our data (Table 1). Reconstructed peak thermobarometric conditions (Tetiker et al. 2009a, Fig. 8; 2009b, Fig. 17) of 14 Kb/500 °C for the LKC and 5 Kb/300° C for the UKC are in agreement with our temperature reconstructions constrained by multiple methods.

The results of this study and the preexisting data available in the literature are still insufficient to fully discriminate among the various hypotheses put forward to explain the development of the Karakaya Complex. For the LKC a wealth of data on textural features, mineral associations, clay/phyllosilicate transformations, typical index minerals, and crystallochemistry of various mineral species points to HP/LT conditions in a compressional basin (Okay & Moniè 1997; Rojay & Göncüoğlu 1997; Okay et al. 2002;

Tetiker et al. 2009a, b). More difficult is the interpretation of the UKC for which a rather limited dataset is available. According to Tetiker et al. (2009b), the Upper Karakaya units (Orhanlar, Hodul, Çal, and their eastern equivalents) reflect the diagenetic/metamorphic characteristics of an extensional basin dominated by low heat flow. We do not share their opinion as low heat flow is a hallmark of sedimentary basins located along subduction zones and partly or totally superposed on subduction-accretion complexes such as forearc, trench-slope, or peripheral foreland basins (e.g. Ingersoll & Busby-Spera 1995; Allen & Allen 2005). The thermal evolution of the Karakaya Complex may be envisaged as the result of Permian-Triassic subduction-accretion related to the progressive closure of the Paleotethys (Figure 6). Within the framework of the oceanic-plateau hypothesis of Okay (2000), during the Middle Triassic time while the Lower Karakaya (Nilüfer Unit) oceanic plateau was moving towards the southern active margin of Laurasia, the greywacke series of the Upper Karakaya (Orhanlar Unit) were probably already part of the accretionary complex. In the Late Triassic, the LKC was accreted, as testified by the presence of the eclogite and blueschist facies slices. During this stage, deformation along the Laurasian margin induced erosion of granitic basement and sedimentation of arkosic detritus (Hodul Unit) onto the accretionary wedge. The different temperature peaks (120-376°C) recorded in the Upper Karakaya are the results of different degree of involvement of the units in the complex dynamic processes of the accretionary wedge. Portions of these units experienced higher temperatures as they were incorporated in the accretionary wedge, whereas others remained at relatively higher structural levels.

At the Triassic-Jurassic boundary time the Karakaya Complex suffered an erosional episode (Cimmeride orogeny), and was then regionally overlain by relatively undeformed Early Jurassic shallow-marine sandstone and limestone (Figure 2). In the Bursa region, a new AFT age from the overlying Early Jurassic sandstone (Bayırköy Formation) yielded a Middle Jurassic age (184±22 Ma) showing that such sandstone was never buried more than

a few kilometers (Okay et al. 2008). This result constrains the exhumation history of the Karakaya Complex, which recorded Late Triassic peak temperatures and during Jurassic time was already at relatively shallow crustal depth, at least in the Bursa region.

Conclusions

Integrated analytical methods for the determination of organic and inorganic parameters - including clay mineralogy, vitrinite reflectance and Raman spectroscopy on carbonaceous material- were applied to the Karakaya Complex of northern Anatolia to constrain its thermal structure and evolution. Such multi-method investigation shows a good degree of correlation among the results of these methods, and demonstrates that Raman spectroscopy on carbonaceous material can be applied successfully to temperature ranges of 200-350°C, thus extending the application of this method from higher grade metamorphic contexts (Bollinger et al. 2004; Beyssac et al. 2007; Gabalda et al. 2009) to lower grade metamorphic conditions.

Our data from the Lower Karakaya Complex (Nilüfer Unit) indicate a range of peak temperatures up to about 500°C (upper greenschist facies), with higher temperatures reached in Bursa, Eskişehir and in the Tokat Massif areas. The Hodul and the Orhanlar Units of the Upper Karakaya Complex yielded heterogeneous temperature peaks (125-376°C) across the study area. Deep diagenetic conditions (4-5 km depth), were present in the Biga peninsula whereas towards the east anchizone up to epizone conditions (9-10 km) prevailed. The graywackes of the Orhanlar Unit and the arkoses of the Hodul Unit experienced a common range of peak temperatures across the study area.

The thermal evolution of the Karakaya Complex as a whole is the result of complex accretionary wedge dynamics during the progressive closure of the Paleotethys in Permo-

Triassic time. At the Triassic-Jurassic boundary the Karakaya Complex was further deformed, uplifted and eroded during the Cimmerian collisional orogeny. The Complex is overlain by a relatively undeformed Early Jurassic succession which was never buried more than a few kilometers, suggesting that (i) most Karakaya Complex was already at shallow crustal depth by Early Jurassic time and hence (ii) its thermal evolution can be ascribed to subduction-accretion processes.

Acknowledgments

Two anonymous reviews provided insightful criticism and helped improving the manuscript substantially. This research was sponsored by MIUR (Italian Dept. of Public Education, University and Research) and by TÜBA (The Turkish Academy of Sciences). Field assistance by Selvihan Goktak is gratefully acknowledged.

References

ABAD, I., GUITIERREZ-ALONSO, G., NIETO, F., GERTNER, I., BECKER, A. & CABRO, A. 2003. The structure and the phyllosilicates (chemistry, crystallinity and texture) of Talas Ala-Tau (Tien Shan, Kyrgyz Republic): comparison with more recent subduction complexes. *Tectonophysics* **365**, 103-127.

AKYÜREK, B. BILGINER, E. AKBAŞ, B., HEPŞEN, N., PEHLIVAN, Ş., SUNU, O., SOYSAL, Y., DAĞER, Z., ÇATAL, E., SÖZERI, B., YLDIRIM, H. & HAKYEMEZ Y. 1984. Basic geological features of the Ankara-Elmadağ-Kalecik region. *Jeoloji Mühendisliği* **20**, 31-46 [in Turkish with English abstract].

AKYÜREK, B. & SOYSAL, Y. 1983. Basic geological features of the region south of the Biga Peninsula (Savaştepe-Kırkağaç-Bergama-Ayvalık). *Maden Tetkik ve Arama Enstitütü (MTA) Dergisi* **95/96**, 1-13 [in Turkish with English abstract].

ALDEGA, L., BOTTI, F., CORRADO, S. 2007a. Clay mineral assemblages and vitrinite reflectance in the Laga Basin (Central Apennines, Italy): What do they record? *Clays and Clay Minerals* **55**, 504-518.

ALDEGA, L., CORRADO, S., GRASSO, M. & MANISCALCO, R. 2007b. Correlation of diagenetic data from organic and inorganic studies in the Apenninic-Maghrebian fold-and-thrust belt: a case study from Eastern Sicily. *The Journal of Geology* **115**, 335-353.

ALLEN, P.A. & ALLEN, J.R. 2005. Basin Analysis – Principles and Applications. Blackwell Publishing.

ALTINER, D. & KOÇYIĞIT, A. 1993. Third remark on the geology of the Karakaya basin. An Anisian megablock in northern central Anatolia: micropaleontologic, stratigraphic and structural implications for the rifting stage of the Karakaya basin. *Revue de Paléobiologie* **12**, 1-17.

ÁRKAI, P. 1991. Chlorite crystallinity: an empirical-approach and correlation with illite crystallinity, coal rank and mineral facies as exemplified by Paleozoic and Mesozoic rocks of Northeast Hungary. *Journal of Metamorphic Geology* **9**, 723-734.

ÁRKAI, P., FERREIRO MÄHLMANN, R., SUCHY, V., BALOGH, K., SYKOROVA, I & FREY, M. 2002. Possible effects of tectonic shear strain on phyllosilicate: a case study from the Kandersteg area, Helvetic domain, Central Alps Switzerland. *Schweizerische Mineralogische und Petrographische Mitteilungen* **82**, 273-290.

BEYSSAC, O., BOLLINGER, L., AVOUAC, J.P. & GOFFÈ, B., 2004. Thermal metamorphism in the lesser Himalaya of Nepal determined from Raman spectroscopy of carbonaceous material. *Earth and Planetary Science Letters* **225**, 233-241.

BEYSSAC, O., GOFFÈ, B., CHOPIN, C. & ROUZAUD J.N. 2002. Raman spectra of carbonaceous material in metasediments: a new geothermometer. *Journal of Metamorphic Geology* **20**, 859-871.

BEYSSAC, O., GOFFÈ, B., PETITET, J.P., FROIGNEUX, E., MOREAU, M. & ROUZAUD J.N. 2003. on the characterization of disordered and heterogeneous carbonaceous materials by Raman spectroscopy. *Spectrochimica Acta Part A* **59**, 2267-2276.

BEYSSAC, O., SIMOES, M., AVOUAC, J.P., FARLEY, K.A., CHEN, Y.G., CHAN Y.C. & GOFFÈ, B., 2007. Late Cenozoic metamorphic evolution and exhumation of Taiwan. *Tectonics* **26**, TC6001, doi:10.1029/2006TC002064.

BINGÖL, E., AKYÜREK, B. & KORKMAZER, B. 1975. Geology of the Biga Peninsula and some characteristic of the Karakaya blocky series. In: *Congress of Earth Sciences on the occasion of the 50th anniversary of the Turkish Republic* (Ed M.T.v.a. Enstitüsü), 70-77, Ankara [In Turkish with English abstract].

BISCAYE, P.E. 1965. Mineralogy and sedimentation of recent dee-sea clay in the Atlantic ocean and adiacent seas and oceans. *Geological Society of America Bullettin* **76**, 803-832.

BOLLINGER, L., AVOUAC, J.P., BEYSSAC, O., CATLOS, E.J., HARRISON, T.M., GROVE, M., GOFFÈ, B. & SAPKOTA, S. 2004. Thermal structure and exhumation history of the Lesser Himalaya in central Nepal. *Tectonics* **23**, TC5015, doi: 10.1029/2003TC001564.

BUSTIN, R.M., BARNES, M.A. & BARNES, W.C. 1990. Determining levels of organic diagenesis in sediments of fossil fuels. In: McIlreath, I.A. & Morrow, D.W. (eds), Diagenesis, *Geoscience Canada Reprint*, 205-226.

CAVAZZA, W., FEDERICI, I., OKAY, A.I. & ZATTIN M. 2009. Pre-Cenozoic amalgamation of the İstanbul and Sakarya terranes (NW Turkey) – evidence from low-temperature thermochronology. *Terra Nova*, submitted.

CORRADO, S., ALDEGA, L., DI LEO, P., GIAMPAOLO, C., INVERNIZZI, C., MAZZOLI, S. & ZATTIN, M., 2005. Thermal maturity of the axial zone of the Southern Apennines fold-and thrust-belt (Italy) from multiple organic and inorganic indicators. *Terra Nova* **17** (1), 56-65.

DELLISANTI, F., PINI G., TATEO, F. & BAUDIN, F. 2008. The role of tectonic shear strain on the illitization mechanism of mixed-layers illite–smectite. A case study from a fault zone in the Northern Apennines, Italy. *International Journal of Earth Sciences,* **97**, 601-616.

FERREIRO MÄHLMANN, R. 2001. Correlation of very low grade data to calibrate a thermal maturity model in a nappe tectonic setting, a case study from the Alps. *Tectonophysics* **334**, 1-33.

GABALDA, S., BEYSSAC, O., JOLIVET, L., AGARD, P. & CHOPIN C. 2009. Thermal structure of fossil subduction wedge in the Western Alps. *Terra Nova* **21**, 28-34.

GENÇ, Ş.C. & YILMAZ, Y. 1995. Evolution of the Triassic continental margin, northwest Anatolia. *Tectonophysics* **243**, 193-207.

GÖNCÜOĞLU, M.C., KUWAHARA, K., TEKIN, U.K. & TURHAN, N. 2004. Upper Permian (Changxingian) Radiolarian Cherts within the Clastic Successions of the "Karakaya Complex" in NW Anatolia. *Turkish Journal of Earth Sciences*, **13**, 201–213.

GÖNCÜOĞLU, M.C., TURHAN, N., ŞENTÜRK, K., ÖZCAN, A. & UYSAL, Ş. 2000. A geotraverse across NW Turkey: tectonic units of the central Sakarya region and their tectonic evolution. In: Bozkurt E., Winchester J.A. & Piper J.A.D. (eds) *Tectonics and Magmatism in Turkey and Surrounding Area. Geological Society, London, Special Publication* **173**, 139-161.

GUGGENHEIM, S., BAIN D.C., BERGAYA, F., BRIGATTI, M.F., DRITS, V.A., EBERL, D.D., FORMOSO, M.L.L., GALAN, E., MERRIMAN, R.J., PEACOR, D.R., STANJEK, H. & WATANABE, T. 2002. Report of the Association Internationale pour l'Etude des Argiles (AIPEA) Nomenclature Committee for 2001: order, disorder and crystallinity in phyllosilicates and the use of the 'Crystallinity Index'. *Clay Minerals,* **37**, 389-393.

INGERSOLL, R.V. & BUBSY-SPERA, C.J. 1995. Tectonics of Sedimentary Basins. Blackwell Science.

JUDIK, K., RANTITSCH, G., RAINER, T.M., ÁRKAI, P. & TOMLJENOVIĆ, B. 2008. Alpine metamorphism of organic matter in metasedimentary rocks from Mt. Medvednica (Croatia). *Swiss Journal of Geoscience* **101**, 605–616.

KAYA, O. & MOSTLER, H. 1992. A Middle-Triassic age for low-grade greenschist facies metamorphic sequence in Bergama (Izmir), western Turkey: the first paleontological age assignment and structural-stratigraphic implications. *Newsletter for Stratigraphy* **26**, 1-17.

KAYA, O., WIEDMANN, J. & KOZUR, H. 1986. Preliminary report on the stratigraphy, age and structure of the so-called Late Paleozoic and/or Triassic "mélange" or "suture zone complex" of northwestern and western Turkey. *Yerbilimleri* **13**, 1-16.

KISCH, H.J. 1987. Correlation between indicators of very low-grade metamorphism. In: *Low Temperature Metamorphism*, ed. Frey M., Blackie, Glasgow, 227-300.

KISCH, H.J. 1991. Illite crystallinity - Recommendations on sample preparation, X-ray-diffraction settings, and interlaboratory samples. *Journal of Metamorphic Geology* **9**, 665-670.

KISCH, H.J., SASSI, R. & SASSI, F.P. 2006. The b_0 lattice parameter and chemistry of phengites from HP/LT metapelites. *European Journal of Mineralogy*, **18**, 207-222.

KOÇYIĞIT, A. 1987. Tectonostratigraphy of the Hasanoğlan (Ankara) region: evolution of the Karakaya orogenic belt. *Yerbilmeri* **14**, 269-294 [In Turkish with English abstract].

KRUMM, S. 1996. WINFIT 1.0 - A computer program for X-ray diffraction line profile analysis. *Acta Universitatis Carolinae Geologica,* **38**, 253-261.

KOZUR, H., AYDIN, M., DEMIR, O., YAKAR, H., GÖNCÜOĞLU, M.C. & KURU, F. 2000. New stratigraphic and palaeogeographic results from Palaeozoic and Early-Mesozoic of the Middle Pontides (northern Turkey) in the Azdavay, Devrekani, Küre and Inebolu areas. Implications for the Carboniferous-Early Cretaceous geodynamic evolution and some related remarks to the Karakaya oceanic rift basin. *Geologica Croatica* **53**, 209-268.

KÜBLER, B. 1967. La cristallinité de l'illite et les zones tout à fait supérieures du métamorphisme. Pp. 105-121 in: *Etages Tectoniques, Colloque de Neuchâtel 1966*. Université Neuchâtel, Switzerland.

LAHFID, A. 2008. Etablissement d'un géothermomètre à maxima pour les séries argileuses peu matures. *PhD Dissertation, Université Paris 7*.

LEVEN, E.J.A. & OKAY, A.I. 1996. Foraminifera from the exotic Permo-Carboniferous limestone blocks in the Karakaya Complex, northwest Turkey. *Rivista Italiana di Paleontologia e Stratigrafia* **102**, 139-174.

LEZZERINI, M., SARTORI, F. & TAMPONI, M. 1995. Effect of amount of material used on sedimentation slides in the control of illite crystallinity measurements. *European Journal of Mineralogy,* **7**, 819-823.

MERRIMAN, R.J. 2005. Clay minerals and sedimentary basin history. *European Journal of Mineralogy*, **17**, 7–20.

MERRIMAN, R.J. & FREY, M. 1999. Patterns of very low-grade metamorphism in metapelitic rocks. In *Low-Grade Metamorphism*, ed. Frey & Robinson, Blackwell, 61-107.

NORRIS, R.J., RUPKE, N.A. 1986. Development of slaty cleavage in a mudstone unit from the Cantabrian Mountains, northern Spain. *Journal of Structural Geology* **8**, 871-878.

OKAY, A.I. 2000. Was the Late Triassic orogeny in Turkey caused by the collision of an oceanic plateau? In: Bozkurt E., Winchester J.A. & Piper J.A.D. (eds) *Tectonics and Magmatism in Turkey and Surrounding Area. Geological Society, London, Special Pubblication* **173**, 25-41.

OKAY, A.I. 2004. Tectonics and high-pressure metamorphism in Northwest Turkey. *32nd International Geological Congress, Florence, Italy. Field trip guide book P01* 56 pp.

OKAY, A.I. & ALTINER, D. 2004. Uppermost Triassic limestone in the Karakaya Complex: Stratigraphic and Tectonic Significance. *Turkish Journal of Earth Sciences* **13**, 187-199.

OKAY, A.I. & GÖNCÜOĞLU, M.C. 2004. The Karakaya Complex: a review of data and concepts. *Turkish Journal of Earth Sciences* **13**, 77-95.

OKAY, A.I. & MONIÈ, P. 1997. Early Mesozoic subduction in the Eastern Mediterranean: evidence of Triassic eclogite in northwest Turkey. *Geology* **25**, 595-598.

OKAY, A.I., MONOD, O. & MONIÈ, P. 2002. Triassic blueschists and eclogites from northwest Turkey: vestige of the Paloe-Tethyan subduction. *Lithos* **64**, 155-178.

OKAY, A.I., SATIR, M., ZATTIN, M., CAVAZZA,W. & TOPUZ, G. 2008. An Oligocene ductile strike-slip shear zone: the Uludağ Massif, northwest Turkey – implication for the westward translation of Anatolia. *Geological Society of American Bulletin* **120**, 893-911.

OKAY, A.I., SIYAKO, M. & BURKAN, K.A. 1991. Geology and tectonic evolution of the Biga Peninsula, northwest Turkey. *Bulletin of the Technical University of Istanbul* **44**, 191-256.

OKAY, A.I. & TÜYSÜZ, O. 1999. Tethyan sutures of northern Turkey. In: Durand B., Jolivet L., Horvàth F. & Sèranne M. (eds) *The Mediterranean Basin: Tertiary Extension Within the Alpine Orogen. Geological Society, London, Special Pubblication* **156**, 475-515.

OKAY, A.I., TÜYSÜZ, O., SATIR, M., ÖZKAN-ALTINER, S., ALTINER, D., SHERLOCK, S. & EREN, R.H. 2006. Cretaceous and Triassic subduction-accretion, high-pressure/low-temperature metamorphism and continental growth in the Central Pontides, Turkey. *Geological Society of America Bulletin* **118**, 1247-1269.

PICKETT, E.A. 1994. *Tectonic evolution of the PalaeoTethys Ocean in NW Turkey*. PhD Dissertation, University of Edinburgh [unpublished].

PICKETT, E.A. & ROBERTSON, A.H.F. 1996. Formation of the Late Palaeozoic-Early Mesozoic Karakaya Complex and related ophiolites in NW Turkey by paleotethyan subduction-accretion. *Journal of Geological Society, London* **153**, 995-1009.

PICKETT, E.A. & ROBERTSON, A.H.F. 2004. Significance of the volcanogenic Nilüfer Unit and related components of the Triassic Karakaya Complex for Tethyan subduction/accretion processes in NW Turkey. *Turkish Journal of Earth Sciences* **13**, 97-143.

POTEL, S., FERREIRO MÄHLMANN, R., STERN, W.B., MULLIS, J. & FREY, M. 2006. Very low-grade metamorphic evolution of pelitic rocks under high-pressure/low-temperature condition, NW New Caledonia (SW Pacific). *Journal of Petrology* **47**, 991-1015.

RANTITSCH, G., GROGGER, W., TEICHERT, C., EBNER, F., HOFER, C., MAURER E.M., SCHAFFER, B & TOTH, M. 2004. Conversion of carbonaceous material to graphite within the Greywacke Zone of the Eastern Alps. *International Journal of Earth Science* **93**, 959-973.

RANTITSCH, G., SACHSENHOFER, R.F., HASENHÜTTL, C., RUSSEGGER, B. & RAINER, T.M. 2005. Thermal evolution of an extensional detachment as constrained by organic

metamorphic data and thermal modeling: Graz Paleozoic Nappe Complex (Eastern Alps). *Tectonophysics* **411**, 57–72.

REYNOLDS, R.C. 1985. NEWMOD, a computer program for the calculation of one-dimensional diffraction patterns of mixed-layer clays.

ROJAY, B. & GÖNCÜOĞLU, M.C. 1997. Tectonic setting of some pre-Jurassic low-grade metamorphics in northern Anatolia. *Yerbilimleri* **19**, 109-118.

SAYIT, K. & GÖNCÜOĞLU, M.C. 2009. Geochemistry of mafic rocks of the Karakaya complex, Turkey: evidence for plume-involvement in the Palaeotethyan extensional regime during the Middle and Late Triassic. *International Journal of Earth Sciences* **98**, 367-385.

ŞENGÖR, A.M.C. 1984. The Cimmeride Orogenic system and the tectonics of Eurasia. *Geological Society of America, Special paper* **195**, 82pp.

ŞENGÖR, A.M.C. & YILMAZ, Y. 1981. Thethyan evolution of Turkey: a plate tectonic approach. *Tectonophysics* **75**, 181-241.

ŞENGÖR, A.M.C., YILMAZ, Y. & SUNGURLU, O. 1984. Tectonic of the Mediterranean Cimmerides: nature and evolution of the western termination of Paleo-Tethys. In: Dixon J.E. & Robertson A.H.F. (eds), *The Geological Evolution of the Eastern Mediterranean. Geological Society, London, Special Pubblication* **17**, 77-112.

STAMPFLI, G.M. & BOREL, G.D. 2004. The TRANSMED Transects in Space and Time: Constrains on the Paleotectonic Evolution of the Mediterranean Domain. In: Cavazza W., Roure F. M., Spakman W., Stampfli G. M. & Ziegler P. A. (eds), *The TRANSMED Atlas – The Mediterranean Region from crust to Mantle. Springer, Berlin Heidelberg*, pp. 53–80, (see also Appendix 3).

STERN, W.B., MULLIS, J., RAHN, M. & FREY, M. 1991. Deconvolution of the first “illite” basal reflection. *Schweizerische Mineralogische Und Petrographische Mitteilungen* **71**, 453-462.

TEKELİ, O. 1981. Subduction complex of pre-Jurassic age, northern Anatolia, Turkey. *Geology* **9**, 68-72.

TETİKER, S., YALÇIN, H. & BOZKAYA, Ö. 2009a. Low grade metamorphism of the units from Karakaya Complex (Tokat region). Proceedings of 14th National Clay Symposium, p.155-173 [In Turkish with English abstract].

TETİKER, S., YALÇIN, H. & BOZKAYA, Ö. 2009b. Diagenesis and low grade metamorphism of Karakaya Complex in the NW Anatolia. *Yerbilimleri* **30**, 193–212 [In Turkish with English abstract].

TOPUZ, G., ALTHERR, R., KALT, A., SATIR, M., WERNER O. & SCHWARTZ W.H. 2004a. Aluminous granulites from the Pulur Complex, NE Turkey: a case of partial melting, efficient melt extraction and crystallisation. *Lithos* **72**, 183-207.

TOPUZ, G., ALTHERR, R., SATIR, M. & SCHWARTZ, W.H. 2004b. Low-grade metamorphic rocks from the Pulur Complex, NE Turkey: implication for the pre-Liassic evolution of the Eastern Pontides. *International Journal of Earth Sciences* **93**, 72-91.

WARR, L.N. & RICE, A.H.N. 1994. Interlaboratory standardization and calibration of clay mineral crystallinity and crystallite size data. *Journal of Metamorphic Geology* **12**, 141-152.

WIEDMANN, J. KOZUR, H. & KAYA, O. 1992. Faunas and age significance of the pre-Jurassic turbidite-olistostrome unit in the western parts of Turkey. *Newsletter for Stratigraphy* **26**, 133-144.

YILMAZ, Y. 1981. Tectonic evolution of the southern margin of the Sakarya Continent. *Istanbul Yerbimileri* **1**, 33-52.

YILMAZ, A. & YILMAZ, H. 2004. Geology and structural evolution of the Tokat Massif (Eastern Pontides, Turkey). *Turkish Journal of Earth Sciences* **13**, 231-246.

Figure captions

Figure 1. Simplified tectonic map of Turkey and the surrounding regions. Modified from Okay and Tüysüz (1999).

Figure 2. Tectonostratigraphy of the Karakarya Complex showing the tectonic relationships between its Lower and Upper portions. Modified from Okay (2000).

Figure 3. Geologic map of the western-central Pontides with Kübler Index and vitrinite reflectance data, and Raman spectroscopy temperatures from the Karakaya Complex. Modified from Okay & Göncüoğlu (2004).

Figure 4. Raman spectra of carbonaceous material obtained in various units of the Karakaya in order of increasing metamorphic grade. Location are indicated in Figure 3. Position of the graphite G band and D1, D2 defects bands are indicated. For each spectrum, the value of the mean R2 ratio (R2= D1/[G+D1+D2] peak area ratio) obtained after 10 decomposition and corresponding RSCM temperature is given.

Figure 5. Regional distribution of clay mineral, vitrinite reflectance, and Raman spectroscopy data. For ÁI only values between 0.33 and 0.26 are reported. For RSCM the mean temperatures are indicated.

Figure 6. Schematic cross-section showing the hypothetical tectonic evolution of the Karakaya Complex during the (a) Middle Triassic and (b) Late Triassic. Modified from Okay (2000).

Table 1. Clay mineralogy and vitrinite reflectance data and Raman spectroscopy temperatures.

Table 2. Raman spectroscopy data with paleotemperatures higher than 350°C.

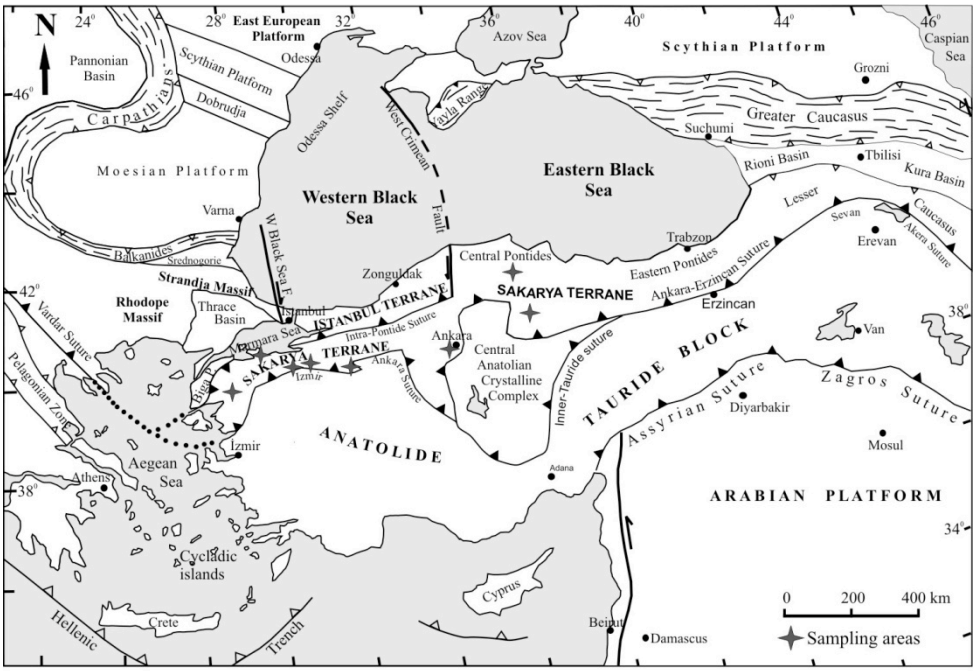

Federici *et al.* Figure 1

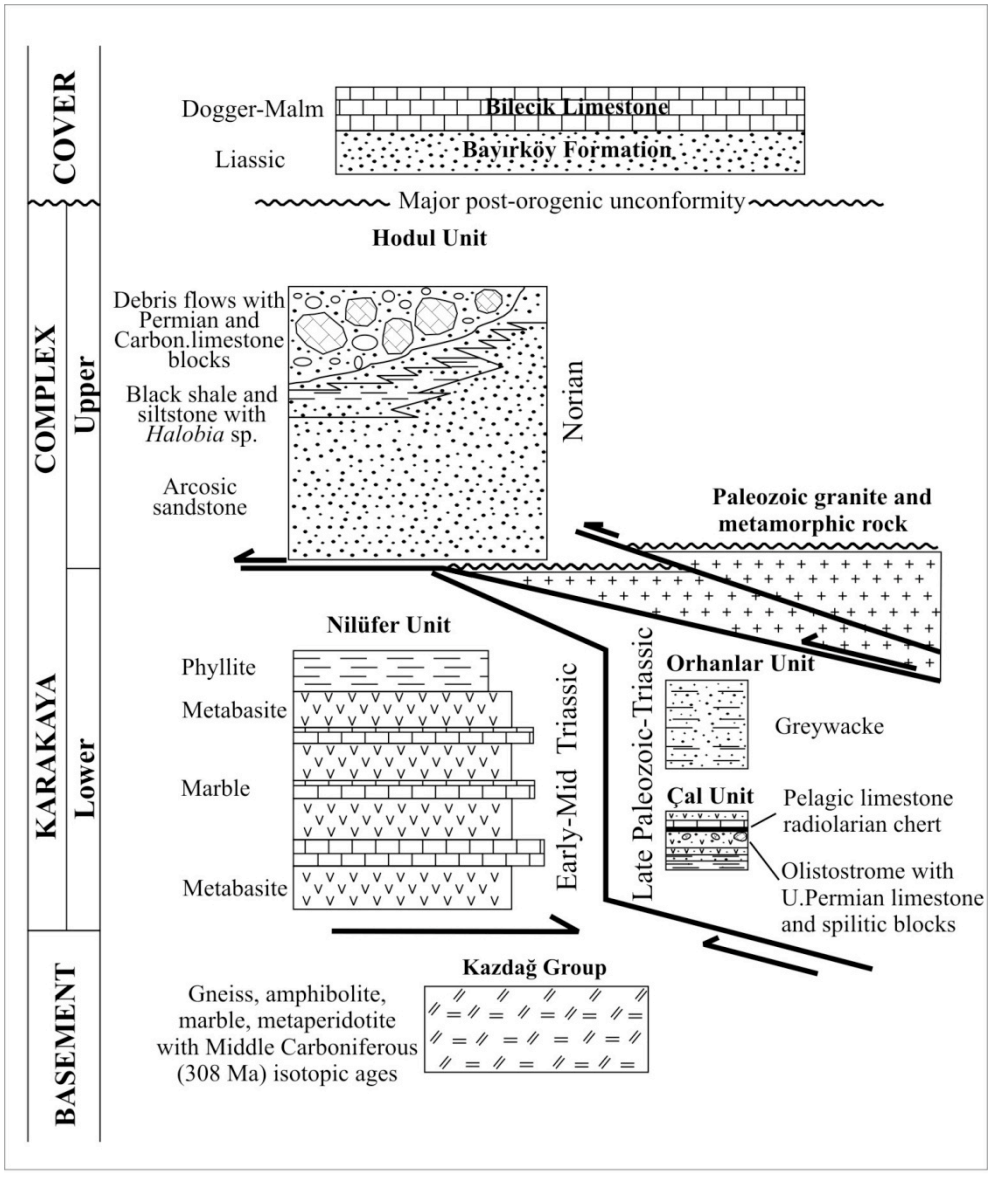

Federici *et al.* Figure 2

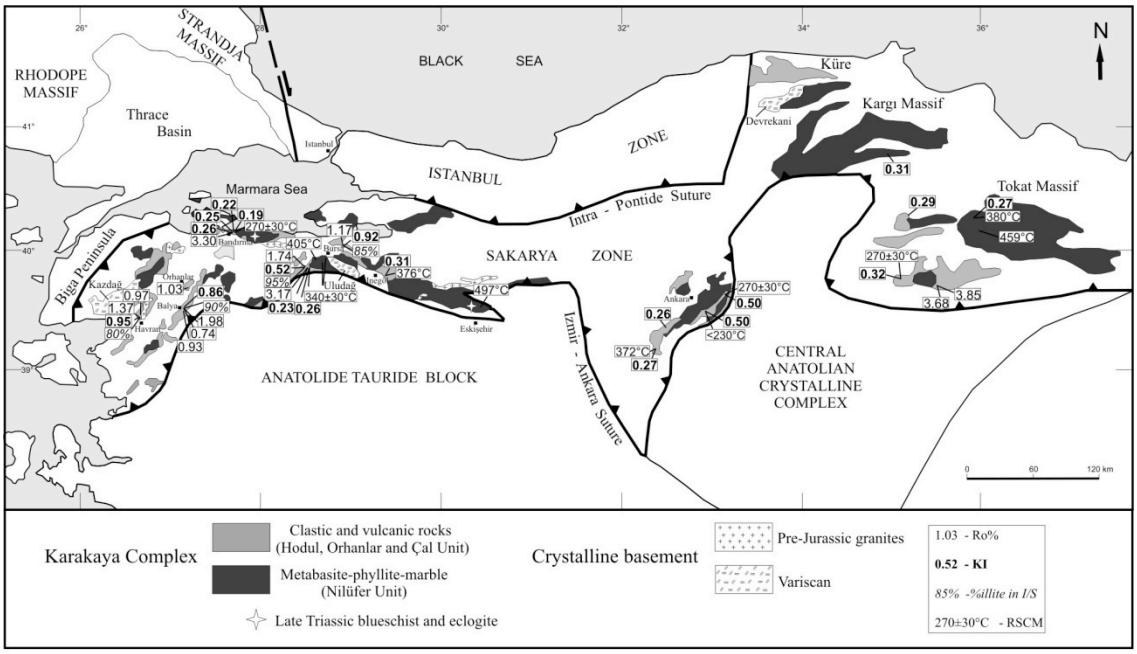

Federici *et al.* Figure 3

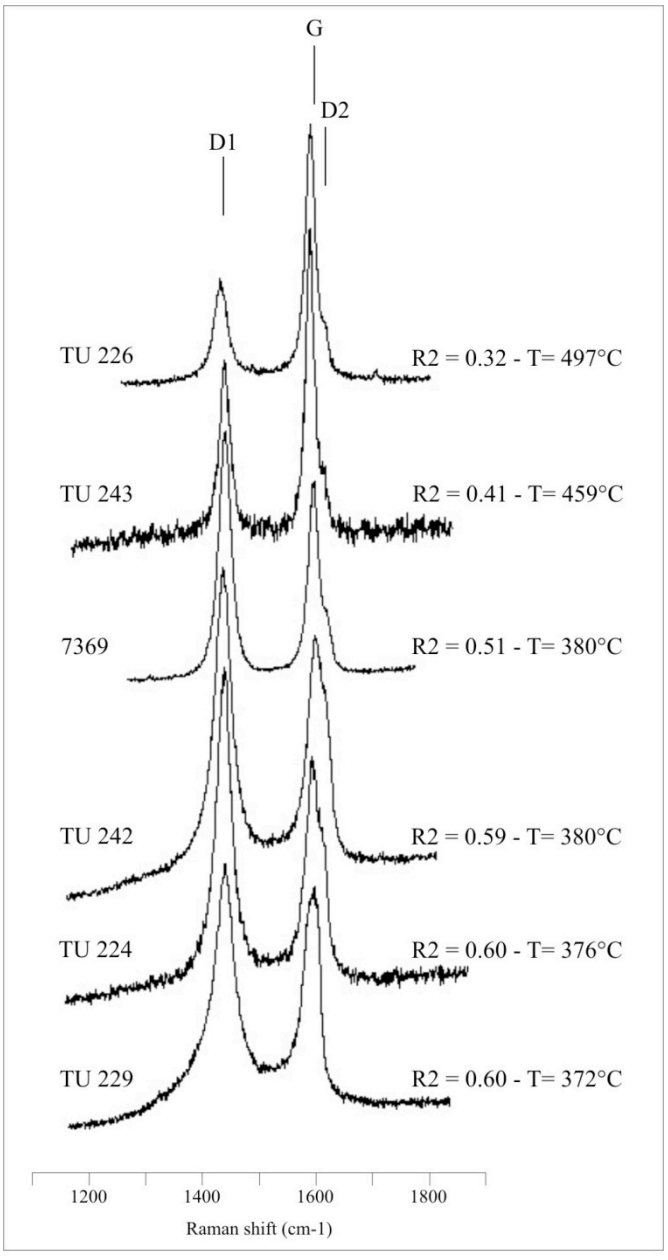

Federici *et al.* Figure 4

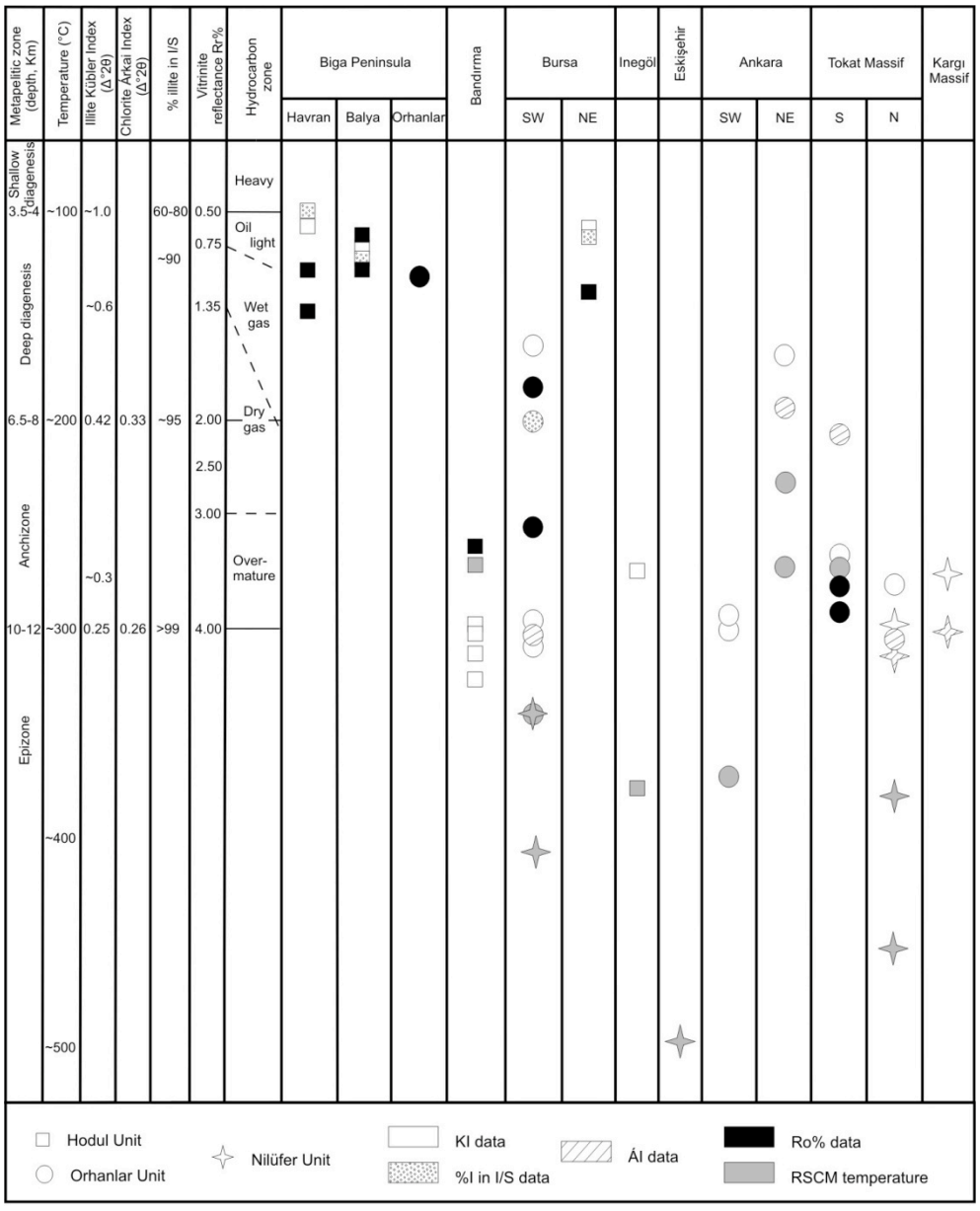

Federici *et al.* Figure 5

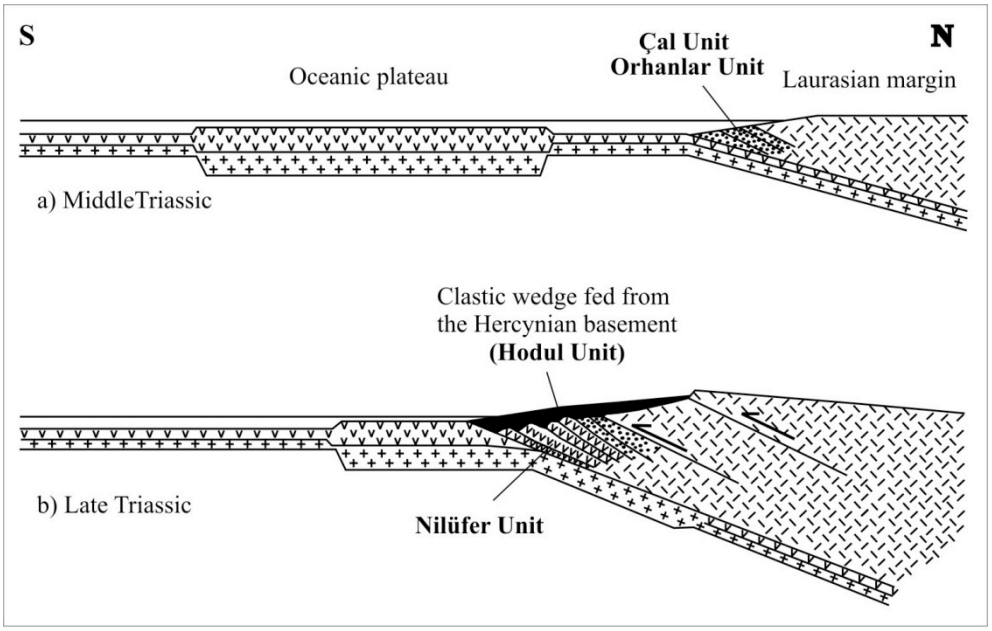

Federici *et al.* Figure 6

TABLE 1. Organic matter maturity, clay mineralogy data and Raman spectroscopy temperatures.

Locality		Sample	Coordinates	Unit	Lithology	%Ro±s.d. (n. measurements)	KI (001) 10Å	ÁI (002) 7Å	% I in I/S (<2μm)	X-Ray semiquantitative analyses		RSCM (T°C)
										bulk	<2μm	
Biga Peninsula	Havran	IF 24	N39°35'53.018" E27°10'49.364"	Hodul Unit	Dark brown siltite with numerous mineral fragments and macrofossils, alterated	1.377±0.14 (45)	0.95		80	$Ms_{25}Chl_{15}Qtz_{40}Pl_{20}$	$Ill_{45}Chl_{54}I/S_1$	
		IF 23	N39°36'05.265" E27°10'58.537"	Hodul Unit	Medium-grained greenish brown sandstone, alterated	0.97±0.07 (21)						
	Balya	IF 17	N39°44'27.208" E27°35'29.662"	Hodul Unit	Fine-grained greenish brown sandstone	0.74±0.09 (42)						
		IF 19	N39°44'48.299" E27°35'53.373"	Hodul Unit	Dark grey argillite	1.984±0.06 (55)	0.86		90	$Ms_{25}Chl_{15}Qtz_{30}Pl_{30}$	$Ill_{74}Chl_{26}I/S_1$	
		IF 20	N39°44'16.031" E27°39'39.086"	Hodul Unit	Fine-grained greenish brown siltite	0.934±0.09 (33)						
	Orhanlar	IF 13	N39°53'04.123" E27°36'53.926"	Orhanlar Unit	Fine to medium-grained grey greywacke with vein of calcite	1.039±0.04 (15)						
	Bandırma	IF 28	N40°21'14.582" E28°00'20.098"	Hodul Unit	Brown grey mudstone with slaty cleavage		0.26			$Ms_{65}Chl_{10}Qtz_5K\text{-}fd_{10}Pl_{10}$	$Ill_{95}C/S_5$	270±30
		IF 29	N40°21'14.582" E28°00'20.098"	Hodul Unit	Brown grey mudstone with slaty cleavage		0.25			$Ms_{65}Chl_{10}Qtz_5K\text{-}fd_5Pl_{10}Cal_5$	$Ill_{85}Chl_{10}C/S_5$	270±30
		IF 31	N40°21'14.099" E28°00'19.794"	Hodul Unit	Brown grey mudstone with slaty cleavage		0.22			$Ms_{60}Chl_5Qtz_{15}K\text{-}fd_5Pl_5Cal_{10}$	$Ill_{95}C/S_5$	270±30
		IF 33	N40°21'14.582" E28°00'20.098"	Hodul Unit	Brown grey mudstone with slaty cleavage and veins of calcite	3.306±0.10 (26)	0.19			$Ms_5Chl_5Qtz_{20}Pl_5Cal_{65}$	$Ill_{85}Chl_{10}C/S_5$	270±30
		IF 34	N40°21'14.841" E28°00'20.187"	Hodul Unit	Brown grey mudstone with slaty cleavage and veins of calcite		0.22			$Ms_{15}Chl_5Qtz_{25}Pl_{15}Cal_{40}$	$Ill_{90}Chl_5C/S_5$	270±30
Bursa area	SW	7249	N40°04'43.240" E29°00'22.452"	Nilüfer Unit	Phyllites							340±30
		7370	N40°05'50.376" E28°56'28.779"	Nilüfer Unit	Marble							340±30
		7369	N40°10'34.850" E28°58'26.259"	Nilüfer Unit	Marble							405±24
		IF 36	N40°04'25.935" E28°59'53.575"	Orhanlar Unit	Dark grey mudstone with slaty cleavage	3.177±0.13 (36)	0.23	0.26		$Ms_{30}Chl_{20}Qtz_{15}Pl_{30}Cal_5$	$Ill_{60}Chl_{40}$	
		IF 37	N40°04'25.935" E28°59'53.575"	Orhanlar Unit	Dark grey mudstone with slaty cleavage		0.26	0.26		$Ms_{20}Chl_{25}Qtz_{20}Pl_{35}$	$Ill_{50}Chl_{50}$	340±30
		IF 39	N40°04'23.375" E28°59'08.330"	Orhanlar Unit	Grey mudstone	1.747±0.09 (46)	0.52	0.44	95	$Ms_{15}Chl_{15}Qtz_{35}Pl_{35}$	$Ill_{65}Chl_{35}$	
	NE	IF 7	N40°15'34.206" E29°13'01.968"	Hodul Unit	Grey mudstone	1.176±0.08 (51)	0.92		85	$Ms_{25}Qtz_{55}Pl_{20}$	$Ill_{99}I/S_1$	

Note: %Ro -vitrinite reflectance; KI -Kübler Index; ÁI -Árkai Index; %I in I/S -illite content in illite-smectite; RSCM -raman spectroscopy on carbonaceous material; Ms -muscovite; Chl -chlorite; Qtz -quartz; K-feldspar; Pl -plagioclase; Cal -calcite; Kln -kaolinite Ill -illite; I/S -illite/smectite; C/S -chlorite/smectite.

TABLE 1. Organic matter maturity, clay mineralogy data and Raman spectroscopy temperatures.

	Locality	Sample	Coordinates	Unit	Lithology	%Ro±s.d. (n. measurements)	KI (001) 10Å	ÁI (002) 7Å	% I in I/S (<2μm)	X-Ray semiquantitative analyses		RSCM (T°C)
										bulk	<2μm	
	Inegöl	TU 224	N40°02'35.546" E29°43'03.227"	Hodul Unit	Brown grey mudstone, closely spaced scaly cleavage, altered		0.31			$Ms_{65}Chl_{15}Qtz_5Pl_{15}$	$Ill_{85}Chl_{10}C/S_5$	376
	Eskişehir	TU 226	N39°51'26.062" E30°37'58.748"	Nilüfer Unit	Marble							497
Ankara area	SW	TU 229	N39°47'05.589" E32°42'41.332"	Orhanlar Unit	Grey mudstone with closely spaces slaty cleavage		0.27			$Ms_{75}Chl_{15}K\text{-}fd_5Pl_5$	$Ill_{85}Chl_{10}C/S_5$	372
		TU 231	N39°50'29.850" E32°48'11.121"	Orhanlar Unit	Brow to grey mudstone with closely slaty cleavage		0.26			$Ms_{55}Chl_{25}Qtz_5K\text{-}fd_5Pl_{10}$	$Ill_{65}Chl_{35}$	
	NE	TU 233	N39°52'34.235" E32°48'45.792"	Orhanlar Unit	Dark grey mudstone with discrete spaced scaly cleavage and veins of calcite		0.50	0.34		$Ms_{10}Chl_{15}Qtz_{30}Pl_{40}Cal_5$	$Ill_{40}Chl_{60}$	<230
		TU 235	N39°57'50.628" E33°05'43.668"	Orhanlar Unit	Dark grey mudstone with discrete spaced scaly cleavage and veins of calcite		0.50	0.39		$Ms_{20}Chl_{15}Qtz_{30}Pl_{15}Cal_{20}$	$Ill_{55}Chl_{45}$	270±30
Tokat Massif	S	TU 237	N40°07'08.656" E34°50'30.959"	Orhanlar Unit	Dark grey mudstone with slaty cleavage		0.32	0.30		$Ms_{50}Chl_{30}Qtz_{10}Pl_{10}$	$Ill_{50}Chl_{50}$	270±30
		TU 238	N40°05'01.753" E35°14'59.381"	Orhanlar Unit	Fine to medium-grained grey greywacke weakly altered	3.681±0.13 (16)						
		TU 239	N40°05'01.753" E35°14'59.381"	Orhanlar Unit	Dark grey mudstone with slaty cleavage	3.852±0.10 (8)				$Ms_{35}Chl_{45}Qtz_{10}Pl_{10}$	$Ill_{70}Chl_{30}$	
	N	TU 241	N40°33'15.145" E35°25'19.986"	Orhanlar Unit	Dark grey mudstone with discrete spaced scaly cleavage		0.29	0.23		$Ms_{20}Chl_{20}Qtz_{33}Pl_{25}Cal_2$	$Ill_{50}Chl_{50}$	
		TU 242	N40°31'58.344" E35°45'20.904"	Nilüfer Unit	Dark grey mudstone with closely spaced slaty cleavage		0.27	0.17		$Ms_{35}Chl_{45}Qtz_{15}Pl_5$	$Ill_{70}Chl_{30}$	380
		TU 243	N40°29'36.406" E35°47'25.146"	Nilüfer Unit	Grey violaceous mudstone with closely spaced slaty cleavage					$Ms_{60}Kln_{20}Qtz_{10}K\text{-}fd_5Pl_5$	$Ill_{70}Chl_{30}$	459
	Kargı Massif	TU 244	N41°07'34.410" E34°46'16.609"	Nilüfer Unit	Grey mudstone with veins of calcite		0.31	0.25		$Ms_{45}Chl_{20}Qtz_{25}Pl_5Cal_5$	$Ill_{60}Chl_{40}$	

Note: %Ro -vitrinite reflectance; KI -Kübler Index; ÁI -Árkai Index; %I in I/S -illite content in illite-smectite; RSCM -raman spectroscopy on carbonaceous material; Ms -muscovite; Chl -chlorite; Qtz -quartz; K-feldspar; Pl -plagioclase; Cal -calcite; Kln -kaolinite Ill -illite; I/S -illite/smectite; C/S -chlorite/smectite.

TABLE 2. Raman spectroscopy details and temperatures.

Sample	Coordinates	Tectonostratigraphic Unit	Lithology	R2	SD	T(°C)	n	SE
7369	N40°10'34.850" E28°58'26.259"	Nilüfer Unit	Marble	0,51	0,06	405	13	7
TU 224	N40°02'35.546" E29°43'03.227"	Hodul Unit	Pelites	0,60	0,02	376	10	3
TU 226	N39°51'26.062" E30°37'58.748"	Nilüfer Unit	Marble	0,32	0,03	497	12	4
TU 229	N39°47'05.589" E32°42'41.332"	Orhanlar Unit	Slate	0,60	0,04	372	13	5
TU 242	N40°31'58.344" E35°45'20.904"	Nilüfer Unit	Phyllite	0,59	0,02	380	11	3
TU 243	N40°29'36.406" E35°47'25.146"	Nilüfer Unit	Phyllite	0,41	0,03	459	10	5

Note: Raman spectroscopy data. R2 is R2 ratio (D1 / (G+D1+D2)), SD is standard deviation for R2, T(°C) is temperature, n is number of spectra, and SE is standard error. Temperatures are calculated using the equation of Beyssac *et al.* (2002): T(°C) = -445R2 + 641.

CHAPTER 3

This chapter consists of the manuscript titled "Pre-Cenozoic amalgamation of the İstanbul and Sakarya terranes (NW Turkey) – evidence from low-temperature thermochronology" by William Cavazza, Ilaria Federici, Aral I. Okay and Massimiliano Zattin. The manuscript was submitted to "Terra Nova" on October 19th, 2009.

Running head: Pre-Cenozoic amalgamation of the İstanbul and Sakarya terranes

Pre-Cenozoic amalgamation of the İstanbul and Sakarya terranes (NW Turkey) – evidence from low-temperature thermochronology

William Cavazza[1], Ilaria Federici[1], Aral I. Okay[2] and Massimiliano Zattin[3]

[1]Dipartimento di Scienze della Terra e Geologico-Ambientali, Università di Bologna, Piazza di Porta San Donato 1, 40126 Bologna, Italy; [2]Avrasya Yerbilimleri Enstitüsü ve Jeoloji Mühendisliği Bölümü, Maden Fakültesi, İstanbul Teknik Üniversitesi, Maslak, 34469 İstanbul, Turkey; [3]Dipartimento di Geoscienze, Università di Padova, Via Giotto 1, 35137 Padova, Italy

ABSTRACT

Apatite fission-track (AFT) analyses of a large number of rock samples collected from the İstanbul terrane (İT) and the adjacent Sakarya terrane (ST) of northwestern Turkey isolate three discrete episodes of exhumation. (1) Paleocene - early Eocene AFT ages reflect the closure of the Izmir-Ankara ocean. (2) Late Eocene – earliest Oligocene ages are the result of renewed tectonic activity along the Izmir-Ankara suture. (3) Late Oligocene - early Miocene ages reflect the onset and development of northern Aegean extension. AFT ages cluster identically both north and south of the tectonic contact between İT and ST, thus implying that such terranes were amalgamated in pre-Cenozoic times.

Correspondence: William Cavazza, Department of Earth and Geoenvironmental Sciences, Piazza di Porta San Donato 1, 40126 Bologna, Italy. Tel.: 00 39 051 2094939; fax: 00 39 051 2094522; e-mail: william.cavazza@unibo.it

Introduction

The Pontides are an east-west trending orogenic belt stretching some 1,400 km, from SE Bulgaria to the Lesser Caucasus (Fig. 1). They repeatedly underwent deformation during the Variscan (Carboniferous), Cimmerian (Triassic), and Alpine (Late Cretaceous-Paleogene) orogenies (Yılmaz et al., 1997; Tüysüz, 1999), with widespread reactivation of older structures and creation of complex tectonostratigraphic relationships. Although presently constituting a discrete and continuous orographic element, the Pontides result from the amalgamation of three tectono-stratigraphic terranes: the Strandja massif, the İstanbul terrane (İT) (also known as İstanbul Zone), and the Sakarya terrane (ST) (also known as Sakarya Zone). The Intra-Pontide suture, i.e. the tectonic boundary between İT and ST, is considered by Okay and Tüysüz (1999) the result of the progressive closure of an Intra-Pontide ocean during the Senonian. In contrast, according to Şengör and Yılmaz (1985), the Intra-Pontide suture formed in the early Eocene after an orthogonal opening between İT and ST during the Liassic. Stampfli and Hochard (2009) support a middle Jurassic collision between İT and ST. Akbayram et al. (2009) favor a Cenomanian collision.

In this paper, based on a large number of AFT ages derived from rock units cropping out north and south of the Intra-Pontide suture, we document that İT and ST were mechanically coupled at least from the Paleocene and thus they were amalgamated in pre-Cenozoic times. This result has significant bearing on paleogeographic-paleotectonic reconstructions of the eastern Mediterranean region.

Geological overview

As mentioned above, the Pontides are made of three distinct tectonostratigraphic terrane: the Strandja massif, the İT, and the ST (Fig. 1). The Strandja massif constitutes the easternmost part of the vast crystalline basement massif that includes the Rhodope and Serbo-Macedonian massifs. It consists of a Variscan crystalline basement nonconformably overlain by a Triassic-Jurassic sedimentary succession (Aydın, 1974; Okay and Tüysüz, 1999; Sunal et al., 2006). Senonian andesites and associated granodiorites are widespread (Moore et al., 1980), and form a distinctive Late Cretaceous magmatic belt that can be followed all along the Pontides along the Black Sea and represents a magmatic arc developed above the northward subducting Neotethyan Ocean.

The İT is a fragment of continental lithosphere about 400 km long (Figs. 1, 2). It is made of a late Precambrian basement complex overlain by a continuous Ordovician-to-Carboniferous sedimentary succession, which was deformed during the Hercynian orogeny (Dean et al., 1997; Görür et al., 1997). The İT shows a Paleozoic-Mesozoic stratigraphy similar to that of the Moesian

platform and -according to Okay et al. (1994)- prior to the Late Cretaceous opening of the western Black Sea it was situated south of the Odessa shelf (Fig. 1).

The ST is an elongate lithospheric ribbon stretching >1,500 km from the Aegean Sea to the Lesser Caucasus (Fig. 1). It is characterized by the absence of *in situ* Paleozoic sedimentary rocks, by the presence of a characteristic Permo-Triassic subduction-accretion complex (Karakaya-Küre Complex), and by a ubiquitous early to mid-Jurassic transgression (Okay and Göncüoğlu, 2004).

Analytical methods

Fission-track dating is a tool to unravel the cooling histories experienced by rocks in the upper crustal levels and to give a measure of their motion toward the surface (for a review, see Donelick et al., 2005). Fission tracks in apatites all have the same initial length of about 16 μm (Green, 1988) but anneal at rates proportional to temperatures, starting at about 60°C. Over geological time scales, partial annealing of fission tracks occurs at temperatures between about 60 and 125°C (the Partial Annealing Zone: PAZ; Gleadow and Fitzgerald, 1987). Because tracks shorten in relation to the degree and duration of heating, the measurement of fission track lengths gives information about thermal evolution in the PAZ temperature range. A quantitative evaluation of the thermal history can be carried out through modelling procedures, which find a range of cooling paths compatible with the AFT data (Ketcham, 2005). In this work, inverse modelling of track-length data was performed using the HeFTy program (Ehlers et al., 2005), which generates the possible T-t paths by a Monte Carlo algorithm.

Discussion of analytical results

Samples were collected from most of the suitable stratigraphic units across a large area of the İT and the ST (Fig. 2). Figure 2 shows the areal distribution of AFT ages in the study area; complete results are listed in Table 1. All youngest, Neogene AFT ages were yielded by rock samples collected in the western portion of the study area around the Marmara Sea. Except for the Neogene ages, all other AFT ages do not show any consistent geographic distribution (Fig. 2). Similarly, there is no relationship between FT ages and sample elevations (Table 1).

AFT ages from the western portion of our study area confirm the results of Zattin et al. (2009) that most exhumation in the peri-Marmara region occurred in latest Oligocene – early Miocene times, when the Aegean domain was beginning to form by extension. Detachments are widespread in the Cyclades as well as in the northern Rhodope and western Turkey (e.g. Gautier and Brun, 1994; Dinter, 1998). For example, the two youngest AFT ages (16.8 ± 1.9 and 16.3 ± 1.4 Ma) of our entire dataset were yielded by samples taken from pre-Jurassic units a few km east of the

Kazdağ core complex (Table 1, Fig. 2), a major Aegean-related extensional feature exposing mid-crustal level (Okay and Satır, 2000; Cavazza et al., 2008). Zattin et al. (2005, 2009) and Okay et al. (2008) provide evidence that the present-day western portion of the North Anatolian Fault system – widening to ca. 100 km in a north-south direction in the Marmara-Biga region- is superposed on older, generally east-west trending, tectonic structures with a significant vertical component, thus capable of inducing exhumation.

The oldest AFT age of our entire dataset (106.6 ± 5.7 Ma) was yielded by a sandstone sample (TU 116, Table 1) from the Carboniferous fluvio-deltaic Karadon Formation along the coast of the Black Sea (Fig. 2). This is the only evidence in the study area of the thermochronological effects of the opening of the western Black Sea. The FT age of this sample fits well with the time span covered by the western Black Sea break-up unconformity between the Cağlayan Fm. (Aptian-Albian) an the Kapanboğazi Fm. (Cenomanian) in the area of Sinop and the correlative hyatuses to the west (Tüysüz, 1999, Fig. 3). Such distinctive thermotectonic event was likely registered by other rock units but then erased by younger thermochronological events.

If we exclude the Neogene AFT ages from the westernmost samples and the one Early Cretaceous age discussed above, all other twenty-two AFT ages cluster into two discrete groups (Fig. 3). Such groups are neither geographically nor geologically defined, as samples from both the İT and the ST concur to the composition of each group. The first cluster comprises Paleocene-Ypresian AFT ages and if we exclude sample TU 41 (65.8 ± 5.0 Ma), the age distribution of the other ten samples within this cluster ranges narrowly between 62.3 (late Danian) and 50.3 Ma (late Ypresian). The second cluster comprises eleven samples ranging in age between 43.5 (late Lutetian; TU 120) and 32.3 Ma (early Rupelian; TU 114). Excluding sample TU 120, the entire late Ypresian – early Bartonian time span, covering about >10 Ma, is devoid of AFT ages. Similarly, the early Rupelian – early Chattian time span is also devoid of AFT ages (Fig. 3).

The coherent AFT ages distribution along the western-central Pontides, with three discrete clusters of ages alternating with two relatively long periods of little or null exhumation, requires a geologically meaningful explanation. The absence of any regular spatial pattern in the geographic distribution of the older AFT ages derives from the complex tectonic history of the Pontides, with multiple, superposed deformation episodes –including Plio-Quaternary strike-slip deformation with large horizontal offset- which have generated complex tectonostratigraphic relationships and jumbled any previous spatially coherent exhumation trend(s). From this viewpoint, it is not surprising that the only areally defined exhumation trend is determined by the youngest cluster of ages concentrated in the westernmost portion of the study area (Figs. 2, 3). In fact, such cluster (late

Oligocene – early Miocene) relates to northern Aegean regional extension, i.e. *the latest tectonic event capable of generating significant vertical separation*.

The older age cluster (Paleocene – late Ypresian; Fig. 3) can be explained as the result of deformation induced by the closure of the İzmir-Ankara oceanic domain and the ensuing collision in the Paleocene – early Eocene between the ST to the north and the Anatolide-Tauride Block to the south (Okay and Tüysüz, 1999; Okay et al., 2001). All our samples are within 100 km from the trace of the İzmir-Ankara suture (Fig. 2) and the entire study area provides ample evidence of deformation related to the development of such suture (e.g. Okay et al., 2001). Our data are supported by similar Paleocene – early Eocene AFT ages from the Dereli–Şebinkarahisar granitoids in the Eastern Pontides (Boztuğ et al., 2004), also interpreted as the result of fast exhumation related to the collision.

The Bartonian – early Rupelian age cluster (Fig. 3) corresponds to the second phase of deformation along the Pontides characterized by the termination of deposition and deformation in the internal basins (Okay et al., 2001; Fig. 13). Alternatively, Robinson et al. (2005, Fig. 8) interpreted a widespread stratigraphic hyatus covering the same time span in the eastern Pontides as the result of rifting and opening of the eastern Black Sea, while compression induced by the closure of the Neotethys would have occurred much later in the late Eocene - Oligocene

Modeling of fission-track data was performed on the five samples with the highest numbers of measured tracks (Table 1) and provided more quantitative constraints on their cooling paths (Fig. 4). Sample TU 41 from early Eocene turbidites north of İzmit Bay within the İT yielded an AFT age of 65.8 Ma, i.e. older than its depositional age. This implies that (i) we dated fast cooling and exhumation in the sediment source area in the latest Cretaceous time, and (ii) the flysch has never been buried at the bottom of the PAZ after deposition. Sample TU 46 from a granitoid unit within the ST also points to an early Paleocene episode of exhumation. Cooling occurred over a wide time span until the early Oligocene, with a discrete period of no exhumation during the middle Eocene, in line with the overall absence of AFT ages in this period throughout the study area (Fig. 3). TU 116 was taken from Westphalian fluvio-deltaic deposits along the coast of the Black Sea and yielded an Albian AFT age. In spite of relatively scarce constraints for the pre-Cretaceous history, thermochronological modeling indicates a long phase of Mesozoic subsidence followed by steady exhumation during Cretaceous times. TU 117 was also taken along the Black Sea coast, from Triassic continental to shallow-marine deposits. Its modelled thermochronological evolution is similar to the one of TU 116, with a long phase of early-middle Jurassic subsidence followed by exhumation beginning in the late Jurassic and taking up speed starting at about 110 Ma. The somewhat younger early Paleocene AFT age (61.0 Ma) of TU 117 derives from the short tracks

(mean confined track lengths = 11.76 μm; Table 1), indicating a long period of residence of the sample within the partial annealing zone. TU 123 from a Precambrian granite of the İT yielded an AFT age of 38.3 Ma (late Bartonian). Inverse modelling of track-length data indicates fairly steady, low rates of cooling.

The clustering of AFT data from both the İT and ST into two coherent groups (Danian-Ypresian and late Lutetian - early Rupelian) indicates that they were amalgamated by earliest Paleocene time and then suffered the same tectonic events. Both exhumation episodes correlates well with phases of deformation along the Izmir-Ankara suture, as discussed above. The overall Cenozoic chronostratigraphy of sedimentary successions in the Pontides within relatively short distance from the Izmir-Ankara suture (<50 km) agrees with our thermochronologic data, as major supraregional hyatuses correspond to the two older clusters of AFT ages (Fig. 5). Other independent data substantiate the hypothesis of a pre-Cenozoic amalgamation of the İT and ST. (1) Within the Pontides, the Turonian-Campanian magmatic arc related to northward subduction of the Izmir-Ankara ocean stretches continuosly some 1,500 km from Bulgaria to the Caucasus, crossing the tectonic boundaries between the Strandja massif, the İT, and the ST without any significant interruption or offset. (2) Tüysüz (1999) showed that İT and the ST in the central Pontides share a common Senonian stratigraphy while they differ in their pre-Senonian stratigraphy and evolution, thus indicating that amalgamation must be Cenomanian or older. The question arises if amalgamation took place during the Cenomanian, i.e. concomitant with the opening of the western Black Sea (Okay et al., 2001; Akbayram et al., 2009), or earlier (i.e. in the middle Jurassic, as shown in the paleotectonic reconstructions by Stampfli and Hochard, 2009).

Conclusions

The complex areal distribution of exhumation ages documented in this paper in the western and central Pontides results from the superposition of discrete tectonic events. The western portion of the study area is dominated by late Oligocene – early Miocene AFT ages which obliterated any previous thermotectonic event. We suggest that extension that affected the Aegean region (e.g. Jolivet et al., 2004) gave rise to exhumation at a regional scale. These exhumation ages are in agreement with the thermochronologic and structural data of Zattin et al. (2005, 2009) and Okay et al. (2008) for the southern and western Marmara region, indicating that the present-day North Anatolian Fault –which branches into a ca. 100 km wide fault system in the Marmara-Biga region- is superposed on older, generally east-west trending, tectonic structures capable of inducing significant exhumation.

All older exhumation ages in the study area do not show an ordered geographic distribution yet they cluster coherently into two discrete groups: late Danian - late Ypresian (62.3-50.3 Ma) and late Lutetian - early Rupelian (43.5-32.3 Ma). Both exhumation episodes correlates well with phases of deformation along the Izmir-Ankara suture. Since the thermochronological effects of the two exhumation episodes are widespread in both the İstanbul and Sakarya terranes, our data indicates that their amalgamation occurred in pre-Cenozoic times.

Acknowledgments

This research was sponsored by MIUR (Italian Dept. of Public Education, University and Research) and by TÜBA (The Turkish Academy of Sciences). Field assistance by Selvihan Goktak is gratefully acknowledged.

References

Akbayram, K., Okay, A.I., Satir, M. and Topuz, G., 2009. New U-Pb, Pb-Pb and Rb-Sr ages from northwest Turkey: Early Cretaceous continental collision in the Western Pontides. 2nd Int. Symp. Geol. Black Sea, Abs. Book, 11-12.

Aydın, Y. 1974. Etude pétrographique et géochimique de la parte centrale du Massif d'Istranca (Turquie). PhD Thesis, Université de Nancy, 131 pp.

Beccaletto, L., Bartolini, A.C., Martini, R., Hochuli, P.A. and Kozur, H., 2005. Biostratigraphic data from the Çetmi melange, northwest Turkey: palaeogeographic and tectonic implications. *Palaeogeography, Paleoclimatology, Palaeoecology*, **221**, 215–244.

Bonev, N. and Beccaletto, L., 2007. From syn- to post-orogenic Tertiary extension in the north Aegean region: constraints on the kinematics in the eastern Rhodope-Thrace, Bulgaria-Greece and the Biga Peninsula, NW Turkey. In: The Geodynamics of Aegean and Anatolia (T. Taymaz, T., Y. Yilmaz, and Y. Dilek, eds), *Geol. Soc. London Spec. Publ.,* **291**, 113-142.

Boztuğ, D., Jonckheere, R., Wagner, G.A. and Yeğingil, Z., 2004. Slow Senonian and fast Palaeocene–Early Eocene uplift of the granitoids in the Central Eastern Pontides, Turkey: apatite fission-track results. *Tectonophysics*, **382**, 213– 228

Cavazza, W., Okay, A.I. and Zattin, M., 2009. Rapid early-middle Miocene exhumation of the Kazdağ metamophic core complex (Western Anatolia). *Int. J. Earth Sci.*, DOI 10.1007/s00531-008-0353-9.

Dean, W.T., Martin, F., Monod, O., Demir, O., Rickards, R.B., Bultynck, P. and Bozdogan, N., 1997. Lower Paleozoic stratigraphy, Karadere–Zirze area, Central Pontides. In: Göncüoğlu, M.C. and Derman A.S. (eds) Early Palaeozoic Evolution in NW Gondwana. *Turkish Ass. Petrol. Geol. Spec. Publ.*, **3**, 32–38.

Dinter, D.A., 1998. Late Cenozoic extension of Alpine collisional orogen, northeastern Greece: origin of the north Aegean basin. *Geol. Soc. Am. Bull.,* **110**, 1208-1230.

Donelick, R.A., O'Sullivan, P.B. and Ketcham, R.A., 2005. Apatite fission-track analysis. *Rev. Min. Geochem.*, **58**, 49-94.

Fleischer, R.L., Price, P.B. and Walker, R.M., 1975. *Nuclear tracks in solids: principles and techniques.* University of California Press, Berkeley.

Gailbraith, R.F., 1981. On statistical models for fission tracks counts. *Math. Geol.*, **13**, 471-478.

Gallagher, K., 1995. Evolving temperature histories from apatite fission-track data. *Earth Planet. Sci. Lett.*, **136**, 421-435.

Gleadow, A.J.W., Duddy, I.R., Green, P.F. and Lovering, J.F., 1986. Confined fission track lengths in apatite: a diagnostic tool for thermal history analysis. *Contr. Miner. Petrol.*, **94**, 405-415.

Gleadow, A.J.W. and Fitzgerald, P.G., 1987. Uplift history and structure of the Transantarctic Mountains: new evidence from fission track dating of basement apatites in the Dry Valleys area, southern Victoria Land. *Earth Planet. Sci. Lett.*, **82**, 1-14.

Görür, N. and Okay, A.I., 1996. A fore-arc origin for the Thrace Basin, NW Turkey. *Geol. Rund.*, **85**, 662-668.

Green, P.F., 1988. The relationship between track shortening and fission track age reduction in apatite: combined influences of inherent instability, annealing anisotropy, length bias and system calibration. *Earth Planet. Sci. Lett.*, **89**, 335-352.

Green, P.F., Duddy, I.R., Laslett, G.M., Hegarty, K.A., Gleadow, A.J.W. and Lovering, J.F., 1989. Thermal annealing of fission tracks in apatite: 4. Quantitative modelling techniques and extension to geological timescales. *Chem. Geol.*, **79**, 155-182.

Jolivet, L., Famin, V., Mehl, C., Parra, T., Aubourg, C., Hébert, R. and Phillippot, P., 2004. Strain localization during crustal-scale boudinage to form extensional metamorphic domes in the Aegean Sea. In: Gneiss domes in orogeny (D.L. Whitney, C. Teyssier and C.S. Siddoway, eds). Geol. Soc. Am. Spec. Paper, **380**, 185-210.

Ketcham, R.A., 2005. Forward and inverse modeling of low-temperature thermochronometry data. *Rev. Min. Geochem.*, **58**, 275-314.

Ketcham, R.A., Carter, A., Donelick, R.A., Barbarand, J. and Hurford, A.J., 2007. Improved modeling of fission-track annealing in apatite. *Am. Miner.*, **92**, 799-810.

Ketcham, R.A., Donelick, R.A. and Carlson, W.D., 1999. Variability of apatite fission-track annealing kinetics III: extrapolation to geological time scales. *Am. Miner.*, **84**, 1235-1255.

Ketcham, R.A., Donelick, R.A. and Donelick, M.B., 2000. AFTSolve: a program for multi-kinetic modeling of apatite fission-track data. *Geol. Mater. Res.*, **1**, 1-32.

Laslett, G.M., Green, P.F., Duddy, I.R. and Gleadow, A.J.W., 1987. Thermal annealing of fission tracks in apatite: 2. A quantitative analysis. *Chem. Geol.*, **65**, 1-13.

Moore, W.J., McKee, E.H. and Akinci, Ö., 1980. Chemistry and chronology of plutonic rocks in the Pontid Mountains, northern Turkey. *Europ. Copper Dep.*, **1**, 209-216.

Okay, A.I. and Göncüoğlu, M.C., 2004. The Karakaya Complex: A review of data and concepts. *Turk. J. Earth Sci*., **13**, 77-96.

Okay, A.I., Satir, M., Zattin, M., Cavazza, W. and Topuz, G., 2008. An Oligocene ductile strike-slip zone: Uludag Massif, northwest Turkey – implications for escape tectonics. *Geol. Soc. Am. Bull.*, **120**, 893-911.

Okay, A.I., Satir, M. and Siebel, W., 2006. Pre-Alpide Palaeozoic and Mesozoic orogenic events in the Eastern Mediterranean region. In: European Lithosphere Dynamics (D.G. Gee and R.A.

Stephenson, eds). *Geol. Soc. London Mem.,* **32**, 389–405.

Okay, A.I., Şengör, A.M.C. and Görür, N., 1994. Kinematic history of the opening of the Black Sea and its effect on the surrounding regions. *Geology,* **22**, 267-270.

Okay, A.I., Tansel, İ. and Tüysüz, O., 2001. Obduction, subduction and collision as reflected in the Upper Cretaceous-Lower Eocene sedimentary record of western Turkey. *Geological Magazine*, **138**, 117-142.

Okay, A.I. and Tüysüz, O., 1999. Tethyan sutures of the northern Turkey. In: Durand, B., Jolivet, L., Horvát, F. & Sérrane, M. (eds) The Mediterranean basins: Tertiary extension within the Alpine Orogen. *Geol. Soc. London Spec. Publ.*, **156**, 475-515.

Özcan, Z., 2009. İstanbul karadeniz sahil şeridi ili Bursa avasindaki üst Kretase-Eosen birimlerinin stratigrafik gelişmi ve korelasyonu. PhD dissertation, İstanbul Technical University, 185 pp.

Robertson, A.H.F. and Ustaomer, T. 2004. Tectonic evolution of the Intra-Pontide suture zone in the Armutlu Peninsula, NW Turkey. *Tectonophysics,* **381**, 175–209.

Robinson, A.G., (ed), 1997, Regional and petroleum geology of the Black Sea and surrounding regions. Am. Ass. Petrol. Geol. Mem., 68, Tulsa.

Robinson, A.G., Banks, C.J., Rutheford, M.M., and Hirst, J.P.P., 1995. Stratigraphic and structural development of the Eastern Pontides, Turkey. *J. Geol. Soc. London*, **152**, 861-872.

Şengör, A.M.C. and Yılmaz, Y., 1981. Tethyan evolution of Turkey: a plate tectonic approach. *Tectonophysics*, **75**, 181-241.

Stampfli, G. and Hochard, C., 2009. *Geol. Soc. London Memoir*, in press.

Sunal, G., Natal'in, B., Satır, M. and Toraman, E., 2006. Paleozoic magmatic events in the Strandja Massif, NW Turkey. *Geodin. Acta*, **19**, 283–300.

Tüysüz, O., 1999. Geology of the Cretaceous sedimentary basins of the Western Pontides. *Geol. J.*, **34**, 75-93.

van der Beek, P., Cloetingh, S. and Andriessen, P., 1994. Mechanisms of extensional basin formation and vertical motions at rift flanks: Constraints from tectonic modelling and fission track thermochronology. *Earth Planet. Sci. Lett.,* **121**, 417–433.

Yılmaz, Y., Tüysüz, O., Yiğitbas, E., Can Genc, Ş., and Şengör, A.M.C., 1997. Geology and tectonic evolution of the Pontides. In: Regional and petroleum geology of the Black Sea and surrounding regions (A.G. Robinson, ed). *Am. Ass. Petrol. Geol. Mem.,* **68**, 183-226.

Zattin, M., Cavazza, W., Okay, A.I., Federici, I., Fellin, G., Pignalosa, A. and Reiners, P., 2009. A precursor of the North Anatolian Fault in the Marmara Sea region. *J. Asian Earth Sci.*, submitted.

Zattin, M., Landuzzi, A., Picotti, V. and Zuffa, G.G., 2000. Discriminating between tectonic and sedimentary burial in a foredeep succession, Northern Apennines. *J. Geol. Soc. London*, **157**, 629-633.

Zattin, M., Okay, A.I. and Cavazza, W., 2005. Fission-track evidence for late Oligocene and mid-Miocene activity along the North Anatolian Fault in southwestern Thrace. *Terra Nova*, **17**, 95–101.

Figure captions

Figure 1. Simplified tectonic map of Asia Minor and the surrounding regions showing the major terranes and sutures. Modified from Okay and Tüysüz (1999).

Figure 2. Geologic map of the western-central Pontides with apatite fission-track ages (black) from the İstanbul and Sakarya Zones. Modified from Okay *et al.* (2008).

Figure 3. Age distribution of apatite fission-track data from the İstanbul (black bars) and Sakarya (gray bars) Zones. See Fig. 2 for location of samples.

Figure 4. Time-temperature paths obtained from inverse modelling using the HeFTy program (Ehlers et al., 2005), which generates the possible T-t paths by a Monte Carlo algorithm. Predicted AFT data were calculated according to the Ketcham et al. (2007) annealing model and the Donelick et al. (1999) c-axis projection. Shaded areas mark envelopes of statistically acceptable fit and the thick lines correspond to the most probable thermal histories. Thermal paths out of the partial annealing zone are largely inferential as fission-track data cannot give reliable information out of this temperature range. In each diagram, parameters (model and measured age, model and measured mean length) related to inverse modelling are reported. GOF gives an indication about the fit between observed and predicted data (values close to 1 are best).

Figure 5. Simplified chronostratigraphic sections for selected localities in the Sakarya terrane. Major hyatuses correspond to exhumation episodes defined by AFT age clusters of Fig. 2.

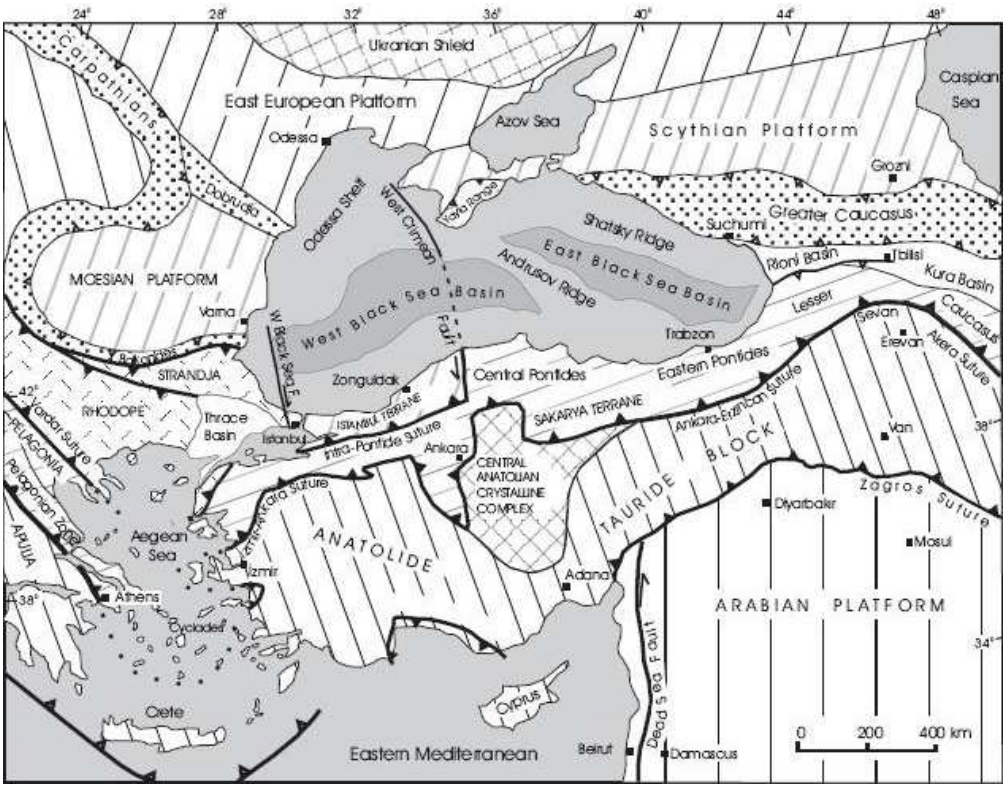

Geological framework
166x130mm (96 x 96 DPI)

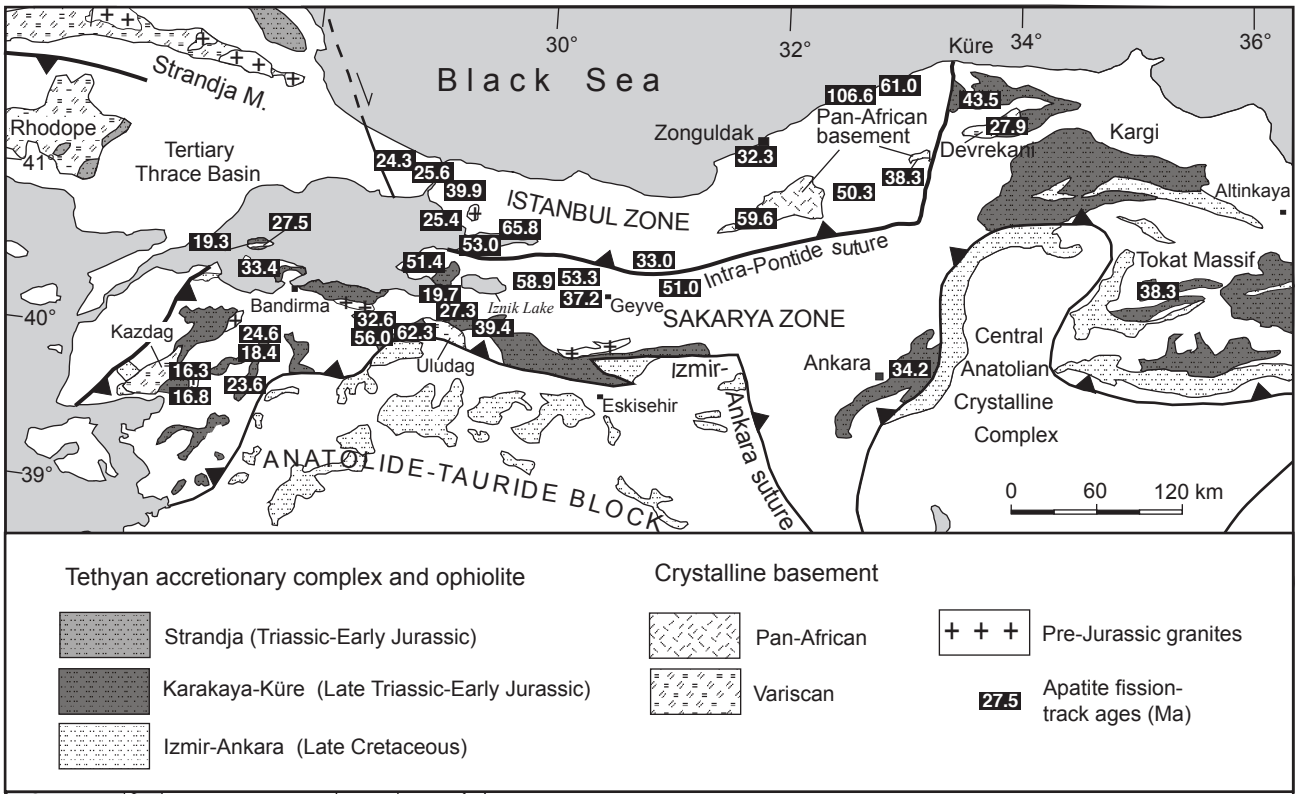
Black Sea
Strandja M.
Rhodope
Tertiary
Thrace Basin
ISTANBUL ZONE
Intra-Pontide suture
SAKARYA ZONE
ANATOLIDE-TAURIDE BLOCK
Izmir-
Ankara suture
Zonguldak
Pan-African
basement
Devrekani
Kargi
Altinkaya
Tokat Massif
Central
Anatolian
Crystalline
Complex
Ankara
Eskisehir
Geyve
Izmik Lake
Bandirma
Kazdag
Uludag
Küre
30°
32°
34°
36°
41°
40°
39°
0
60
120 km
106.6
61.0
43.5
27.9
32.3
38.3
50.3
59.6
24.3
25.6
39.9
25.4
65.8
53.0
27.5
19.3
33.4
51.4
33.0
58.9
53.3
51.0
37.2
19.7
27.3
32.6
56.0
62.3
39.4
24.6
18.4
16.3
16.8
23.6
34.2
38.3
Tethyan accretionary complex and ophiolite
Strandja (Triassic-Early Jurassic)
Karakaya-Küre (Late Triassic-Early Jurassic)
Izmir-Ankara (Late Cretaceous)
Crystalline basement
Pan-African
Variscan
Pre-Jurassic granites
Apatite fission-track ages (Ma)

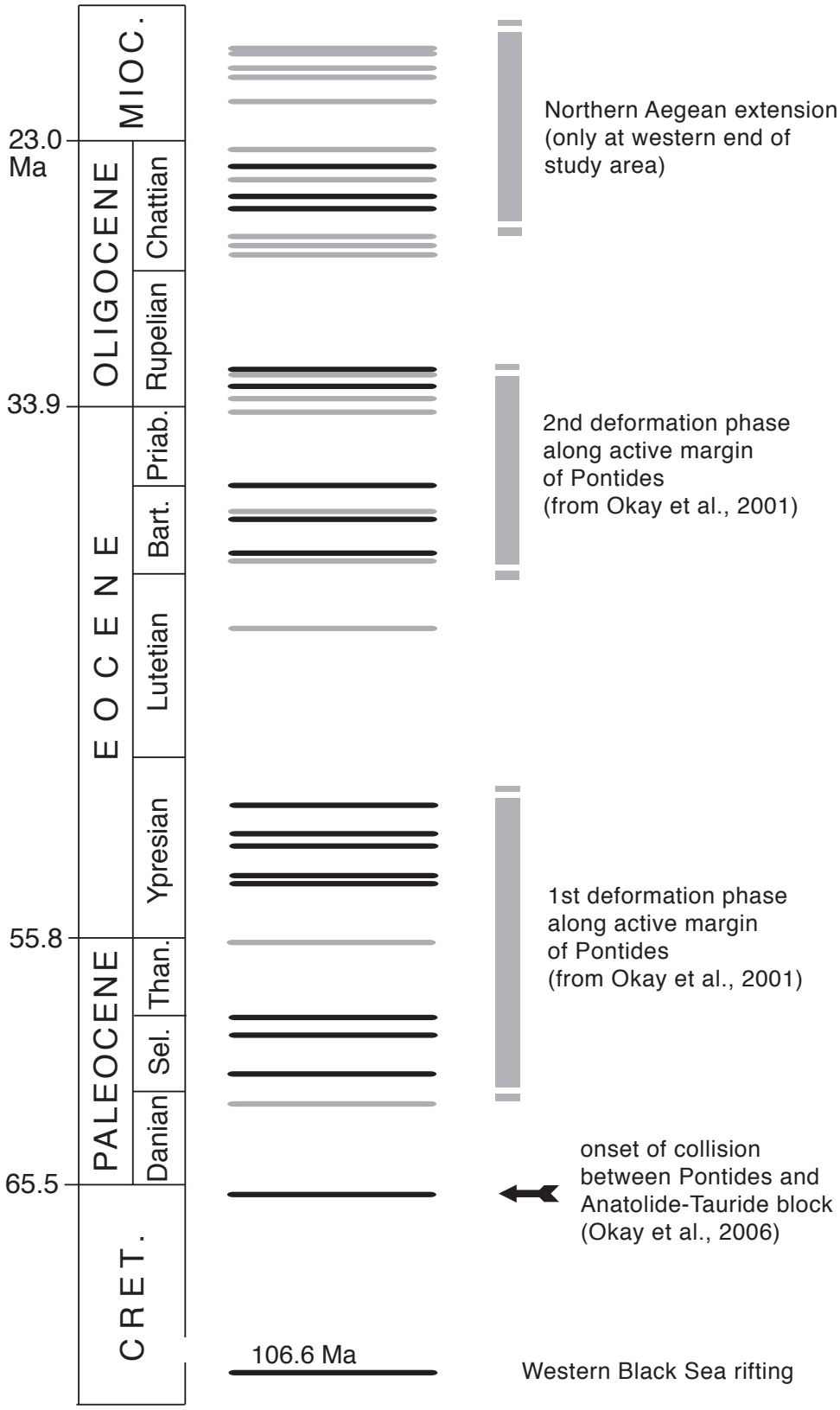
MIOC.
OLIGOCENE
Chattian
Rupelian
EOCENE
Priab.
Bart.
Lutetian
Ypresian
PALEOCENE
Than.
Sel.
Danian
CRET.
23.0 Ma
33.9
55.8
65.5
106.6 Ma
Northern Aegean extension (only at western end of study area)
2nd deformation phase along active margin of Pontides (from Okay et al., 2001)
1st deformation phase along active margin of Pontides (from Okay et al., 2001)
onset of collision between Pontides and Anatolide-Tauride block (Okay et al., 2006)
Western Black Sea rifting

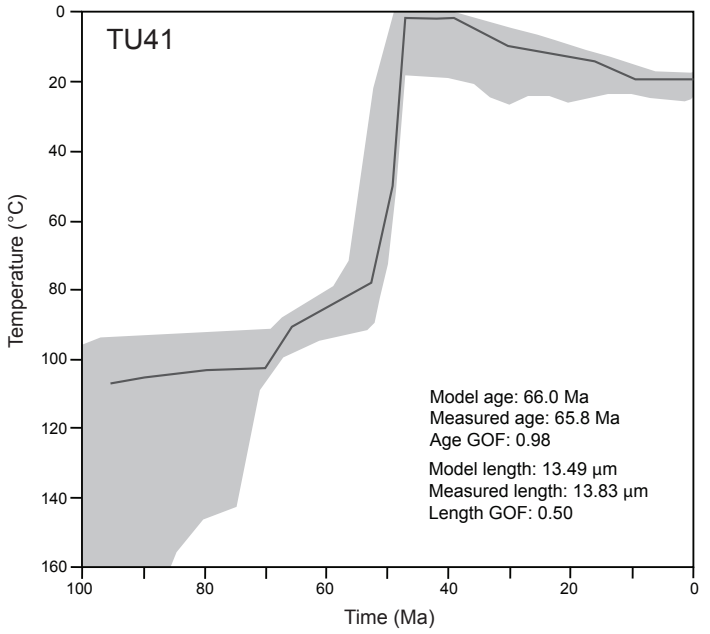
TU41
Temperature (°C)
Time (Ma)
Model age: 66.0 Ma
Measured age: 65.8 Ma
Age GOF: 0.98
Model length: 13.49 µm
Measured length: 13.83 µm
Length GOF: 0.50

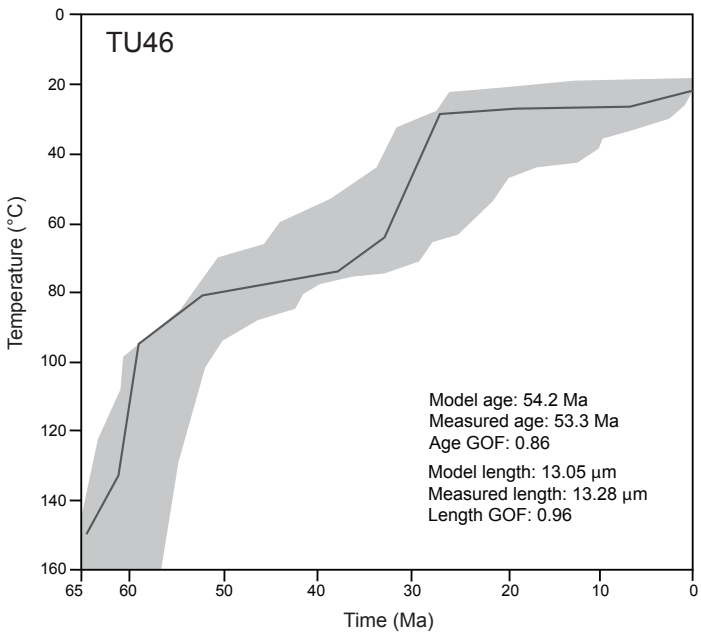
TU46
Temperature (°C)
Time (Ma)
Model age: 54.2 Ma
Measured age: 53.3 Ma
Age GOF: 0.86
Model length: 13.05 µm
Measured length: 13.28 µm
Length GOF: 0.96

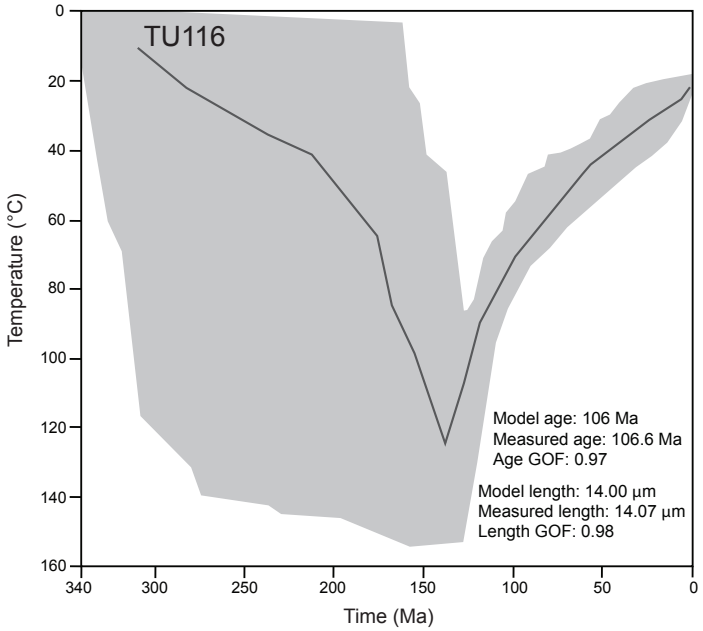
TU116
Temperature (°C)
Time (Ma)
Model age: 106 Ma
Measured age: 106.6 Ma
Age GOF: 0.97
Model length: 14.00 µm
Measured length: 14.07 µm
Length GOF: 0.98

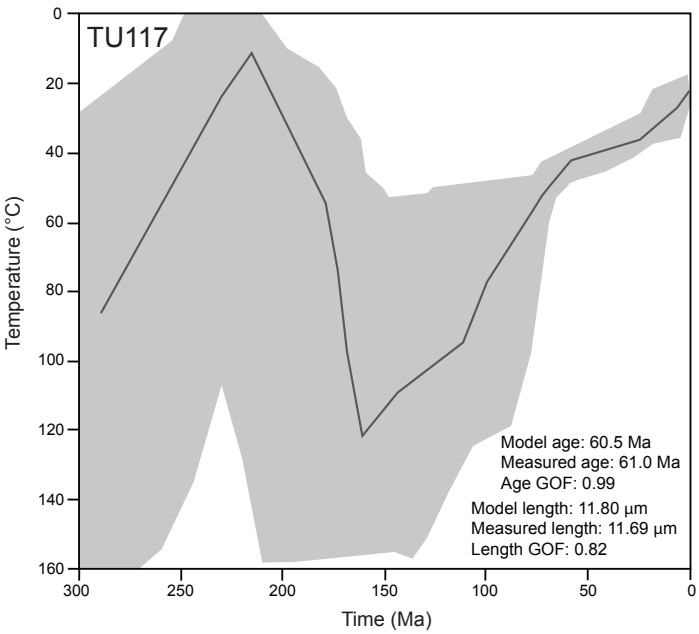
TU117
Temperature (°C)
Time (Ma)
Model age: 60.5 Ma
Measured age: 61.0 Ma
Age GOF: 0.99
Model length: 11.80 µm
Measured length: 11.69 µm
Length GOF: 0.82

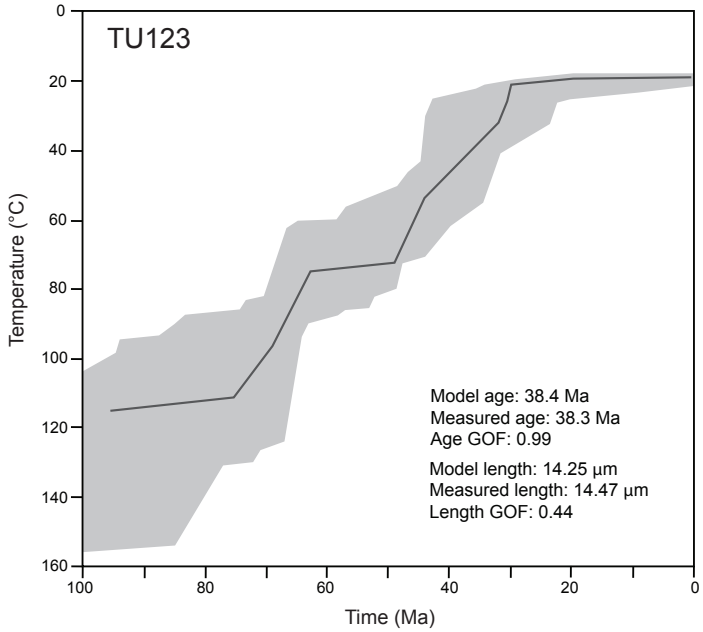
TU123
Temperature (°C)
Time (Ma)
Model age: 38.4 Ma
Measured age: 38.3 Ma
Age GOF: 0.99
Model length: 14.25 µm
Measured length: 14.47 µm
Length GOF: 0.44

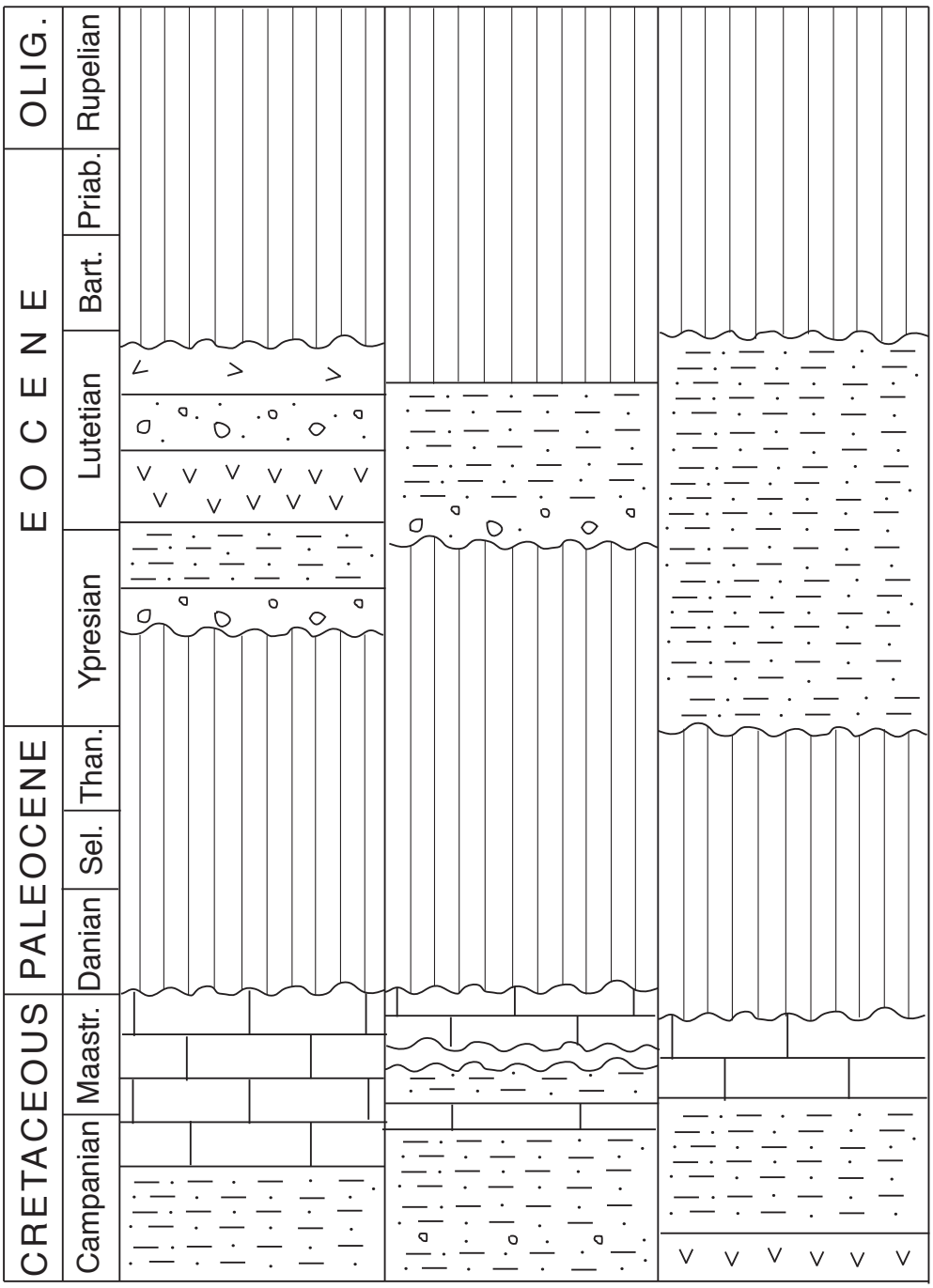
OLIG.
Rupelian
Priab.
Bart.
EOCENE
Lutetian
Ypresian
Than.
PALEOCENE
Sel.
Danian
Maastr.
CRETACEOUS
Campanian
South Iznik Lake
(Ozcan, 2009)
Geyve
(Okay et al., 2001)
Altinkaya
(Robinson et al., 2005)

Table 1. Apatite fission-track analyses. See Fig. 2 for location of samples.

Sample number	Rock unit	UTM coordinates	Elevation (m)	No. of crystals	Spontaneous		Induced		$P(\chi)^2$	Dosimeter		Age (Ma) ± 1s	Mean confined track length (mm) ± std. err.	Std. dev.	No. of tracks measured
					ρs	Ns	ρi	Ni		ρd	Nd				
TU 38^	Eocene granodiorite	0667110 4497786	424	15	3.51	193	1.16	636	20.2	0.94	4474	51.4 ± 4.8	13.43 ± 0.33	1.91	33
TU 39^	?Oligocene tuffite	0711381 4503904	-	20	1.66	124	0.60	448	98.9	1.05	4982	53.0 ± 5.5	15.46 ± 0.11	1.07	100
TU 41^	Early Eocene turbidite	0730648 4522849	-	20	5.83	255	1.51	661	99.9	0.94	4444	65.8 ± 5.0	13.83 ± 0.18	1.79	100
TU 46^	granite	0274412 4495581	-	20	2.34	157	0.85	570	67.6	1.06	5021	53.3 ± 4.9	13.28 ± 0.34	1.71	52
TU 47^	Eocene granite	0560460 4485269	25	20	2.46	199	1.44	1164	86.6	1.07	5059	33.4 ± 2.6	14.15 ± 0.15	1.04	49
TU 48^	Eocene granite	0545966 4494013	20	20	0.51	67	0.46	597	91.6	0.94	4458	19.3 ± 2.5	14.12 ± 0.16	1.31	68
TU 49^	Eocene granite	0549675 4495825	709	20	0.64	34	0.44	235	99.6	1.04	4924	27.5 ± 5.1	14.52 ± 0.19	1.16	38
TU 92^	Trakya Fm. ss. (Carb.)	0641940 4555239	31	14	0.27	72	1.95	517	99.9	1.05	4993	24.3 ± 3.1	13.59 ± 0.16	0.80	25
TU 94^	Trakya Fm. ss. (Carb.)	0662767 4556491	-	8	0.34	75	2.36	517	6.9	1.08	5122	25.6 ± 4.1	12.62 ± 0.30	1.46	23
TU 96^	andesite dyke (?K)	0678005 4523039	-	26	0.10	137	0.71	937	84.8	1.07	5085	25.4 ± 2.6	-	-	-
TU 100^	Çavuşbaşı granite (?K)	0681234 4552295	92	21	0.18	151	0.79	664	85.3	1.06	5030	39.9 ± 3.7	13.77 ± 0.23	1.20	27
TU 101	Bayırköy Formation (early J.)	0667147 4436914	-	10	0.46	72	1.31	204	43.2	1.07	5067	62.3 ± 8.7	-	-	-
TU 109*	Hodul Unit (Triassic)	0693970 4451364	-	19	5.66	336	2.63	1562	0.0	1.12	5291	39.4 ± 4.8	-	-	-
TU 110	Pamukova granite (Prec.)	0255732 4490386	348	12	1.19	307	3.74	964	0.0	1.07	5103	58.9 ± 12.5	11.42 ± 0.31	1.47	22
TU 111	Geyve gneiss (Prec.)	0274851 4502255	108	15	0.33	72	1.47	321	98.8	1.00	4750	37.2 ± 4.9	-	-	-
TU 112	Bolu Dagi granodiorite (Prec.)	0421837 4545342	607	22	0.43	140	1.26	413	62.2	1.06	5048	59.6 ± 6.1	11.83 ± 0.27	1.40	27
TU 113	Ulus Fm. ss. (Aptian-Albian)	0446093 4561816	208	9	0.28	38	0.94	129	57.5	1.03	4907	50.3 ± 9.4	-	-	-
TU 114	Carboniferous ss.	0402256 4589029	80	14	0.31	119	1.65	640	65.8	1.05	4975	32.3 ± 3.3	14.08 ± 0.29	1.21	17
TU 116	Karadon Fm. ss. (Carb.)	0444679 4619235	10	19	1.15	925	1.88	1521	13.7	1.06	5047	106.6 ± 5.7	13.04 ± 0.12	1.25	100
TU 117	Çakraz Fm. ss. (Triassic)	0456851 4625629	5	21	0.78	379	2.23	1088	14.7	1.05	5012	61.0 ± 4.5	11.76 ± 0.16	1.44	86
TU 120	?Jurassic granitoid	0554312 4619561	1237	6	0.72	87	2.89	349	93.5	1.05	5006	43.5 ± 5.3	12.49 ± 0.38	1.63	18
TU 121	Hercynian granitoid	0579170 4606995	1183	20	1.14	849	7.09	5277	83.4	1.04	4965	27.9 ± 1.2	13.52 ± 0.09	0.92	100
TU 123	Iğdir granite (Prec.)	0512004 4574545	1167	14	0.69	258	3.04	1137	60.7	1.02	4842	38.3 ± 2.8	13.59 ± 0.16	1.16	54
TU 125	Mudurnu Fm. ss. (middle J.)	0338444 4487906	447	3	1.15	11	0.39	37	82.5	1.04	4924	51.0 ± 17.6	-	-	-
TU 126	granite (Prec.)	0329991 4495829	571	18	0.34	203	1.77	1049	99.6	1.03	4883	33.0 ± 2.6	13.51 ± 0.20	1.30	42
TU 234	Elmadağ Fm (middle-late Tr.)	0508153 4423773	900	20	0.28	210	2.00	1517	71.8	1.49	7088	34.2 ± 2.6	13.74 ± 0.25	1.00	16
TU 236	Devecidağ Complex (Triassic)	0656958 4442603	840	5	0.39	66	2.57	429	25.5	1.50	7138	38.3 ± 5.1	-	-	-
IF 6	Hodul Unit (Triassic)	0687071 4459898	172	21	0.36	181	3.72	1863	1.9	1.16	5498	19.7 ± 2.1	13.13 ± 0.19	1.15	38
IF 8	Hodul Unit (Triassic)	0688559 4458907	253	8	0.27	58	1.91	404	96.2	1.15	5457	27.3 ± 3.9	-	-	-
IF 12	Orhanlar Greywacke (Tr.)	0553203 4414050	263	24	0.08	36	0.61	270	51.4	1.11	5293	24.6 ± 4.4	-	-	-
IF 14	Orhanlar Greywacke (Tr.)	0552629 4415471	231	14	0.36	79	3.54	787	5.5	1.14	5416	18.4 ± 3.0	12.56 ± 0.47	1.25	7
IF 16	Hodul Unit (Triassic)	0550687 4399167	293	10	0.40	61	3.15	485	57.7	1.13	5375	23.6 ± 3.2	-	-	-
IF 21	Çamlık Granodiorite	0515901 4384381	376	21	0.17	93	1.91	1030	96.0	1.12	5334	16.8 ± 1.9	12.81 ± 0.26	1.24	22
IF 24	Hodul Unit (Triassic)	0515487 4383163	241	17	0.51	254	5.67	2842	11.0	1.11	5252	16.3 ± 1.4	12.77 ± 0.18	1.18	42
IF 35	Orhanlar Greywacke (Tr.)	0670389 4437874	422	23	0.22	92	1.20	509	60.5	1.09	5170	32.6 ± 3.8	-	-	-
IF 38	Orhanlar Greywacke (Tr.)	0669326 4437757	561	13	0.85	193	2.79	632	6.1	1.08	5129	56.0 ± 6.1	11.16 ± 0.39	1.93	25

Notes. Central ages calculated using dosimeter glass CN5 and ζ-CN5=332.54±5.55. ρs: spontaneous track densities (x 10^6 cm $^{-2}$) measured in internal mineral surfaces; N_s: total number of spontaneous tracks; ρi and ρd: induced and dosimeter track densities (x 10^6 cm^{-2}) on external mica detectors (g=0.5); N_i and N_d: total numbers of tracks; $P(\chi^2)$: probability of obtaining χ^2-value for ν degrees of freedom (where ν=number of crystals-1); a probability >5% is indicative of an homogenous population. Predicted AFT data were calculated according to the Ketcham et al. (1999) annealing model and the Donelick et al. (1999) c-axis projection. Procedures for sample preparation and analysis are described in Zattin et al. (2000). *Published in Okay et

CHAPTER 4

This chapter consists of the manuscript titled “A precursor of the North Anatolian Fault in the Marmara Sea region” by Massimiliano Zattin, William Cavazza, Aral I. Okay, Ilaria Federici, Maria Giuditta Fellin, Antonio Pignalosa and Peter Reiners. The manuscript was submitted to the “Journal of Asia Earth Sciences” on May 20th, 2009, and accepted on March 11th 2010.

A precursor of the North Anatolian Fault in the Marmara Sea region

M. ZATTIN [a*], W. CAVAZZA [b], A.I. OKAY [c], I. FEDERICI [b], M.G. FELLIN [d], A. PIGNALOSA [b] & P. REINERS [e]

[a] *Dipartimento di Geoscienze, Università di Padova, Via Giotto 1, 35137 Padova, Italy*

[b] *Dipartimento di Scienze della Terra e Geologico-Ambientali, Università di Bologna, Piazza di Porta San Donato 1, 40126 Bologna, Italy*

[c] *Avrasya Yerbilimleri Enstitüsü ve Jeoloji Mühendisliği Bölümü, Maden Fakültesi, İstanbul Teknik Üniversitesi, Maslak, 34469 İstanbul , Turkey*

[d] *Institut für Isotopengeologie und Mineralische Rohstoffe, ETH, Clausiusstrasse 25, 8092 Zürich, Switzerland*

[e] *Department of Geosciences, University of Arizona, Gould-Simpson Building #77, Tucson, AZ 85721, USA*

** Corresponding Author (massimiliano.zattin@unipd.it; fax: ++39 049 8272070)*

Abstract

Apatite (U-Th)/He and fission-track analyses of both basement and sedimentary cover samples collected around the Marmara Sea point to the existence of a system of major E-W-trending structural discontinuities active at least from the Late Oligocene. In the Early Pliocene, inception of the present-day North Anatolian Fault (NAF) system in the Marmara region occurred by reactivation of these older tectonic structures. This is particularly evident across the Ganos fault in southern Thrace, as exhumation south of it occurred during the latest Oligocene and north of it during the mid-Miocene. In this area, large tectonic structures long interpreted as the results of Plio-Quaternary NAF-related transpressional deformation (i.e. the Ganos monocline, the Korudağ anticline, and the Gelibolu folds) were in fact produced during the Late Oligocene – Early Miocene. The overall lack of significant (U-Th)/He age differences across the NAF indicates that the Early

Pliocene inception of strike-slip motion in the Marmara region represents a relatively minor episode. At the scale of the entire Marmara region, the geographic pattern of exhumation ages shown in this study results instead from the complex superposition of older tectonic events including (i) the amalgamation of Sakarya and Anatolide-Tauride terranes, and (ii) Aegean-related extension.

Keywords

Thermochronology, exhumation, North Anatolian Fault, Marmara Sea.

The Marmara Sea consists essentially of depressions and ridges aligned along the E-W trend of the North Anatolian Fault (NAF). This fault system, about 1500 km long, is characterized by a right-lateral strike-slip motion and constitutes the northern boundary of the westward moving Anatolian block (e.g. Jackson and McKenzie, 1988; Barka, 1992). According to the common interpretation, the NAF nucleated in eastern Anatolia (Bitlis-Zagros suture zone) during the Late Miocene (ca. 11 Ma) following the collision of the Arabia and Anatolian plates, and propagated westward reaching the Marmara region during the Pliocene (e.g. Barka, 1992; Hubert-Ferrari et al., 2002; Şengör et al., 2005). In this region, the NAF widens into a complex fault zone stretching some 100 km in a N-S direction, from Ganos Mt. in southern Thrace (Okay et al., 2004) to Kazdağ in the southern Biga peninsula (Cavazza et al., 2008). Such configuration translates into a high degree of structural complexity, with coexisting deep basins, push-up structures, and block rotations (e.g. Seeber et al., 2004). The inception of the NAF activity has been inferred based on the study of the associated sedimentary basins, with earlier studies relying mainly on the scarce palaeontological data from terrestrial sedimentary records (see Şengör et al., 2005, for a review). The oldest basins are Middle to Late Miocene in age, whereas the youngest are hardly older than the Pleistocene. Based on apatite fission-track analysis of limited number of samples, Zattin et al. (2005) suggested that the Ganos segment of the NAF follows a preexisting structural discontinuity in existence at

least by the latest Oligocene. Late Oligocene age displacement along the NAF is also supported by Uysal et al. (2006) who studied a ca. 500 km long segment of the NAF east of the Marmara Sea by radiometric dating of fault gouges. They found that an early event of significant strike-slip was initiated at about 57 Ma, but further intensified at ~26 Ma and later than ~8 Ma. Kaymakci et al. (2007), on the basis of palaeomagnetic data, proposed that the Ganos fault and other ENE-trending faults experienced dextral strike-slip activity before the Late Pliocene development of the NAF. An Oligocene major strike-slip shear zone in western Anatolia, with an estimated right-lateral offset of 100±20 km, was described also by Okay et al. (2008) in the Uludağ area, located close to the city of Bursa, about 30 km south of the Marmara Sea. All these papers support the idea that pre-existing mechanical weakness zones such as faults and shear zones greatly influence the locus of subsequent tectonic activity (e.g. Holdsworth et al., 1997).

In this paper, we build on the results by Zattin et al. (2005) to give a more complete picture of the tectonic evolution of the western NAF by using (U-Th)/He and fission-track dating on apatite. Samples were therefore collected all around the Marmara Sea and across the main strands of the fault. Our data confirm that the Marmara segments of the active NAF, regarded as post-Miocene structures, have had instead a complex evolution, as shown by the presence of pre-Late Miocene structural discontinuities along which significant vertical displacements occurred. The exact age of these earlier discontinuities is difficult to determine but should be older than the extension that affected the Aegean region since the Late Oligocene (e.g. Seyitoğlu et al., 1992; Jolivet and Faccenna, 2000). Thermochronological data by Zattin et al. (2005) demonstrate that in the Late Oligocene vertical displacements occurred along a precursor of the Ganos fault. The additional dataset presented in this paper suggests that the location and kinematics of the western NAF are controlled by position and geometry of the basement block margins inherited from Mesozoic–Cenozoic closure of oceanic basins belonging to the Tethyan realm and the ensuing collision between the bordering microcontinents.

Geologic setting

The Neogene tectonics of the Marmara region has been controlled by the interaction of the extensional regime driven by slab retreat along the Aegean subduction zone (e.g., Jolivet, 2001) and the westward escape of the Anatolian microplate (moving with respect to the Eurasian plate at a velocity of ~21 mm/yr; e.g., Reilinger et al., 2006) guided by the NAF. In central Anatolia, over 90% of this movement is concentrated on this fault, which forms a well-defined narrow plate boundary. In the Aegean region, the rigid westward translation of the Anatolian microplate combined with back-arc spreading behind the Aegean Trench gave way to distributed north-south extension along E-W–trending normal faults. This extension resulted in the formation of E-W trending grabens, which are the most prominent neotectonic feature of western Anatolia (Bozkurt, 2001). The same structural trend is observed in the Marmara Sea region, where the NAF developed as a complex fault system. East of the Marmara Sea, the NAF splits into two branches which, divided into sub-branches, form a zone of distributed deformation more than 120 km wide (Fig. 1; Şengör et al., 1985). However, GPS studies show that over 90% of the present-day strike-slip deformation occurs along the main northern branch of NAF passing through the Marmara Sea and continuing westward into Thrace as the Ganos segment (McClusky, 2000; Meade et al., 2002). The Marmara Sea comprises a broad shelf to the south and three deep step-over sub-basins to the north (Barka, 1997; Okay et al., 2000; Le Pichon et al., 2001; Imren et al., 2001; Armijo et al., 2002). Transpressional uplift and transtensional subsidence are associated with the Ganos fault in the western Marmara region (Okay et al., 2004; Seeber et al., 2004).

The present-day tectonic framework of Anatolia is the result of a complex evolution that initiated in the Late Cretaceous with the convergence between the African and Eurasian plates. This resulted in the progressive closure of the Neotethyan Ocean and the amalgamation of the surrounding continental fragments. The consequent subduction–accretion complexes and emplacement of ophiolites produced the present-day crustal configuration.

In western Anatolia an extensional phase occurred during latest Oligocene-Miocene time, as testified by exhumation of the Kazdağ massif in the southern Biga Peninsula (Okay and Satir, 2000; Cavazza et al., 2008) and in the Simav complex in the northern Menderes Massif (Isik et al., 2004; Thomson and Ring, 2006). In both cases, Neogene tectonic evolution involved rapid exhumation through low-angle detachment faults followed by relative quiescence, at least in terms of vertical tectonics. The history of this extensional phase is consistent with that of the Aegean post-orogenic back-arc extension, widely recognised in the central Aegean region (e.g. Jolivet et al., 2008).

The terranes of the Marmara region

Geologically, the Marmara region resulted from the amalgamation of relatively small continental fragments: the Sakarya Zone to the south, the İstanbul Zone to the northeast and the Strandja-Rhodopian terrane cropping out all along the northern, western and southern margins of the Thrace Basin (Fig. 1; Görür and Okay 1996; Okay and Tüysüz 1999). According to Şengör and Yılmaz (1981), the tectonic boundary between the Sakarya and İstanbul zones –the so-called Intra-Pontide suture- formed in the early Eocene after an orthogonal opening between the İstanbul and Sakarya terranes during the Liassic. Okay and Tüysüz (1999) advocated a Senonian closure of the Intra-Pontide ocean. Beccaletto et al. (2005) pointed out that the Intra-Pontide suture cannot be traced in the western Marmara region. Following is a concise description of the peri-Marmara terranes.

The Sakarya Zone is a terrane characterised by the presence of a Triassic subduction-accretion complex (Karakaya Complex), which forms a strongly deformed and partly metamorphosed basement. The final phase of deformation occurred during the latest Triassic and was followed by sedimentation of Jurassic continental to shallow-marine deposits, Cretaceous carbonates, and finally by Senonian andesites (Altıner et al., 1991; Tüysüz, 1993).

The İstanbul Zone is made of Precambrian crystalline basement overlain by a continuous transgressive sedimentary succession ranging from Ordovician to Carboniferous which was

deformed during the Hercynian orogeny (Dean et al., 1997; Görür et al., 1997). The deformed Paleozoic succession is unconformably overlain by a Mesozoic succession. Senonian andesites and small acidic intrusions are widespread and are related to the northward subduction of the İzmir-Ankara ocean (Okay and Tüysüz, 1999).

The Strandja zone constitutes the easternmost part of the crystalline basement that includes the Rhodope Massif and, in the Marmara region, is made of metamorphic rocks intruded by Permian granites which are unconformably overlain by a Triassic succession (Aydın, 1974; Okay and Tüysüz, 1999). Basement and Triassic succession were regionally metamorphosed during the mid-Jurassic and then overlain by Cenomanian conglomerates and shallow marine limestones. As in the case of the İstanbul Zone, these are covered by Senonian andesites and intruded by associated granodiorites (Moore et al., 1980).

The crystalline rocks of Strandja-Rhodope represent the basement of the Thrace basin (Görür and Okay 1996). The base of the Thrace basin fill is Early-Middle Eocene (Sakinç et al., 1999; Siyako and Huvaz, 2007) and the following deposits (until the Oligocene) form a shallowing-upward, dominantly clastic succession up to 9000-m-thick. The depocenters of the basin are characterised by locally tuffaceous siliciclastic turbidites, whereas continental to shallow-marine clastics and carbonates with subordinate volcanoclastics were laid along the margins and on elongate bathymetric highs. Dramatic lateral facies changes and the corresponding irregular subsidence patterns during the Middle Eocene (Siyako and Huvaz, 2007) have been interpreted as the result of strike-slip tectonism (e.g. Turgut et al., 1991). During the Early Oligocene, shales and sandy shales were deposited in a shelf to slope environment. Later sedimentation was characterised by coal-bearing clastics and carbonates with some tuffaceous material deposited in marginal marine to terrestrial environments (Turgut et al., 1991). During the latest Miocene–Pliocene, most of the area was characterised by fluvial deposition which lasted until the Late Pleistocene.

Methods

Fission-track dating is a useful tool to unravel the cooling histories experienced by rocks in the upper crustal levels and to give a measure of their motion toward the surface (for a review of the method, see Donelick et al., 2005). Fission tracks in apatites all have the same initial length of about 16 µm (the extact length depending on composition; e.g. Ketcham *et al*., 1999) but anneal at rates proportional to temperatures, starting from about 60°C. Over geological time scales, partial annealing of fission tracks occurs at temperatures between about 60 and 125°C (the Partial Annealing Zone: PAZ; Gleadow and Fitzgerald, 1987). Because tracks shorten in relation to the degree and duration of heating, the measurement of fission track lengths gives information about the thermal evolution in the PAZ temperature range. A quantitative evaluation of the thermal history can be carried out through modelling procedures, which find a range of cooling paths compatible with the apatite fission-track (AFT) data (Ketcham, 2005). In this work, inverse modelling of track length data was performed using the HeFTy program (Ehlers et al., 2005), which generates the possible T-t paths by a Monte Carlo algorithm. Predicted AFT data were calculated according to the Ketcham et al. (1999) annealing model and the Donelick et al. (1999) c-axis projection.

The (U-Th)/He method is based on the accumulation of ^{4}He produced by the decay of ^{238}U, ^{235}U, ^{232}Th and ^{147}Sm. Radiogenic ^{4}He diffuses out of the mineral at a rate determined by the temperature and the He diffusivity of the mineral. The temperature range of the apatite He partial retention zone (PRZ) is estimated to be ~40-80°C (Wolf et al., 1998). Measurements are typically made using a two-stage analytical procedure involving degassing of the crystal by heating and gas-source mass spectrometry to measure ^{4}He, followed by inductively-coupled plasma mass spectrometry on the same crystal to measure U and Th (and, in some cases, Sm). Grain ages typically have a relative standard error of approximately 3% to 5%, as determined by replicate measurements.

Procedures for sample preparation and analysis are outlined in Table 1 and described in more detail in Zattin et al. (2000) and Reiners (2005).

Analytical results

Western Marmara Sea

The westernmost samples come from Gökçeada (Fig. 2a). TU55 was collected from andesites dated at 30.4±0.7 Ma (K/Ar; Ercan et al., 1995) and cutting Eocene-Oligocene flysch. The obtained AFT age (27.2±1.8 Ma) and the very long track lengths (mean length = 15.11 μm; Table 1) indicate fast cooling immediately after the volcanic event. A sample from a sandstone bed of the Upper Eocene-Lower Oligocene Ceylan Fm from the Gökçeada (TU54; see Gelibolu column in Fig. 3) yielded an AFT age of 48.5±5.7 Ma, i.e. older than the depositional age considering 1 sigma error (Fig. 4). Given the AFT age of the andesites, we can infer that the Upper Eocene-Oligocene flysch underwent no major post-depositional burial and, therefore, the AFT age of sample TU54 is related to the cooling of the source rock and does not give any information about the post-depositional history. However, the time of exhumation of the rocks exposed on the island is constrained by AHe dating (11.9±0.1 Ma, sample TU55), which indicates that (i) the andesites were emplaced at a depth above the AHe closure temperature and (ii) final cooling took place in the Serravallian.

Moving to the Gelibolu peninsula, we dated a sample (TU52) collected from a tuffite bed within the Ceylan Fm dated at 30.05±0.49 Ma (Ar-Ar on biotite; Di Vincenzo, pers. comm.). Here AFT data agree with Ar-Ar data (27.2±2.6 Ma), thus indicating minor post-depositional burial. Moreover, Ar-Ar and AFT data indicate that the depositional age of the Ceylan Fm reaches up the end of the Early Oligocene. Exhumation to very shallow levels occurred only in the Late Miocene, as testified by an AHe age of 8.4±0.1 Ma from the same sample. The AHe age indicates some reheating that should have caused some annealing of fission tracks. Actually, the radial plot (Fig. 4) shows some grains older than depositional age that could be related to inherited apatites (i.e. not crystallized during the Oligocene magmatic event) and the younger individual grain ages could therefore be referred to some post-depositional annealing that affected the volcanic apatites. A Late

Oligocene AFT exhumation age (28.3±3.2 Ma) is recorded by sample TU51, collected from the Ceylan Formation (Fig. 3) exposed just south of the NAF, close to the coast of the Saros Gulf. However, here the chi-square test shows a broad dispersion of single grain ages, part of which are older than the stratigraphic age (Fig. 4). Hence, post-depositional burial was not sufficient to reset completely the fission tracks but enough to reset the AHe system which gave a very young age of 2.5±0.1 Ma. Sample TU50, collected from the Keşan Formation exposed just south of the easternmost Ganos fault, gave an AFT age of 22.3±2.5 Ma, slightly younger than AFT ages from previously described samples. Its AHe age is again quite young (4.7±0.1 Ma).

North of sample TU51 and north of the NAF, in the core of the Korudağ anticline sample TU64 yielded an AFT age of 24.9±2.3 Ma, younger than its depositional age (Eocene, Keşan Formation; Fig. 4). In this case, burial temperatures were comprised into the PAZ, as constrained by inverse modelling which was performed by using both AFT and AHe data (Fig. 5). The cooling path is quite complex, with a rapid cooling event at 14-10 Ma followed by very low cooling rates. We performed also some AHe dating on samples from the Ganos Mt. area, previously analysed with the fission-track method by Zattin et al. (2005). The oldest AHe (9.4±0.1 Ma) was detected on sample TU2 collected on the top of Ganos Mountain (Table 2). This age fits well with the cooling path shown by Zattin et al. (2005; Fig. 5). Moving towards the NAF, a slightly younger AHe age (8.8±0.2 Ma) was yielded by a sample from the Gaziköy Fm (Middle Eocene; Figs.2 and 3). The youngest age (5.7±0.1 Ma) was detected on the sample closest to the NAF and at sea level.

On the southern side of the Marmara Sea, a sample (TU56) from the Eocene Karabiga granitoids yielded an AFT age of 24.8±3.4 Ma, in the same range of those obtained along the northern coast.

Two samples were taken on Marmara Island from Eocene granitoids, at sea-level (TU48) and on top of the highest peak (709 m; TU49). As expected, TU49 yielded the oldest AFT age (27.5±5.1 Ma) although the age difference with the sample taken at the sea level (19.3±2.5 Ma) is quite high despite the limited elevation difference. Track lengths demonstrate that both samples

cooled rapidly through the PAZ. The AHe age of sample TU48 (21.2±0.5 Ma) is older than the corresponding AFT age, thus pointing to the some problems in the analytical data such as the possible presence of apatite crystals with anomalous annealing kinetics or some inclusions in the apatite dated with the AHe method.

Another sample was collected south of Marmara Island, along the western coast of the Kapıdağı peninsula (TU47). Its AFT age (33.4±2.6 Ma) is significantly older than those obtained from Marmara Island and from the Eocene flysch of the Ganos area. Again, track lengths indicate a fast cooling through the PAZ, as confirmed by the AHe age of 27.7±0.4 Ma.

Eastern Marmara

Samples were collected from different units across a large area (Fig. 2b). Three samples (TU38, TU39, TU46) located at the same latitude show very similar AFT ages (51-53 Ma). TU39 is from a tuffitic bed interbedded with the Eocene flysch. This sample has very long fission tracks (mean length: 15.46 μm). Given that its AFT age is very close to the depositional age (Fig. 4) we can exclude that we dated the time of exhumation. It is likely that the apatites were derived from syndepositional volcanism, and that the flysch was never buried at the bottom of the PAZ. However, the AHe age (23.0±1.1 Ma) suggests some possible reheating, thus pointing to an interpretation similar to one we proposed for sample TU52. Samples TU38 and TU46 are both from Eocene granites. Their AFT age and track length distribution are very similar and document a moderate cooling after their intrusion. Inverse modelling (Fig. 5) suggests Early Eocene intrusion and very low cooling rates (about 1.3°C/m.y.) in the last 40 m.y. Considering a "normal" geothermal gradient of 30°C/km, this translates into an exhumation rate of 0.04 km/m.y.

Sample TU41 was collected NW of Izmit from the Eocene flysch. This sample yielded an AFT age (65.8±5.0 Ma) older than its depositional age. We can then conclude that (i) we dated cooling and exhumation in the sediment source area, and (ii) the flysch has never been buried at the bottom of the PAZ after deposition. (Although some reset is possible, given that some grains are

younger than the depositional age; Fig. 4.) Four more samples were dated in the İstanbul zone. Two of them (TU92, TU94) were collected from Carboniferous sandstones and cooled in a short time range (24-26 Ma); the same age was detected in a sample from Cretaceous andesites (TU96). Measured track lengths are not sufficient to constrain reliably the thermal history. The oldest AFT age from the İstanbul zone (39.9±3.7 Ma) was obtained from a sample (TU100) collected from a granite emplaced during the Late Cretaceous.

The youngest AFT age (14.9±5.0 Ma) from eastern Marmara region was obtained from a sample collected from a granitic intrusion of Eocene age in the Armutlu peninsula (TU36), although only twelve grains could be dated (no track lengths). Here some problems arise from the comparison with the AHe age (38.9±1.1 Ma), much older than the AFT age. It is likely that AHe age is affected by the presence of small inclusions of zircon.

Discussion

The data presented here, integrated by those by Zattin et al. (2005) and Okay et al. (2008), provide the first regional picture of the thermal evolution in the last 60 m.y. of both crystalline units and sedimentary successions cropping out around the Marmara Sea. Overall, samples collected west of Marmara Island underwent a larger degree of subsidence and a much younger exhumation. Moreover, we document the presence of tectonic denudation related to fault structures which – although following the trace of the present-day NAF- were active well before its inception. Age patterns could be affected by possible deformations of isotherms due to advection and/or topography effects but these processes were probably not really effective due to the low exhumation rates and the very smooth topography, with most of the samples collected at very low elevation (the only relevant relief is Ganos mountain, as discussed here below).

The oldest ages have been recorded in the eastern Marmara region. Here, AFT analyses date to the Early Eocene the exhumation of the crystalline units exposed along the Armutlu peninsula and are in the same age range of the K-Ar dating of illite from the fault rocks along the NAF (Uysal

et al., 2006). These data could be related to the closure of the İzmir-Ankara oceanic domain and the ensuing collision between the Sakarya terrane to the north and the Anatolide-Tauride Block to the south (Okay and Tüysüz, 1999; Okay et al., 2001). AFT ages, including the data from the sample located just north of Izmit (TU41), may indicate the timing of the final uplift related to the end of collision. This exhumation event was followed by very little if not null subsidence and no other important uplift episodes, as testified by mean track lengths, which suggest quite a fast cooling at time of exhumation, and by the AHe ages, which document that the sampled rocks were already near the surface at the end of the Oligocene.

Low-temperature thermochronometers cannot provide evidence of Eocene tectonics in western Marmara as widespread Oligo-Miocene exhumation removed any older thermal signals. At that time, the region around the Ganos fault was exhuming, confirming the conclusions by Zattin et al. (2005). AFT age differences across the Ganos fault support the presence of a nearly E-W oriented structure that was active during the Oligocene (although horizontal displacement due to Plio-Pleistocene strike-slip must be considered when comparing ages across the fault). Rocks north and south of the fault followed markedly different T-t paths (table 1, Fig. 2 and Fig. 3 in Zattin et al., 2005). Exhumation of the southern block across the fission-track closure isotherm took place in the latest Oligocene – earliest Miocene, while the northern block was exhumed in the mid-Miocene (16.4-11.7 Ma). Such different AFT ages and thermochronologic evolutions for samples of similar depositional age and lithology suggest that a precursor of the Ganos Fault was active by late Oligocene time. This conclusion is supported also by the local stratigraphy, as the two clusters of AFT ages ages north and south of the fault correspond to hiatuses in the respective sedimentary successions (Fig. 3). For example, during the late Oligocene deposition came to an end in the southernmost Thrace basin, and was followed by uplift and erosion. In contrast, the Eocene succession north of the fault was still at several kilometres depth by the late Oligocene and was exhumed above the fission-track closure isotherm (110° C) only during the Middle Miocene, when continental to marginal-marine sandstones were being deposited south of the fault (Fig. 3).

During late Oligocene time the whole Kapıdağı-Marmara Island region was being exhumed and some exhumation occurred also in the Thrace basin (Korudağ high). This structure can be linked to the uplifting shoulders related to the formation of the graben in the Gulf of Saros and to the contemporaneous development of the Kuleli-Babaeski high in the northern Thrace basin (Çağatay et al., 1998; Coskun, 2000). Furthermore, our data along the Gelibolu peninsula match well the subsidence rate curves of Coskun (2000) who shows a maximum subsidence in the Oligocene and the inversion of the basin since 26 Ma. Siyako and Huvaz (2007) postdate the inversion of the basin at 20 Ma but their reconstruction was made in a depocentral area about 40 kilometers northeast of the Ganos region.

AFT ages document that most exhumation occurred in a period during which the Aegean area was dominated by extension. During this stage, the Aegean Sea began to form and exhumation led to crustal thinning and formation of sedimentary basins in the hanging walls of detachments. Detachments are widespread in the Cyclades as well as in the northern Rhodope and western Turkey (e.g. Gautier and Brun, 1994; Dinter, 1998). This extensional phase caused erosional unroofing which is well recorded by our thermochronological data although, in the Marmara region, there is no evidence of tectonic exhumation along a discrete tectonic structure, as detected, for example, in the Kazdağ core complex to the south (Okay and Satır, 2000; Cavazza et al., 2008). However, the age differences across the Ganos fault document that some tectonic lineament(s) nearly E-W oriented were active.

Integration of our results with preexisting data indicates that tectonic structures with the same strike of the NAF were active in the Marmara region well before its inception (from 13 to 4 Ma according to different interpretations; see Şengör et al., 2005 for a review). For example, significant Oligocene E-W-trending strike-slip shear zones in the middle crust have been documented in the granitoids of the Kapıdağı peninsula (Aksoy, 1998) and in the late Oligocene gneisses and granitoids of Uludag (Okay et al., 2008). However, movement along the precursor of the WSW-ENE-trending Ganos Fault had a significant dip-slip component (Zattin et al., 2005),

given the marked AFT age difference north and south of the fault. The final collision of the Arabian and Eurasian plates in the mid-Miocene (Dewey et al., 1986; Robertson et al., 2007; Okay et al., in press) and the ensuing change of stress regime resulted in a switch of these structures (both compressional and extensional) to NAF-related faults. This relatively simplistic scenario is much complicated by extension in the Aegean domain.

While Eocene collision and Oligocene-Miocene extension generated some erosion that is well recorded by low-temperature thermochronology, the new strike-slip regime produced no major vertical displacements, as shown by the relationships between AFT ages and sample elevations along the Ganos fault (Fig. 6; Zattin et al., 2005). The increase of AHe ages with elevation confirm this evidence as we could calculate a vertical displacement in the order of 2 kilometers at a mean cooling rate of about 10°C/m.y. in the last 5 m.y. (i.e. an exhumation rate of about 0.3 km/m.y., considering a normal geothermal gradient of 30°C/km). The absence of significant differences in AHe ages across the Ganos fault - at least in its easternmost sector - implies that Pliocene motion along the NAF was predominantly strike-slip. However, some vertical offset and corresponding tectonic exhumation, occurred locally due to the geometry of the fault, probably in the last 3 m.y. For example, along the westernmost sector of the Ganos fault, we found the youngest AHe age (2.5 Ma), documenting a cooling rate of about 25°C/m.y. (corresponding to an exhumation rate of about 0.8 km/m.y. considering a geothermal gradient of 30°C/km). Oblique slip on a non-vertical master fault, which may accommodate transtension and transpression, was described in detail by Seeber et al. (2004) for a curved segment of the Ganos fault. However, it is possible that youngest ages could be related to some late cooling due to hydrothermal activity. Although the region north of Marmara Sea is characterized by normal present-day heat flow values up to 55 mW/m^2 (Pfister et al., 1998), there is the evidence of hydrothermal mineralizations during the Pleistocene on rocks close to faults related to the NAF (Ece et al., 2008).

The last stages of exhumation testified by AHe data are confirmed by stratigraphic hiatuses that document periods of no sedimentation and/or erosion. Çağatay et al. (2006) refer the presence

of an erosional unconformity dated at the base of the late Pliocene in the area of the Gulf of Saros. The same age is given by Yaltırak et al. (1998) for folding and denudation of the westernmost Gelibolu peninsula. Along the Ganos fault, no Pliocene deposits are preserved, therefore confirming the enhanced erosion detected by AHe data. These age data disagree with the notion that the folds in the Gelibolu peninsula occurred in a short period of time ($<10^6$ years) and, above all, that they were well eroded during the Messinian salinity crisis (Armijo et al., 1999). In fact, AHe ages along the Ganos fault are younger than the base of the Alçitepe Formation (top of the Miocene), where Armijo et al. (1999) placed the main erosional unconformity.

AHe indicate that the activity of the NAF (or a paleo-NAF) in the Armutlu peninsula produced only minor vertical displacements (i.e. total offset < 1.5 km). Nonetheless exhumation was sufficient to generate an 800-m-thick fining-upward clastic sequence of Sarmatian to Lower Pliocene age (Sengor et al., 2005) in Yalova Basin. The Manyas and Ulubat basins contain fluvial-to-lacustrine sediments whose deposition started in the late Miocene (Pontian) and continued into Early Pliocene (Yaltırak and Alpar, 2002), reaching a total thickness of about 700 m (Yalçın, 1997; Emre et al., 1998). The Mudanya basin is presently bordered on the south by the Uludağ Massif, whose exhumation was recently described by Okay et al. (2008). Here we report an AHe of 10 Ma from a sample collected at the very border of the Uludağ Massif, indicating that, in this area, a fault with a significant dip-slip component was present before the inception of the NAF.

Conclusions

Integration of our thermochronologic data (AFT and AHe) with preexisting structural information (Aksoy, 1998; Okay et al., 2008) indicates that during the Oligocene E-W-trending tectonic structures were active throughout the Marmara region. Both strike-slip and dip-slip movements occurred across this wide deformation zone. Locally, these structures had significant vertical displacements and generated topographic lows and highs capable of exhuming the partial-annealing zone of apatite. For example, our data show that the present-day Ganos segment of the

NAF follows the trace of a pre-existing structural discontinuity active by late Oligocene time, thus confirming the hypothesis advanced by Zattin et al. (2005). The western Marmara region south of the NAF is characterised by Late Oligocene AFT ages. We suggest that the extension that affected the region, caused by the southward migration (*rollback*) of the Aegean subduction zone, gave rise to tectonic denudation at a regional scale.

Significant vertical displacements of Neogene age are absent across most of eastern Marmara. Here thermochronological data around the Armutlu peninsula document a rapid exhumation in the Early Eocene and indicate that, at that time, all the different units were already at very shallow crustal levels. This exhumation event is probably related to the collision between the Sakarya terrane to the north and the Anatolide-Tauride Block to the south. This erosion event is recorded both in İstanbul and Sakarya terranes, thus indicating that their amalgamation occurred in pre-Eocene times (Cavazza et al., unpublished results). The NAF system in the Marmara region seems to have undergone a two-stage development dominated by (i) dip-slip movements (both compressional and extensional) in the Oligo-Miocene and (ii) dextral strike-slip with negligible vertical movements during the Plio-Quaternary. The second stage is shown by (i) the absence of significant AHe age differences across the main branches of the fault system, and (ii) the virtual absence of ages younger than Pliocene.

Acknowledgments

This research was sponsored by MIUR (Italian Dept. of Public Education, University and Research) and by TUBA (The Turkish Academy of Sciences). Comments by Dr. Halim Mutlu and an anonymous reviewer are gratefully acknowledged.

References

Aksoy, R., 1998. Strain Analysis of the Kapıdagı Peninsula Shear Zone in the Ocaklar Granitoid,

NW Turkey. Turkish Journal of Earth Sciences 7, 79-85.

Altıner, D., Koçyiğit, A., Farinacci, A., Nicosia, U., Conti, M.A., 1991. Jurassic, Lower Cretaceous stratigraphy and paleogeographic evolution of the southern part of the northwestern Anatolia. Geologica Romana 18, 13–80.

Armijo, R., Meyer, B., Hubert, A., Barka, A., 1999. Westward propagation of the North Anatolian fault into the northern Aegean: timing and kinematics. Geology 27, 267-270.

Armijo, R., Meyer, B., Navarro, S., King, G., 2002. Slip partitioning in the Sea of Marmara pull-apart: a clue to propagation processes of the North Anatolian Fault. Terra Nova 14, 80–86.

Aydın, Y., 1974. Etude pétrographique et géochimique de la parte centrale du Massif d'Istranca (Turquie). PhD Thesis, Université de Nancy, p. 131.

Barka, A.A., 1992. The North Anatolian Fault zone. Annales Tectonicae 6, 164–195.

Barka, A.A., 1997. Neotectonics of the Marmara region in active tectonics of Northwest Anatolia. In: Schindler, C., Pfister, M. (Eds), The Marmara Poly-project. Hochschulverlag ETH, Zurich, 55–87.

Beccaletto, L., Bartolini, A.C., Martini, R., Hochuli, P.A., Kozur, H., 2005. Biostratigraphic data from the Çetmi melange, northwest Turkey: palaeogeographic and tectonic implications. Palaeogeography, Paleoclimatology, Palaeoecology 221, 215–244.

Bozkurt, E., 2001. Neotectonics of Turkey – a synthesis. Geodinamica Acta 14, 3-30.

Çağatay, M.N., Görür, N., Alpar, B., Saatçılar, R., Akkök, R., Sakınç, M., Yüce, H., Yaltırak, C., Kuşcu, I. 1998. Geological evolution of the Gulf of Saros, NE Aegean Sea. Geo-Marine Letters, 18, 1-9.

Cavazza, W., Okay, A.I., Zattin, M., 2008. Rapid early-middle Miocene exhumation of the Kazdağ Massif. International Journal of Earth Sciences, 98, 1935-1947.

Coskun B., 2000. North Anatolian Fault-Saros Gulf relationships and their relevance to hydrocarbon exploration, northern Aegean Sea, Turkey. Marine and Petroleum Geology 17, 751-772.

Dean, W.T., Martin, F., Monod, O., Demir, O., Rickards, R.B., Bultynck, P., Bozdogan, N., 1997. Lower Paleozoic stratigraphy, Karadere–Zirze area, Central Pontides. In: Göncüoğlu, M.C., Derman, A.S. (Eds.), Early Palaeozoic Evolution in NW Gondwana. Turkish Association of Petroleum Geologists, Special Publications 3, 32–38.

Dewey, J.F., Hempton, M.R., Kidd, W.S.F., Şaroğlu, F., Şengör, A.M.C., 1986. Shortening of continental lithosphere: The neotectonics of Eastern Anatolia—a young collision zone. In: Coward, M.P., Ries, A.C. (Eds.) Collision Tectonics. Geological Society, London, Special Publications 19, 3 –36.

Dinter, D.A., 1998. Late Cenozoic extension of Alpine collisional orogen, northeastern Greece: origin of the north Aegean basin. Geological Society of America Bullettin 110, 1208-1230.

Donelick, R.A., Ketcham, R.A., Carlson, W.D., 1999. Variability of apatite fission-track annealing kinetics II: crystallographic orientation effects. American Mineralogist 84, 1224-1234.

Donelick, R.A., O'Sullivan, P.B., Ketcham, R.A., 2005. Apatite fission-track analysis. Review Mineralogy and Geochemistry 58, 49-94.

Ece, Ö.I., Schroeder, P.A., Smilley, M.J., Wampler, J.M., 2008. Acid-sulphate hydrothermal alteration of andesitic tuffs and genesis of halloysite and alunite deposits in the Biga Peninsula, Turkey. Clay Minerals, 43, 281-315.

Ehlers, T.A., Chaudhri, T., Kumar, S., Fuller, C.W., Willett, S.D., Ketcham, R.A., Brandon, M.T., Belton, D.X., Kohn, B.P., Gleadow, A.J.W., Dunai, T.J., Fu, F.Q., 2005. Computational tools for low-temperature thermochronometer interpretation. Review Mineralogy and Geochemistry 58, 589-622.

Emre, O., Erkal, T., Tchapalyga, A., Kazancı, N., Kecer, M., Ünay, E., 1998. Neogene–Quaternary evolution of the eastern Marmara region, northwest Turkey. Bulletin of the Mineral Research and Exploration Institute of Turkey 120, 119– 145.

Ercan, T., Satır, M., Steinitz, G., Dora, A., Sarifakioğlu, E., Adis, C., Walter, H.J., Yildirim, T., 1995. Biga Yarımadası ile Gokceada, Bozcaada ve Tavflan adalarındaki (KB Anadolu) Tersiyer

volkanizmasının ozellikleri. Mineral Research and Exploration Institute of Turkey (MTA) Bulletin 117, 55–86.

Farley, K.A., 2000. Helium diffusion from apatite: General behavior as illustrated by Durango fluorapatite. Journal of Geophysical Research 105, 2903-2914.

Gautier, P., Brun, J.P., 1994. Ductile crust exhumation and extensional detachments in the central Aegean (Cyclades and Evvia islands). Geodinamica Acta 7, 57-85.

Gleadow, A.J.W., Fitzgerald, P.G., 1987. Uplift history and structure of the Transantarctic Mountains: new evidence from fission track dating of basement apatites in the Dry Valleys area, southern Victoria Land. Earth Planetary Science Letters 82, 1–14.

Görür, N., Okay, A., 1996. Origin of the Thrace Basin, NW Turkey. Geologische Rundschau 85, 662–668.

Görür, N., Çağatay, M.N., Sakınç, M., Sümengen, M., Şentürk, K., Yaltirak, C., Tchapalyga, A., 1997. Origin of the Sea of Marmara as deduced from Neogene to Quaternary paleogeographic evolution of its frame. International Geology Review 39, 342–352.

Gradstein, F.M., Odd, J.G., Smith, A.G., 2004. A geologic time scale 2004. Cambridge, UK, Cambridge University Press, pp 589.

Holdsworth, R.E., Butler, C.A., Roberts, A. M., 1997. The recognition of reactivation during continental deformation. Journal of Geological Society of London 154, 73-78.

Hubert-Ferrari, A., Armijo, R., King, G.C.P., Meyer, B., Barka, A., 2002. Morphology, displacement, and slip rates along the North Anatolian Fault, Turkey. Journal Geophysical Research 107, 2235.

İmren, C., Le Pichon, X., Rangin, C., Demirbğ, E., Ecevitoğlu, B., Görür, N., 2001. The North Anatolian Fault within the Sea of Marmara: a new interpretation based on multi-channel seismic and multi-beam bathymetry data. Earth Planetary Science Letters 186, 143–158.

Işık, V., Tekeli, O., Seyitoğlu, G., 2004. The $^{40}Ar/^{39}Ar$ age of extensional ductile deformation and granitoid intrusion in the northern Menderes core complex: implications for the initiation of extensional tectonics in western Turkey. Journal Asian Earth Sciences 23, 555-566.

Jackson, J., McKenzie, D.P., 1988. The relationship between plate motions and seismic moment tensors, and the rates of active deformation in the Mediterranean and Middle East. Geophysical Journal 93, 45–73.

Jolivet, L., 2001. A comparison of geodetic and finite strain pattern in the Aegean, geodynamic implications. Earth Planetary Science Letters 187, 95–104.

Jolivet, L., Faccenna, C., 2000. Mediterranean extension and the Africa-Eurasia collision. Tectonics 19, 1095–1106.

Jolivet., L., Augier, R., Faccenna, C., Negro, F., Rimmele, G., Agard, P., Robin, C., Rossetti, F., Crespo-Blanc, A., 2008. Subduction, convergence and the mode of backarc extension in the Mediterranean region. Bulletin de la Societe Geologique de France, 179, 525-550.

Kaymakci, N., Aldanmaz, E., Langereis, C., Spell, T.L., Gurer, O.F., Zanetti, K.A., 2007. Late Miocene transcurrent tectonics in NW Turkey: evidence from palaeomagnetism and $^{40}Ar–^{39}Ar$ dating of alkaline volcanic rocks. Geological Magazine 144, 379–392.

Ketcham, R.A., 2005. Forward and inverse modeling of low-temperature thermochronometry data. Reviews in Mineralogy and Geochemistry 58, 275-314.

Ketcham, R.A., Donelick, R.A., Carlson, W.D., 1999. Variability of apatite fission-track annealing kinetics III: extrapolation to geological time scales. American Mineralogist 84, 1235-1255.

Le Pichon, X., Şengör, A.M.C., Demirbağ, E., Rangin, C., İmren, C., Armijo, R., Görür, N., Çağatay, M.N., Mercier de Lepinay, B., Meyer, B., Saatcılar, R., Tok, B., 2001. The active Main Marmara Fault. Earth and Planetary Science Letters 192, 595– 616.

McClusky, S., 2000. Global Positioning System constraints on plate kinematics and dynamics in the eastern Mediterranean and Caucasus. Journal of Geophysical Research 105, 5695–5719.

Meade, B.J., Hager, B.H., McClusky, S.C., Reilinger, R.E., Ergintav, S., Onur, L., Barka, A., Özener, H., 2002. Estimates of seismic potential in the Marmara Sea region from block models of secular deformation constrained by Global Positioning System measurements. Bullettin Seismological Society of America 92, 208– 215.

Moore, W.J., McKee, E.H., Akinci, Ö., 1980. Chemistry and chronology of plutonic rocks in the Pontid Mountains, northern Turkey. European Copper Deposits 1, 209-216.

Okay, A.I., Tüysüz, O., 1999. Tethyan sutures of northern Turkey. In: Durand, B., Jolivet, L., Horváth, F., Séranne, M. (Eds.), The Mediterranean Basins: Tertiary Extension within the Alpine Orogen. Geological Society, London, Special Publications 156, 475–515.

Okay, A.I., Kaşlılar-Özcan, A., İmren, C., Boztepe-Güney, A., Demirbağ, E., Kuşçu, I., 2000. Active faults and evolving strike-slip basins in the Marmara Sea, northwest Turkey: a multichannel seismic reflection study. Tectonophysics 321, 189–218.

Okay, A.I., Satır, M., 2000. Coeval plutonism and metamorphism in a latest Oligocene metamorphic core complex in northwest Turkey. Geological Magazine 137, 495-516.

Okay, A.I., Tansel, İ., Tüysüz, O., 2001. Obduction, subduction and collision as reflected in the Upper Cretaceous-Lower Eocene sedimentary record of western Turkey. Geological Magazine, 138, 117-142.

Okay, A.I., Tüysüz, O., Kaya, S., 2004. From transpression to transtension: changes in morphology and structure around a bend on the North Anatolian Fault in the Marmara region. Tectonophysics 391, 259–282.

Okay, A.I., Satir, M., Zattin, M., Cavazza, W., Topuz, G., 2008. An Oligocene ductile strike-slip shear zone: the Uludag Massif, northwest Turkey – implications for the westward translation of Anatolia. Geological Society of America Bullettin 120, 893-911.

Okay, A.I., Zattin, M., Cavazza, W., 2010. Apatite fission-track data for the Miocene Arabia-Eurasia collision. Geology, 38, 35-38.

Okay, A.I., Özcan, E., Cavazza, W., Okay, N., Less, G. Upper Eocene olistostromes, two contrasting basement types, and the initiation of the southern Thrace Basin, NW Turkey. Turkish Journal of Earth Sciences, in press.

Özcan, E., Less, L., Okay, A.I., Báldi-Beke, M., Kollányi, K, Yilmaz, İ.Ö. Stratigraphy and larger Foraminifera of the Eocene shallow-marine and olistostromal units of the southern part of the Thrace Basin, NW Turkey. Turkish Journal of Earth Sciences, in press,

Pfister, M., Rybach, L., Simsek, S., 1998. Geothermal reconaissance of the Marmara Sea region (NW Turkey): surface heat flow density in an area of active continental extension. Tectonophysics, 291, 77-89.

Reilinger, R.E., et al. 2006. GPS constraints on continental deformation in the Africa-Arabia-Eurasia continental collision zone and implications for the dynamics of plate interactions. Journal of Geophysical Research 111, B05411.

Reiners, P.W., 2005. Zircon (U-Th)/He thermochronometry. Review Mineralogy and Geochemistry 58, 151-176.

Robertson, A.H.F., Parlak, O., Rızaoğlu, T., Ünlügenç, Ü., İnan, N., Taslı, K., Ustaömer, T., 2007. Tectonic evolution of the South Tethyan ocean: evidence froom the Eastern Taurus Mountains (Elaziğ region, SE Turkey). In: Ries, A.C., Butler, R.W.H., Graham, R.H. (Eds.), Deformation of continental crust. Geological Society of London, Special Publication 272, 231-270.

Sakinç, M., Yaltırak, C., Oktay, F.Y., 1999. Palaeogeographical evolution of the Thrace Neogene Basin and the Tethys–Paratethys relations at northwestern Turkey (Thrace). Palaeogeography, Palaeoclimatology, Palaeoecology 153, 17–40.

Seeber, L., Emre, O., Cormier, M.-H., Sorlien, C.C., McHugh, C.M.G., Polonia, A., Ozer, N., Çağatay, M.N., 2004. Uplift and subsidence from oblique slip: the Ganos–Marmara bend of the North Anatolian Transform, Western Turkey. Tectonophysics 391, 239-258.

Seyitoğlu, G., Scott, B.C., Rundle, C.C., 1992. Timing of Cenozoic extensional tectonics in west Turkey. Journal Geological Society of London 149, 533–538.

Siyako, M., Huvaz, O., 2007. Eocene stratigraphic evolution of the Thrace Basin, Turkey. Sedimentary Geology 198, 75-91.

Şengör, A.M.C., Yılmaz, Y., 1981. Tethyan evolution of Turkey: a plate tectonic approach. Tectonophysics 75, 181-241.

Şengör, A.M.C., Görür, N., Şaroğlu, F., 1985. Strikeslip faulting and related basin formation in zones of tectonic escape: Turkey as a case study. In*:* Biddle, K.T., Christie-Blick, N. (Eds.), Strike-slip Deformation, Basin Formation, and Sedimentation. Society Economic Paleontology Mineralogy, Special Publications 37, 227–264.

Şengör, A.M.C., Tüysüz, O., İmren, C., Sakınç, M., Eyidoğan, H., Görür, N., Le Pichon, X., Rangin, C., 2005. The North Anatolian Fault: a new look. Annual Review Earth Planetary Science 33, 37–112.

Şentürk, K., Sümengen, M., Terlemez, I. and Karaköse, C., 1998. Bandırma D-4 Sheet and 10 Page Explanatory Text, 1:100 000 Scale Geological Map Series. General Directorate of Mineral Research and Exploration, Ankara.

Sümengen, M., Terlemez, I., 1991. Stratigraphy of the Eocene sediments from the southwestern Thrace. Maden Tetkik ve Arama Dergisi, 113, 17–30.

Thomson, S.N., Ring, U., 2006. Thermochronological evalution of postcollision extension in the Anatolide region, western Turkey. Tectonics, 25, TC3005.

Turgut, S., Türkaslan, M., Perinçek, D., 1991. Evolution of the Thrace sedimentary basin and hydrocarbon prospectivity. In: Spencer, A.M. (Ed.), *Generation*, Accumulation and Production of Europe's Hydrocarbon. European Association of Petroleum Geosciences, Special Publications 1, 415–437.

Tüysüz, O., 1993. Karadeniz'den Orta Anadolu'ya bir jeotravers: Kuzey neo-Tetis'in tektonik evrimi. Türkiye Petrol Jeologlari Derneği Bülteni 5, 1–33.

Uysal, I.T., Mutlu, H., Altunel, E., Karabacak, V., Golding, S.D., 2006. Clay mineralogical and isotopic (K–Ar, $\delta^{18}O$, δD) constraints on the evolution of the North Anatolian Fault Zone, Turkey. Earth and Planetary Science Letters 243, 181-194.

Wolf, R.A., Farley, K.A., Kass, D.M., 1998. A sensitivity analysis of the apatite (U-Th)/He thermochronometer. Chemical Geology 148, 105-114.

Yalçın, T., 1997. Hydrogeological investigation of the Gönen and Ekşidere thermal waters (northwest Turkey). In: Schindler, C., Pfister, M. (Eds.), Active Tectonics of Northwestern Anatolia — The Marmara Poly-Project. Verlag der Fachvereine, Zürich, 275-300.

Yaltırak, C., Alpar, B., Yüce, H., 1998. Tectonic elements controlling evolution of the Gulf of Saros (northeastern Aegean Sea, Turkey). Tectonophysics 300, 227-248.

Yaltırak, C., Alpar, B., 2002. Kinematics and evolution of the northern branch of the North Anatolian fault (Ganos fault) between the Sea of Marmara and the Gulf of Saros. Marine Geology 190, 307– 327.

Yıldız, A., Toker, V., Şengüler, I., 1997. The nannoplankton biostratigraphy of the Middle Eocene-Oligocene units in southern Thrace basin and the surface water temperature variations. Türkiye Petrol Jeologları Derneği Bülteni, 9, 31–44.

Zattin, M., Landuzzi, A., Picotti, V., Zuffa, G.G., 2000. Discriminating between tectonic and sedimentary burial in a foredeep succession, Northern Apennines. Journal of Geological Society of London 157, 629-633.

Zattin, M., Okay, A.I., Cavazza, W., 2005. Fission-track evidence for late Oligocene and mid-Miocene activity along the North Anatolian Fault in southwestern Thrace. Terra Nova 17, 95–101.

Figure captions

Figure 1. Simplified tectonic map of the Marmara region showing the major terranes and sutures, as well as the North Anatolian Fault system. Modified from Okay et al., 2008.

Figure 2. Geologic map of western (A) and eastern (B) Marmara with apatite fission-track (black) and (U-Th)/He (red) ages. Fission-track data in italic are from Zattin et al., 2005.

Figure 3. Chronolitho-stratigraphic chart of main lithostratigraphic units across the North Anatolian Fault in the regions around the Gulf of Saros (left) and Ganos Mountain (right). Exact duration of Oligo-Miocene hiatuses north and south of Ganos fault is poorly constrained. Time scale from Gradstein et al. (2004). Sources: Okay et al. (2009), Özcan et al. (2009), Sümengen and Terlemez (1991), Yıldız et al. (1997) and Şentürk et al. (1998).

Figure 4. Radial plots of samples collected from sedimentary rocks whose depositional age partially overlap the AFT age (see Fig. 2 for sample location). If all the single grain ages are younger than the sample's stratigraphic age, then all the grains have been annealed and maximum temperatures must have been at or greater than the total resetting temperature. As the maximum temperature lowers, the number of grain ages older the stratigraphic age generally increases. If the sample age was close to the depositional age (e.g., an ash), then partial (not only total) resetting will produce AFT ages younger than depositional age.

Dots: single grain ages; horizontal axis: precision of individual grains (1/sigma); vertical axis: bar indicates the standard error of each measurement; dashed line: (U-Th)/He age; shaded area: stratigraphic age.

Figure 5. Time-temperature paths obtained from inverse modelling using the HeFTy program (Ehlers et al., 2005), which generates the possible T-t paths by a Monte Carlo algorithm. Predicted

AFT data were calculated according to the Ketcham et al. (1999) annealing model and the Donelick et al. (1999) c-axis projection whereas AHe data were calculated according to Farley (2000) diffusion model.

Shaded areas mark envelopes of statistically acceptable fit and the thick lines correspond to the most probable thermal histories. Thermal paths out of the partial annealing zone are largely inferential as fission-track data cannot give reliable information out of this temperature range. In each diagram, parameters (model and measured age, model and measured mean length) related to inverse modelling are reported. GOF (Goodness-Of-Fit) gives an indication about the fit between observed and predicted data (values close to 1 are best) as it reveals the probability of failing the null hypothesis that the model and data are different. In general a value of 0.05 or higher is considered not to fail the null hypothesis, and thus reflects an acceptable fit between model and data. In these simulations, the only constraints used are the granite emplacement temperature and age (TU46) and the depositional age (TU64).

Figure 6. Age-elevation plot for AFT (dots) and AHe (squares) data in the Ganos region. Only data from the block north of the Ganos fault have been considered.

Figure 1

Click here to download high resolution image

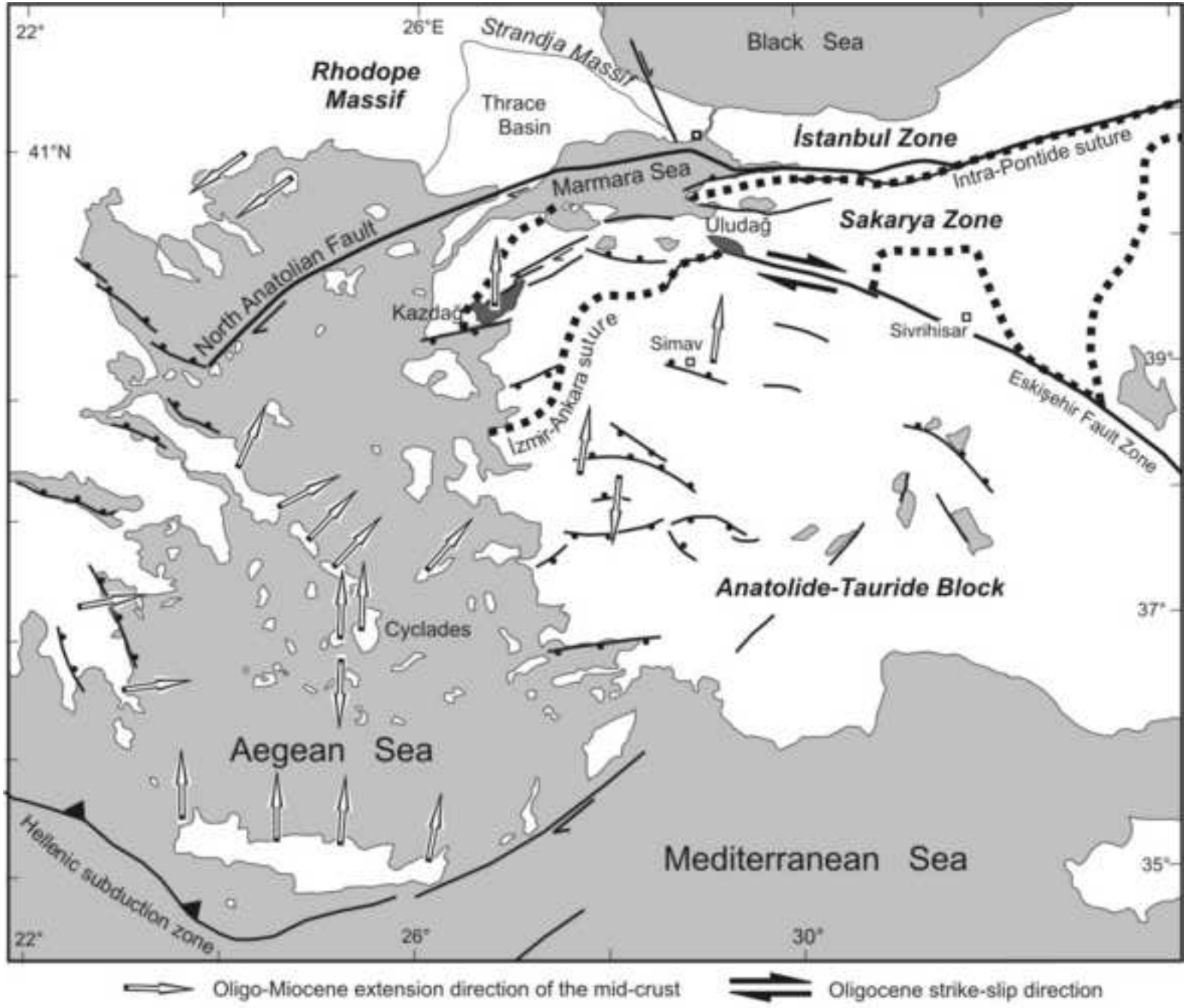

Fig. 1

Figure 2

Click here to download high resolution image

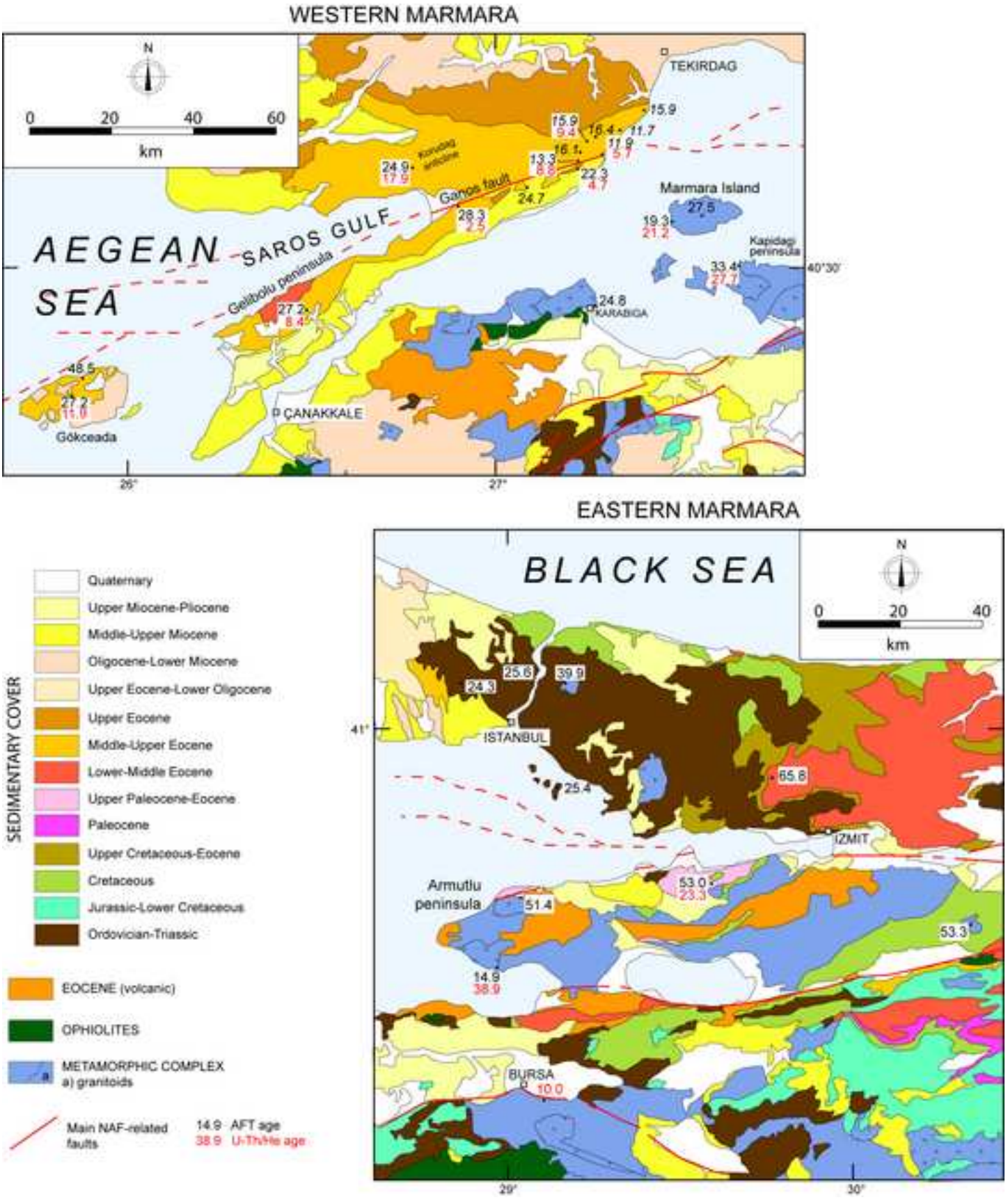

Figure 3

Click here to download high resolution image

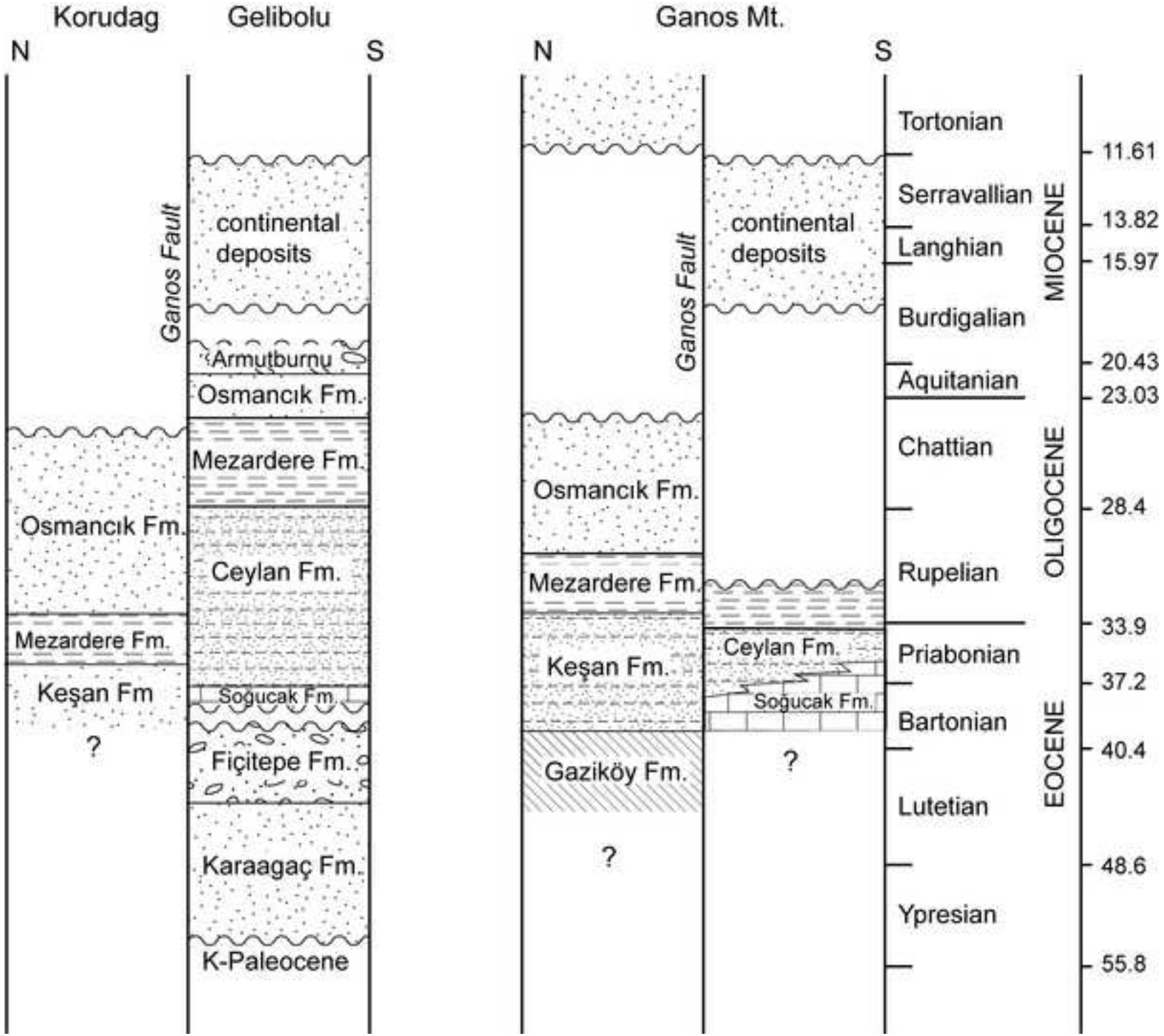

Figure 4

Click here to download high resolution image

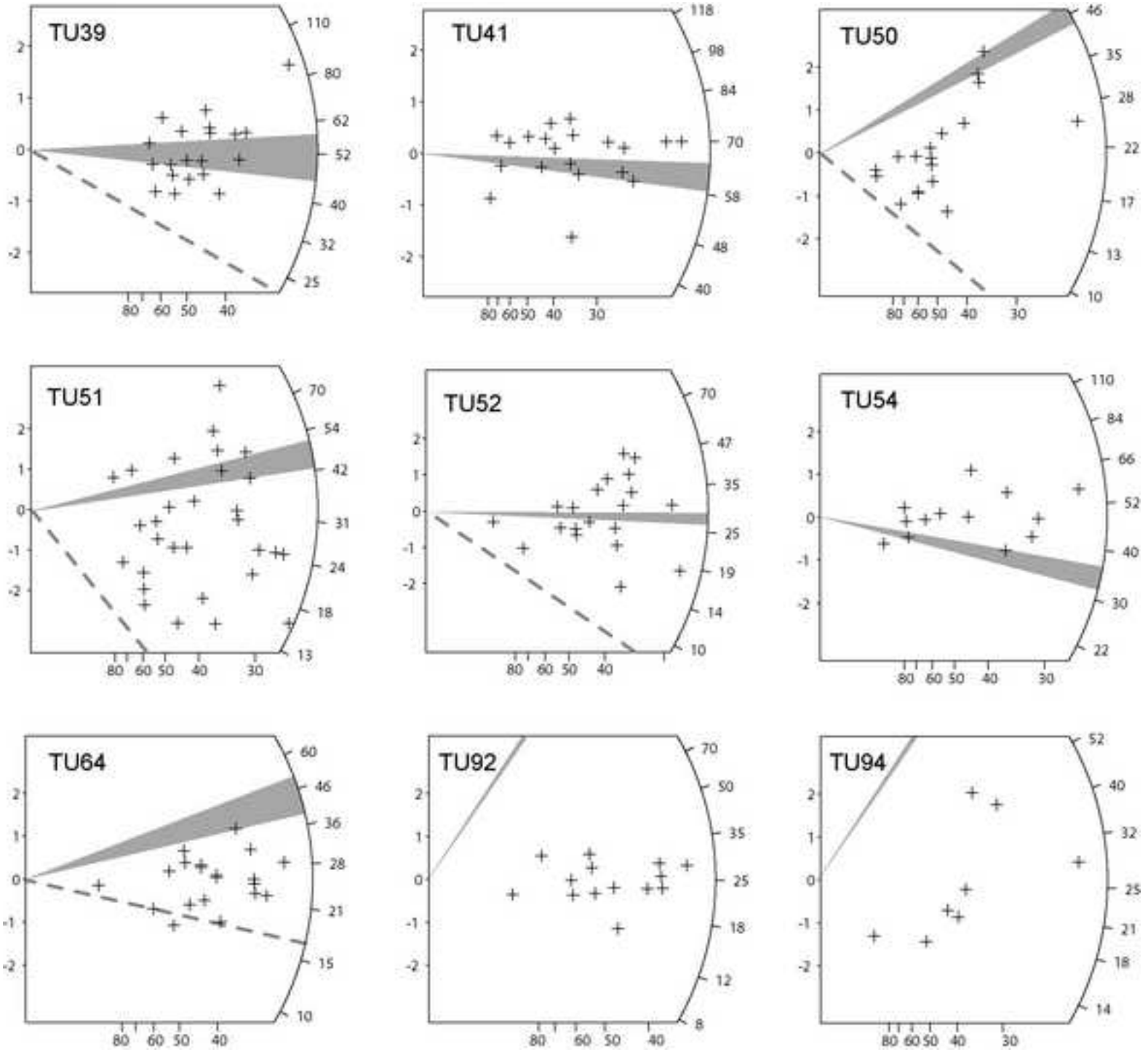

Figure 5

Click here to download high resolution image

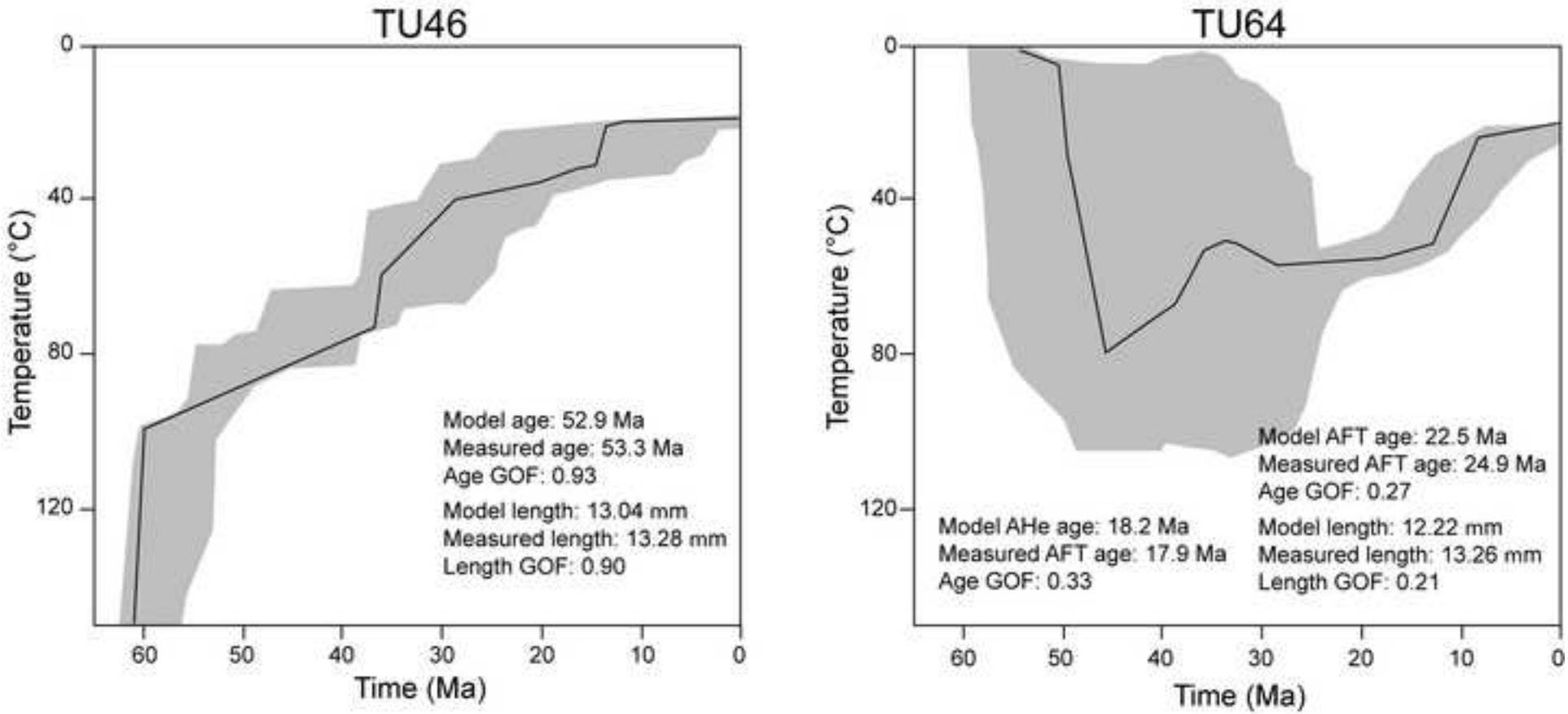

Figure 6

Click here to download high resolution image

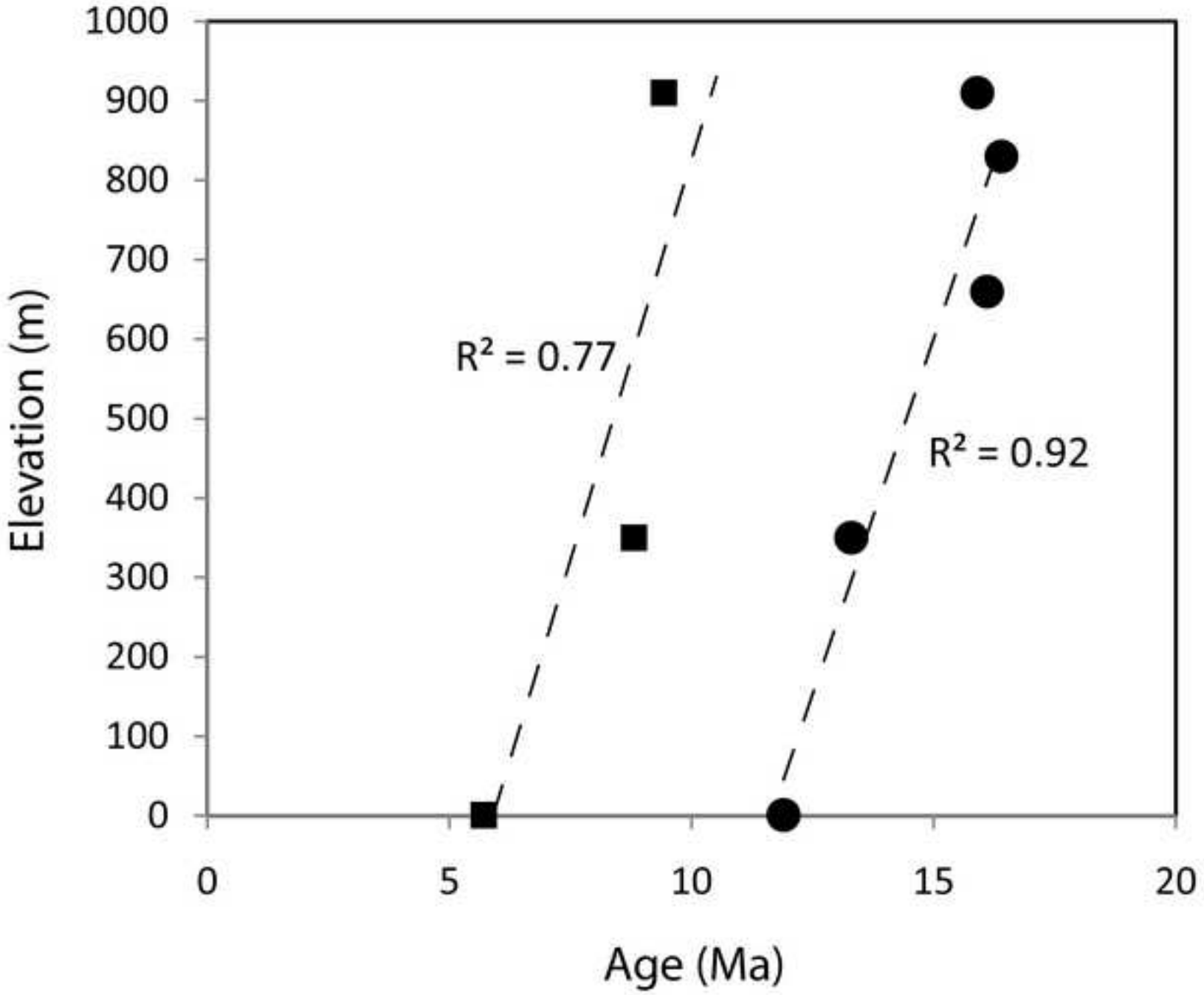

Table 1. *AFT data*

Sample number	Coordinates (UTM)	Elevation (m)	No. of crystals	Spontaneous		Induced		$P(\chi)^2$	Dosimeter		Age (Ma) ± 1σ	Mean confined track lenght (μm) ± std. err	Std. dev.	No. of tracks measured
				ρ_s	N_s	ρ_i	N_i		ρ_d	N_d				
TU1*	35T0526836 4516172	830	20	0.76	44	1.09	634	99.0	1.28	6137	16.4±5.1	13.73±0.23	1.64	53
TU2*	35T0524972 4515051	910	20	1.06	91	1.57	1348	89.0	1.27	6061	15.9±3.4	13.50±0.30	1.91	40
TU3*	35T0523523 4511909	660	20	1.17	80	1.69	1159	92.9	1.27	6022	16.1±3.7	12.93±0.33	1.99	37
TU4*	35T0524381 4510956	350	20	1.45	90	2.53	1565	74.2	1.26	5984	13.3±2.9	14.32±0.34	1.47	19
TU5*	35T0528256 4511674	1	20	2.13	104	3.86	1885	42.5	1.25	5946	11.9±3.2	14.28±0.17	0.76	20
TU6*	35T0508245 4501346	170	20	2.10	286	1.93	2630	94.1	1.24	5908	24.7±3.1	12.60±0.18	1.49	65
TU7*	35T0533648 4519168	350	20	0.67	33	1.29	640	99.9	1.24	5869	11.7±4.2	14.33±0.29	1.25	19
TU9*	35T0538218 4522726	120	20	1.09	74	1.55	1054	18.8	1.22	5793	15.9±4.6	13.53±0.38	2.03	28
TU36	35T0666467 4481129	10	12	0.49	12	0.55	134	48.1	0.95	4504	14.9±5.0	-	-	-
TU38	35T0667110 4497786	200	15	3.51	193	1.16	636	20.2	0.94	4474	51.4±4.8	13.43±0.33	1.91	33
TU39	35T0711381 4503904	70	20	1.66	124	0.60	448	98.9	1.05	4982	53.0±5.5	15.46±0.11	1.07	100
TU41	35T0730648 4522849	301	20	5.83	255	1.51	661	99.9	0.94	4444	65.8±5.0	13.83±0.18	1.79	100
TU46	35T0274412 4495581	80	20	2.34	157	0.85	570	67.6	1.06	5021	53.3±4.9	13.28±0.24	1.71	52
TU47	35T0560460 4485269	25	20	2.46	199	1.44	1164	86.6	1.07	5059	33.4±2.6	14.15±0.15	1.04	49
TU48	35T0545966 4494013	20	20	0.51	67	0.46	597	91.6	0.94	4458	19.3±2.5	14.12±0.16	1.31	68
TU49	35T0549675 4495825	709	20	0.64	34	0.44	235	99.6	1.04	4924	27.5±5.1	14.52±0.19	1.16	38
TU50	35T0519072 4506276	310	20	2.22	103	1.69	783	37.7	0.93	4428	22.3±2.5	-	-	-
TU51	35T0493388 4496841	100	30	1.44	238	1.10	1823	0.0	1.05	4963	28.3±3.2	-	-	-
TU52	35T0456626 4470872	106	20	1.12	149	0.78	940	50.1	0.93	4414	27.2±2.6	14.17±0.16	0.96	36
TU54	35T0405489 4453934	1	14	2.91	93	1.20	385	99.6	1.10	5195	48.5±5.7	-	-	-
TU55	35T0400758 4450867	250	20	2.35	275	1.66	1939	78.4	1.05	5001	27.2±1.8	15.11±0.10	0.98	100
TU56	35T0527608 4474219	30	8	2.81	60	1.92	410	97.7	0.93	4398	24.8±3.4	-	-	-
TU64	35T0480731 4506555	350	20	1.74	139	1.37	1094	99.6	1.07	5079	24.9±2.3	13.26±0.33	2.08	40
TU92	35T0641940 4555239	31	14	2.71	72	1.95	517	99.9	1.05	4993	24.3 ±3.1	13.59 ±0.16	0.80	25
TU94	35T0662767 4556491	27	8	3.43	75	2.36	517	6.9	1.08	5122	25.6 ±4.1	12.62 ±0.30	1.46	23
TU96	35T0678005 4523039	1	26	1.04	137	0.71	937	84.8	1.07	508	25.4±2.6	-	-	-
TU100	35T0681234 4552295	92	21	1.79	151	0.79	664	85.3	1.06	5030	39.9 ±3.7	13.77 ±0.232	1.20	27

Central ages calculated using dosimeter glass CN5 and ζ-CN5=367.45±4.35 (analyst MZ) for all the samples but TU92, TU94, TU96 and TU100 (ζ-CN5=332.54±5.55; analyst: IF). Samples marked by an asterisk are from Zattin et al. (2005). ρ_s: spontaneous track densities (x 10^5 cm^{-2}) measured in internal mineral surfaces; N_s: total number of spontaneous tracks; ρi and ρ_d: induced and dosimeter track densities (x 10^6 cm^{-2}) on external mica detectors (g=0.5); N_i and N_d: total numbers of tracks; $P(\chi^2)$: probability of obtaining χ^2-value for ν degrees of freedom (where ν=number of crystals-1); a probability >5% is indicative of an homogenous population. Samples with a probability <5% have been analyzed with the binomial peak-fitting method.

Table 2. *(U-Th)/He data. Refer to table 1 for sample location.*

Apatite (U-Th)/He analytical data

Sample	Replicates	F_T[a]	Corrected Age[b]	1σ± (Ma)	MWAR (um)[c]	Mass (µg)	Mean Age[d]	1σ± (Ma)
TU2	1	0.650	9.22	0.20	41.0	1.41	**9.43**	**0.14**
	2	0.700	9.61	0.18	47.5	2.14		
TU4	1	0.610	8.81	0.19	35.0	0.78	**8.81**	**0.19**
TU5	1	0.710	5.71	0.14	49.3	2.73	**5.71**	**0.14**
TU29	1	0.728	10.39	0.80	50.9	8.35	**9.99**	**0.42**
	2	0.758	9.83	0.59	56.4	10.74		
TU36	1	0.643	38.88	1.13	38.8	3.53	**38.88**	**1.13**
TU39	1	0.614	23.03	1.09	35.0	2.80	**23.03**	**1.09**
TU47	1	0.653	28.70	0.69	38.1	6.01	**27.75**	**0.39**
	2	0.670	26.35	0.71	42.9	4.04		
	3	0.728	28.04	0.62	52.3	8.14		
TU48	1	0.657	21.22	0.50	38.1	4.26	**21.22**	**0.50**
TU50	1	0.551	4.27	0.12	29.5	1.79	**4.67**	**0.08**
	2	0.618	4.95	0.10	36.1	3.59		
TU51	1	0.692	2.45	0.05	47.8	6.92	**2.52**	**0.04**
	2	0.685	2.58	0.05	45.8	3.75		
TU52	1	0.585	7.66	0.15	33.9	3.10	**8.38**	**0.10**
	2	0.651	9.58	0.19	39.6	4.56		
	3	0.696	8.33	0.17	46.9	8.48		
TU55	1	0.620	12.40	0.26	26.0	4.73	**11.92**	**0.15**
	2	0.654	10.82	0.28	21.9	5.02		
	3	0.695	12.84	0.26	30.9	7.12		
TU64	1	0.594	17.86	0.37	26.7	2.25	**17.86**	**0.37**

AHe age determination are calculate using multigrain-multi-replicate aliquots; Propagated analytical uncertainties are 1σ; Durango apatite measured concurrently with these analyses yielded a weighted mean age of 31.6 ± 0.48 Ma (2σ standard error, n = 9); [a] FT is the alpha-ejection correction of Farley (2000); [b] Alpha ejection corrected age; [c] Mass-weighted average radius;[d] mean ages represent weighted means with weighted errors (1 σ).

CHAPTER 5

CONCLUSIONS

From late Paleozoic to Recent times, the Pontides of northern Turkey have suffered the cumulative effects of a complex structural history, including the Hercynian, Cimmeride, and Alpine orogenies, as well as Aegean extension and significant strike-slip deformation associated with the North Anatolian Fault system (for a review, see Stephenson *et al.* 2004). The determination of the timing of amalgamation of (i) the Rhodopian domain (Strandja Massif), (ii) the İstanbul Zone, and (iii) the Sakarya Zones is of particular interest in deciphering the tectonic evolution of the Pontides and its relationships with the İzmir-Ankara-Erzincan suture to the south. Within this general framework, this dissertation tackled selected aspects of the geological evolution of the Pontides by applying several analytical methods to the thermal evolution of the Cimmeride-age Karakaya subduction-accretion complex, to the thermochronological evolution of the Sakarya and Istanbul exotic terranes, and to the propagation of the North Anatolian Fault system in the Marmara region.

The main results of this dissertation can be summarised as follows.

1) The results of integrated analytical methods for the determination of organic and inorganic parameters -including clay mineralogy, vitrinite reflectance and Raman spectroscopy on carbonaceous material- applied to the **Karakaya Complex** of northern Anatolia show a good degree of correlation and demonstrate that Raman spectroscopy on carbonaceous material can be applied successfully to temperature ranges of 200-330°C, thus extending the application of this method from higher grade metamorphic contexts to lower grade metamorphic conditions.

These data also point out two different thermal histories for the Karakaya Complex: the Nilüfer Unit (Lower Karakaya Complex) recorded a range of peak temperatures between 300°C and 500°C (greenschist facies) The Hodul and Orhanlar Units of the Upper Karakaya Complex yielded peak temperatures of 125-376°C across the study

area. This contradicts the commonly held notion that the Upper Karakaya Complex was unmetamorphosed or only slightly metamorphosed. The peak temperatures from the Upper Karakaya Complex are the results of different degree of involvement of the units in the complex dynamic processes of the accretionary wedge. Portion of these units experienced high temperatures as part of the deepest sections of the accretionary wedge, whereas other remained at relatively shallow depths. In addition, a relatively undeformed Early Jurassic succession overlying the Karakaya Complex which was never buried deeply, suggests that most Karakaya Complex was already at shallow crustal depth by Early Jurassic time.

2) A large number of AFT ages from both **İstanbul and Sakarya terranes** point to three discrete episodes of exhumation related to the complex tectonic evolution of the Pontides. The older AFT ages come from the central and eastern portion of the study area and are clustered into two main exhumation episodes related to deformation along the İzmir-Ankara suture. A first cluster of AFT ages range between 62.3 and 50.3 Ma (Paleocene - early Eocene), and reflect the closure of the İzmir-Ankara ocean and the resulting collision between the Sakarya terrane and the Anatolide-Tauride Block. A second cluster AFT ages ranges between 43.5 and 32.3 Ma (Late Eocene - earliest Oligocene) and is the result of renewed tectonic activity along the İzmir-Ankara suture. Since the same clusters of AFT ages are present north and south of the tectonic boundary between İstanbul and Sakarya terranes (the Intra-Pontide Suture) it is evident that such terranes were amalgamated in pre-Cenozoic times. The youngest AFT ages (Late Oligocene - early Miocene) were yielded by samples taken from the western portion of the study area and are related to the onset and development of northern Aegean extension. This tectonic event probably gave rise to exhumation at a regional scale.

3) Apatite (U-Th)/He and fission-track analyses of both basement and sedimentary cover samples collected around the **Marmara Sea region** yielded exhumation ages spanning the entire duration of the Cenozoic. Exhumation data point to the existence of a system of major E-W-trending structural discontinuities active at least from the late Oligocene. In the early Pliocene, inception of the present-day North Anatolian Fault (NAF) system in the Marmara region occurred by reactivation of these older tectonic structures. The Ganos fault segment of the NAF in southern Thrace represents the best

example of such reactivation, as exhumation south of it occurred during the latest Oligocene and north of it during the mid-Miocene. In this area, large tectonic structures long interpreted as the results of Plio-Quaternary NAF-related transpressional deformation (i.e. the Ganos monocline, the Korudağ anticline, and the Gelibolu folds) were in fact produced during the Late Oligocene – Early Miocene. From a thermochronological viewpoint, the overall lack of significant (U-Th)/He age differences across the NAF indicates that the early Pliocene inception of strike-slip motion in the Marmara region represents a relatively minor episode.

At the scale of the entire study area, the entire geographic pattern of exhumation ages can be related to the complex superposition of tectonic events that affected the Pontides. The western portion of the study area is dominated by the Late Oligocene-Early Miocene AFT ages that obliterated any previous thermotectonic events. This younger exhumation ages are related to the Aegean extension, that probably gave rise to exhumation at a regional scale. The older AFT ages are concentrated in the eastern portion of the study area. The two clusters of exhumation ages (Paleocene - early Eocene and Late Eocene - earliest Oligocene) are related to the activity along the İzmir-Ankara suture, resulting in the collision between the Sakarya terrane to the north and the Anatolide-Tauride Block to the south. The widespread distribution of the AFT ages in both terranes (İstanbul and Sakarya) constrain their amalgamation in pre-Cenozoic times. This result has an important bearing on paleogeographic-paleotectonic reconstructions of the Eastern Mediterranean region.

REFERENCES

All the paper listed below refer to the citations in the Chapter 1, Chapter 5, and the appendixes. The manuscripts enclosed as Chapters 2, 3, and 4 have their own lists of references.

AKSOY, R., 1998. Strain Analysis of the Kapıdagı Peninsula Shear Zone in the Ocaklar Granitoid,NW Turkey. *Turkish Journal of Earth Sciences* **7**, 79-85.

AKYÜREK, B. & SOYSAL, Y., 1983. Basic geological features of the region south of the Biga Peninsula (Savaştepe-Kırkağaç-Bergama-Ayvalık). *Maden Tetkik ve Arama Enstitütü (MTA) Dergisi* **95/96**, 1-13 [in Turkish with English abstract].

AKYÜREK, B., BILGINER, E., AKBAŞ, B., HEPŞEN, N., PEHLIVAN, Ş., SUNU, O., SOYSAL, Y., DAĞER, Z., ÇATAL, E., SÖZERI, B., YLDIRIM, H. & HAKYEMEZ Y., 1984. Basic geological features of the Ankara-Elmadağ-Kalecik region. *Jeoloji Mühendisliği* **20**, 31-46 [in Turkish with English abstract].

ALDEGA, L., BOTTI, F., CORRADO, S., 2007a. Clay mineral assemblages and vitrinite reflectance in the Laga Basin (Central Apennines, Italy): What do they record? *Clays and Clay Minerals* **55**, 504-518.

ALDEGA, L., CORRADO, S., GRASSO, M. & MANISCALCO, R., 2007b. Correlation of diagenetic data from organic and inorganic studies in the Apenninic-Maghrebian fold-and-thrust belt: a case study from Eastern Sicily. *The Journal of Geology* **115**, 335-353.

ALTINER, D. & KOÇYIĞIT, A., 1993. Third remark on the geology of the Karakaya basin. An Anisian megablock in northern central Anatolia: micropaleontologic, stratigraphic and structural implications for the rifting stage of the Karakaya basin. *Revue de Paléobiologie* **12**, 1-17.

ÁRKAI, P., 1991. Chlorite crystallinity: an empirical-approach and correlation with illite crystallinity, coal rank and mineral facies as exemplified by Paleozoic and Mesozoic rocks of Northeast Hungary. *Journal of Metamorphic Geology* **9**, 723-734.

BEYSSAC, O., BOLLINGER, L., AVOUAC, J.P. & GOFFÈ, B., 2004. Thermal metamorphism in the lesser Himalaya of Nepal determined from Raman spectroscopy of carbonaceous material. *Earth and Planetary Science Letters* **225**, 233-241.

BEYSSAC, O., GOFFÈ, B., CHOPIN, C. & ROUZAUD J.N., 2002a. Raman spectra of carbonaceous material in metasediments: a new geothermometer. *Journal of Metamorphic Geology* **20**, 859-871.

BEYSSAC, O., GOFFÈ, B., PETITET, J.P., FROIGNEUX, E., MOREAU, M. & ROUZAUD J.N., 2003. on the characterization of disordered and heterogeneous carbonaceous materials by Raman spectroscopy. *Spectrochimica Acta Part A* **59**, 2267-2276.

BEYSSAC, O., ROUZAUD J.N., GOFFÈ, B., BRUNET, F., & GOFFÈ, B., 2002b. Graphitization in high-pressure, low-temperature metamorphic gradient: a HRTEM and Raman microspectroscopy study. *Contributions to Mineralogy and Petrology* **143**, 19-31.

BEYSSAC, O., SIMOES, M., AVOUAC, J.P., FARLEY, K.A., CHEN, Y.G., CHAN Y.C. & GOFFÈ, B., 2007. Late Cenozoic metamorphic evolution and exumation of Taiwan. *Tectonics* **26**, TC6001, doi:10.1029/2006TC002064.

BINGÖL, E., AKYÜREK, B. & KORKMAZER, B., 1975. Geology of the Biga Peninsula and some characteristic of the Karakaya blocky series. In: *Congress of Earth Sciences on the occasion of the 50th anniversary of the Turkish Republic* (Ed M.T.v.a. Enstitüsü), 70-77, Ankara [In Turkish with English abstract].

BISCAYE, P.E., 1965. Mineralogy and sedimentation of recent deep-sea clay in the Atlantic ocean and adjacent seas and oceans. *Geological Society of America Bulletin* **76**, 803-832.

BOLLINGER, L., AVOUAC, J.P., BEYSSAC, O., CATLOS, E.J., HARRISON, T.M., GROVE, M., GOFFÈ, B. & SAPKOTA, S., 2004. Thermal structure and exhumation history of the Lesser Himalaya in central Nepal. *Tectonics* **23**, TC5015, doi: 10.1029/2003TC001564.

BOZKURT, E., 2001. Neotectonics of Turkey – a synthesis. *Geodinamica Acta* **14**, 3-30.

BRAUN, J., VAN DER BEEK, P. & BATT G., 2006. Quantitative Thermochronology. Numerical Methods for the interpretation of thermochronological data. *Cambridge University Press*, 258 pp.

CORRADO, S., ALDEGA, L., DI LEO, P., GIAMPAOLO, C., INVERNIZZI, C., MAZZOLI, S. & ZATTIN, M., 2005. Thermal maturity of the axial zone of the Southern Apennines fold-and thrust-belt (Italy) from multiple organic and inorganic indicators. *Terra Nova* **17** (1), 56-65.

DELLISANTI, F., PINI G., TATEO, F. & BAUDIN, F., 2008. The role of tectonic shear strain on the illitization mechanism of mixed-layers illite–smectite. A case study from a fault zone in the Northern Apennines, Italy. *International Journal of Earth Sciences,* **97**, 601-616.

DURAND, B., ALPERN, B., PITTION, J.L. & PRADIER, B., 1987. Reflectance of vitrinite as a control of thermal history of sediments. In: Durand, B. (ed). *Thermal history of sedimentary basins. Technip, Paris,* 441-474.

FERREIRO MÄHLMANN, R., 2001. Correlation of very low grade data to calibrate a thermal maturity model in a nappe tectonic setting, a case study from the Alps. *Tectonophysics* **334**, 1-33.

FLEISCHER, R.L., PRICE, P.B. &WALKER, R.M., 1965. The ion explosion spike mechanism for formation of charged particles tracks. *Journal of Applied Physics* **36**, 3645-3652.

GABALDA, S., BEYSSAC, O., JOLIVET, L., AGARD, P. & CHOPIN C., 2009. Thermal structure of fossil subduction wedge in the Western Alps. *Terra Nova* **21**, 28-34.

GAILBRAITH, R.F., 1981. On statistical models for fission tracks counts. *Mathematical Geology* **13**, 471-478.

GENÇ, Ş.C. & YILMAZ, Y., 1995. Evolution of the Triassic continental margin, northwest Anatolia. *Tectonophysics* **243**, 193-207.

GÖNCÜOĞLU, M.C., TURHAN, N., ŞENTÜRK, K., ÖZCAN, A. & UYSAL, Ş., 2000. A geotraverse across NW Turkey: tectonic units of the central Sakarya region and their tectonic evolution. In: Bozkurt E., Winchester J.A. & Piper J.A.D. (eds)

Tectonics and Magmatism in Turkey and Surrounding Area. Geological Society, London, Special Publication **173**, 139-161.

GUGGENHEIM, S., BAIN D.C., BERGAYA, F., BRIGATTI, M.F., DRITS, V.A., EBERL, D.D., FORMOSO, M.L.L., GALAN, E., MERRIMAN, R.J., PEACOR, D.R., STANJEK, H. & WATANABE, T., 2002. Report of the Association Internationale pour l'Etude des Argiles (AIPEA) Nomenclature Committee for 2001: order, disorder and crystallinity in phyllosilicates and the use of the 'Crystallinity Index'. *Clay Minerals,* **37**, 389-393.

HURFORD, A.J. & GREEN, P.F., 1981. A reappraisal of neutron dosimetry and uranium-238λ_f decay values in fission track dating. *Nuclear Tracks* **5**, 53-61.

HURFORD, A.J., 1990. Standardization of fission track dating calibration: recommendation by the Fission Track Working Group of the I.U.G.S. Subcommission on Geochronology. *Chemical Geology (Isotope Geoscience Sector)* **80**, 171-178.

JUDIK, K., RANTITSCH, G., RAINER, T.M., ÁRKAI, P. & TOMLJENOVIĆ, B., 2008. Alpine metamorphism of organic matter in metasedimentary rocks from Mt. Medvednica (Croatia). *Swiss Journal of Geoscience* **101**, 605–616.

KAYA, O., ÖZCOÇAK, O. & LISENBEE, A., 1989. Stratigraphy of the pre.Jurassic blocky sedimentary rocks to the south of Bursa, NW Turkey. *Mineral Research and Exploration of Turkey (MTA) Bulletin* **109**, 15-24.

KOÇYIĞIT, A., 1987. Tectonostratigraphy of the Hasanoğlan (Ankara) region: evolution of the Karakaya orogenic belt. *Yerbilmeri* **14**, 269-294 [In Turkish with English abstract].

KRUMM, S., 1996. WINFIT 1.0 - A computer program for X-ray diffraction line profile analysis. *Acta Universitatis Carolinae Geologica,* **38**, 253-261.

KÜBLER, B., 1967. La cristallinité de l'illite et les zones tout à fait supérieures du métamorphisme. In: *Etages Tectoniques, Colloque de Neuchâtel 1966*. Université Neuchâtel, Switzerland, 105-121.

LAHFID, A., 2008. Etablissement d'un géothermomètre à maxima pour les séries argileuses peu matures. *PhD Dissertation, Université Paris 7*.

LEZZERINI, M., SARTORI, F. & TAMPONI, M., 1995. Effect of amount of material used on sedimentation slides in the control of illite crystallinity measurements. *European Journal of Mineralogy,* **7**, 819-823.

MERRIMAN, R.J. & PEACOR, D.R., 1999. Very low-grade metapelites: mineralogy, microfabrics and measuring reaction progress. In: Frey, M. & Robinson, D. (eds). *Low-grade metamorphism. Blackwell Sciences, Oxford*, 10-60.

MERRIMAN, R.J., 2005. Clay minerals and sedimentary basin history. *European Journal of Mineralogy,* **17**, 7-20.

MOORE, D.M. & REYNOLDS, R.C., 1989. X-ray diffraction and the identification and analysis of clay minerals. *Oxford University Press, Oxford*, 1–327.

MUKHOPADHYAY, P.K., 1994. Vitrinite reflectance as maturity parameter - petrographic and molecular characterization and its applications to basin modelling. In: Mukhopadhyay P.K. & Dow W.G. (eds). *Vitrinite reflectance as a maturity parameter: applications and limitations, American Chemical Society,* 1-24.

OKAY A.I., SATIR M., MALUSKI H., SIYAKO M, MONIE P. METZGER R. & AKYÜZ S., 1996. Paleo- and Neo-Tethyan events in northwest Turkey: geological and geochronological constraints. In: Yin A. & Harrison M. (eds), *Tectonics of Asia. Cambridge University Press*, 420-441.

OKAY, A.I. & TÜYSÜZ, O., 1999. Tethyan sutures of northern Turkey. In: Durand B., Jolivet L., Horvàth F. & Sèranne M. (eds). *The Mediterranean Basin: Tertiary Extension Within the Alpine Orogen. Geological Society, London, Special Pubblication* **156**, 475-515.

OKAY, A.I., 2000. Was the Late Triassic orogeny in Turkey caused by the collision of an oceanic plateau? In: Bozkurt E., Winchester J.A. & Piper J.A.D. (eds) *Tectonics and Magmatism in Turkey and Surrounding Area. Geological Society, London, Special Pubblication* **173**, 25-41.

OKAY, A.I., 2008. Geology of Turkey: a synopsis. *Anschnitt* **21**, 19-42.

OKAY, A.I., SATIR, M., ZATTIN, M., CAVAZZA,W. & TOPUZ, G. 2008. An Oligocene ductile strike-slip shear zone: the Uludağ Massif, northwest Turkey – implication

for the westward translation of Anatolia. *Geological Society of American Bulletin* **120**, 893-911.

OKAY, A.I., SIYAKO, M. & BURKAN, K.A., 1991. Geology and tectonic evolution of the Biga Peninsula, northwest Turkey. *Bulletin of the Technical University of Istanbul* **44**, 191-256.

OKAY, A.I., TANSEL, İ. & TÜYSÜZ, O., 2001. Obduction, subduction and collision as reflected in the Upper Cretaceous-Lower Eocene sedimentary record of western Turkey. *Geological Magazine*, **138**, 117-142.

PEACOR, D.R., 1992. Diagenesis and low-grade metamorphism of shales and slates. In Buseck P.R. ed. *Minerals and Reactions at the Atomic Scale: Transmission Electron Microscopy. Mineralogical Society of America, Reviews in Mineralogy* **27**, 335-380.

PICKETT, E.A. & ROBERTSON, A.H.F., 1996. Formation of the Late Palaeozoic-Early Mesozoic Karakaya Complex and related ophiolites in NW Turkey by paleotethyan subduction-accretion. *Journal of Geological Society, London* **153**, 995-1009.

PICKETT, E.A., 1994. *Tectonic evolution of the PalaeoTethys Ocean in NW Turkey*. PhD Dissertation, University of Edinburgh [unpublished].

PICKETT, E.A., ROBERTSON, A.H.F. & DIXON, J.E., 1995. The Karakaya Complex, NW Turkey: A Palaeo-Tethyan accretionary complex. In: Erler, A., Ercan, T., Bingöl, E. & Örçen, S. (eds). *Geology of the Black Sea Region. Maden Tetkik ve Arama Enstitüsü (MTA), Ankara, Special Pubblication*, 11-18.

POTEL, S., FERREIRO MÄHLMANN, R., STERN, W.B., MULLIS, J. & FREY, M., 2006. Very low-grade metamorphic evolution of pelitic rocks under high-pressure/low-temperature condition, NW New Caledonia (SW Pacific). *Journal of Petrology* **47**, 991-1015.

RANTITSCH, G., GROGGER, W., TEICHERT, C., EBNER, F., HOFER, C., MAURER E.M., SCHAFFER, B & TOTH, M., 2004. Conversion of carbonaceous material to graphite within the Greywacke Zone of the Eastern Alps. *International Journal of Earth Science (Geol Rundsch)* **93**, 959-973.

RANTITSCH, G., SACHSENHOFER, R.F., HASENHÜTTL, C., RUSSEGGER, B. & RAINER, T.M., 2005. Thermal evolution of an extensional detachment as constrained by organic metamorphic data and thermal modeling: Graz Paleozoic Nappe Complex (Eastern Alps). *Tectonophysics* **411**, 57–72.

REYNOLDS, R.C., 1985. NEWMOD, a computer program for the calculation of one-dimensional diffraction patterns of mixed-layer clays.

ŞENGÖR, A.M.C. & YILMAZ, Y., 1981. Thethyan evolution of Turkey: a plate tectonic approach. *Tectonophysics* **75**, 181-241.

ŞENGÖR, A.M.C., 1984. The Cimmeride Orogenic system and the tectonics of Eurasia. *Geological Society of America, Special paper* **195**, 82pp.

ŞENGÖR, A.M.C., YILMAZ, Y. & SUNGURLU, O., 1984. Tectonic of the Mediterranean Cimmerides: nature and evolution of the western termination of Paleo-Tethys. In: Dixon J.E. & Robertson A.H.F. (eds), *The Geological Evolution of the Eastern Mediterranean. Geological Society, London, Special Pubblication* **17**, 77-112.

STAMPFL,I G.M. & HOCHARD, C., 2009. Plate tectonic of the Alpine realm. In: Murphy J.B., Keppie J.D. & Hynes A.J. (eds). Ancient Orogens and Modern Analogues. *Geological Society, London, Special Publication* **327**, 89-111, in press.

STEPHENSON, R., MART, Y.,OKAY, A.I., ROBERTSON, A.H.F., SAINTOT, A., STOVBA, S. & KHRIACHTCHEVSKAYA, O., 2004. TRANSMED Transect VIII. In: Cavazza, W., Roure, F., Spakman, W., Stampfli, G.M. & Ziegler, P. (eds). *The TRANSMED Atlas: The Mediterranean region from Crust to Mantle*. Springer Verlag.

STERN, W.B., MULLIS, J., RAHN, M. & FREY, M., 1991. Deconvolution of the first “illite” basal reflection. *Schweizerische Mineralogische Und Petrographische Mitteilungen* **71**, 453-462.

TEKELİ, O., 1981. Subduction complex of pre-Jurassic age, northern Anatolia, Turkey. *Geology* **9**, 68-72.

TÜYSÜZ, O., 1999. Geology of the Cretaceous sedimentary basins of the Western Pontides. *Geological Journal* **34**, 75-93.

WAGNER, G & REIMER, G.M., 1972. Fission track tectonics<. The tectonic interpretation of fission track ages. *Earth and Planetary Sciences Letters* **14**, 263.268.

WAGNER, G. & VAN DEN HAUTE, P., 1992. Fission track dating. *Kluwer, Dordecht*, 286 pp.

WARR, L.N. & RICE, A.H.N., 1994. Interlaboratory standardization and calibration of clay mineral crystallinity and crystallite size data. *Journal of Metamorphic Geology* **12**, 141-152.

YILMAZ, Y., 1981. Tectonic evolution of the southern margin of the Sakarya Continent. *Istanbul Yerbimileri* **1**, 33-52.

YILMAZ, Y., TÜYSÜZ, O., YIĞITBAS, E., CAN GENC, Ş. & ŞENGÖR, A.M.C., 1997. Geology and tectonic evolution of the Pontides. In: A.G. Robinson (ed) *Regional and petroleum geology of the Black Sea and surrounding regions. American Association of Petroleum Geologists Memorial* **68**, 183-226.

ZATTIN, M., OKAY, A.I. AND CAVAZZA, W., 2005. Fission-track evidence for late Oligocene and mid-Miocene activity along the North Anatolian Fault in southwestern Thrace. *Terra Nova*, **17**, 95–101.

APPENDIX 1

Clay mineralogy

Sample preparation

Whole-rock samples were disaggregated in a mortar and pestle to obtain fragments between 1 and 0.5 cm. These fragments were further disaggregate by shaking in demineralised water and ultrasonic disaggregation for up to 15 minutes. Samples were then dried.

For bulk rock analysis samples were mounted on glass slides. The <2μm fraction was obtained by differential settling, putting samples into settling tubes with demineralised water for 24 hours, according to Stokes Law. The <2μm powder was then dried. Smeared oriented mounts were prepared for each sample taking into account that the amount of clay on the glass slide was at least 3mg/cm2 (Lezzerini *et al.* 1995).

X-ray diffraction analysis

Mineralogical composition of the bulk rock and clay fraction (air-dried and ethylene glycol solvated samples (50°C overnight)) was carried out by powder X-ray diffraction (XRD) using a Philips PW 1710 diffractometer (CuKα radiation; 40kV/30 mA power supply; graphite secondary monochromator, 1° divergence and scatter slits, 0.1 mm receiving slit; 0.02° 2Θ step size; counting time of 2 s/step).

Parameters determination

Mineralogical parameters were determined via processing of the XRD patterns by WINFIT program (Krumm 1996) using an asymmetrical Pearson VII function (Stern *et al.* 1991; Warr & Rice 1994). The semiquantitative modal composition of the clay fraction was calculated using the method by Biscaye (1965), slightly modified to take into account the occurrence of mixed layer illite-smectite (I-S) and chlorite-smectite (C-S).

The very low-grade metamorphism was estimated by using the illite Kübler Index (KI) obtained by measuring the full-width-at-half-maximum-height (Δ°2θ) on the (001) illite diffraction peak at about 10 Å on air-dried specimen (Kübler 1967; Guggenheim et al. 2002). KI data were calibrated against the CIS scale (Warr & Rice 1994) using the

following regression equation: KI(CIS) = 1.09 KI(Bologna) + 0.02 (R2 = 0.96) (Dellisanti et al. 2008). Chlorite crystallinity was evaluated using the Árkai Index (ÁI) (Árkai 1991) obtained measuring the full-width-at-half-maximum-height (Δ°2θ) on the (002) chlorite diffraction peak at about 7 Å on air-dried specimen (Árkai 1991; Guggenheim et al. 2002).

ÁI data were calibrated using the equation: ÁI(CIS) = 1.13 AI(Bologna) - 0.02 (R2 = 0.84) (Dellisanti et al. 2008). In figure 1 a good correlation between KI and ÁI values is shown. The occurrence of mixed layers I-S and C-S was established on glycolated specimen applying the NEWMOD computer modelling (Reynolds 1985; Moore & Reynolds 1997).

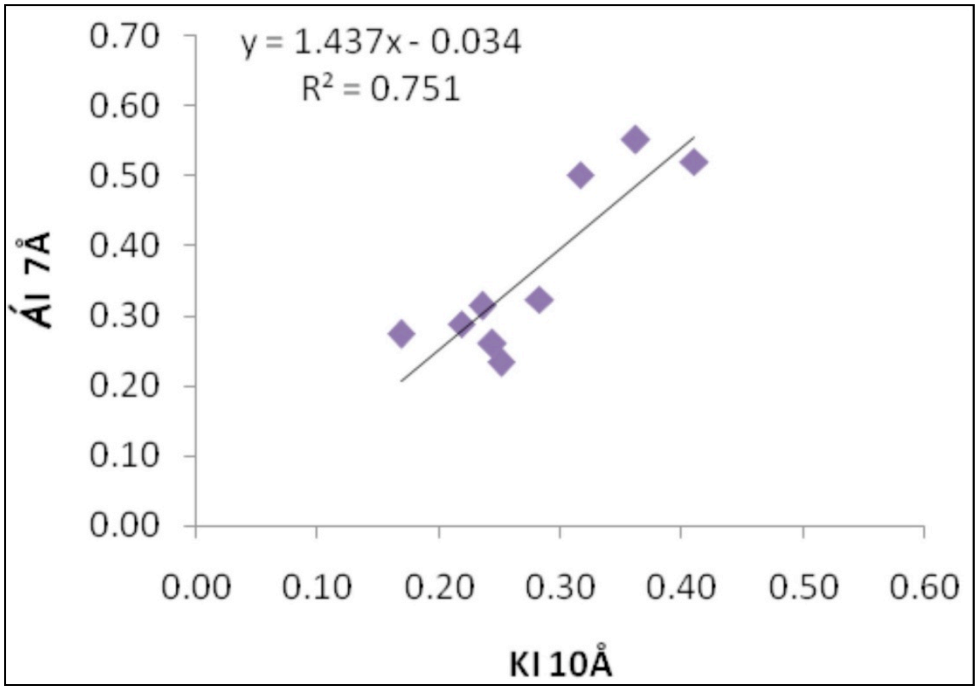

Figura 1. Correlation between KI (10 Å) and ÁI (7 Å) values.

APPENDIX 2

Vitrinite reflectance (Ro%)

Sample preparation

Whole-rock samples were disaggregated in a mortar and pestle. The sample was then analysed with the optical microscope and -where possible- carbonaceous material was isolated by picking, and then put on a plexiglass container. Each sample number was engraved on the container.

A mixture of resin and hardener was prepared just before the mounting procedure. Some resin was then put on the plexiglass with sample and carefully mixed to eliminate possible bubbles of air. The samples were left to harden for about one day. Five-step grinding and polishing processes were then implemented using a polishing machine. The sanding was made with progressively finer sandpaper follow by three-step polishing processes with 1 μm, 0.3 μm and 0.1 μm alumina slurry.

The microscope analysis

Random reflectance (Ro%) was measured under oil immersion, with a Zeiss Axioplan microscope (Fig.2), in reflected monochromatic non-polarised light and at a total magnification of x 50. The microscope was connected with a spectrophotometer MSP200 that recorded the reflected light. A software link with the microscope was used and to record the measures of the reflectance. A instrument calibration by standard samples is needed before measuring.

An average 20 measurements were taken on vitrinite fragments for each sample (never smaller than 5 nm and only slightly fractured and/or altered). Mean reflectance and standard deviation values were calculated for all measurements. The result were represented with a histogram and the indigenous woody fragments were characterized by a gaussian distribution (Fig. 3).

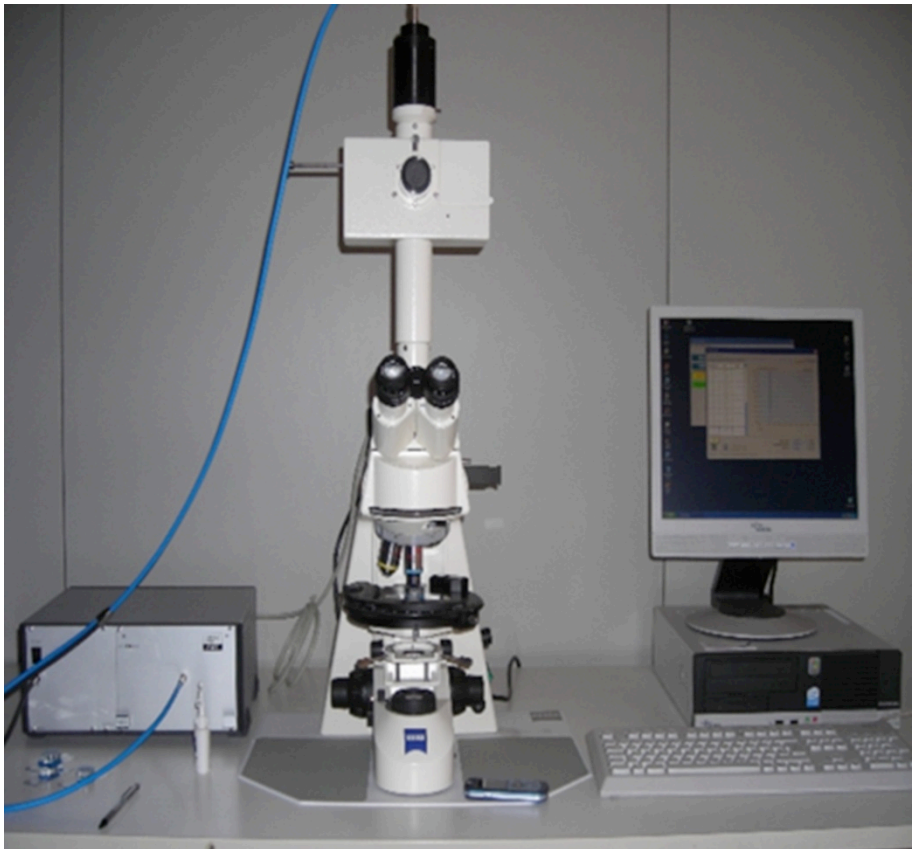

Figura 2. Zeiss Axioplan microscope**.**

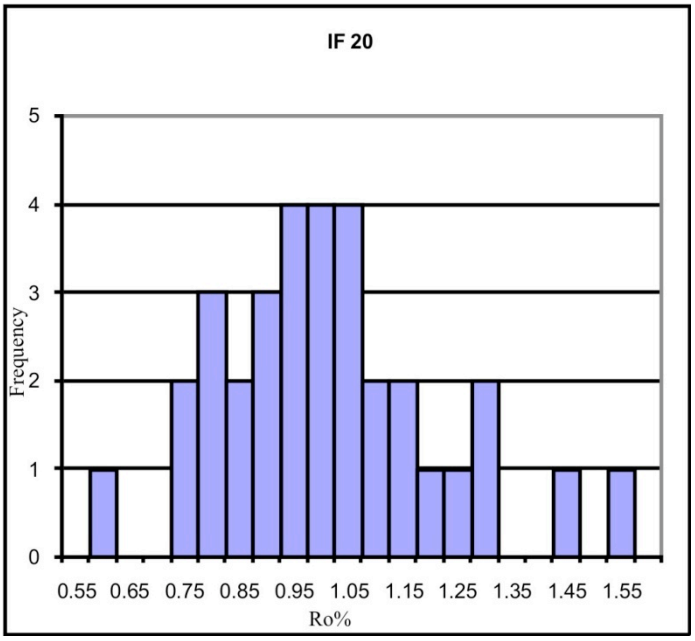

Figura 3. Histogram of sample IF 20.

APPENDIX 3

Appendix 3 - Raman Spectroscopy on carbonaceous material (RSCM)

Samples preparation

Conventional petrographic thin sections cut perpendicularly to the main fabrics (S0, S1) were prepared. The sections have a thickness at least of 30µm and were polished in two stages using a 3µm and a 1µm diamond paste.

The microscope analysis

Raman spectra were obtained using a Renishaw InVIA Reflex microspectrometer (ENS Paris) (Fig. 4). We used a 514 nm Spectra Physics argon laser in circular polarization. The laser was focused on the sample by a DMLM Leica microscope with a 100 × objective (NA=0.90), and the laser power at the sample surface was set around 1 mW.

Figura 4. Renishaw InVIA Reflex microspectrometer (ENS Paris).

The Rayleigh diffusion was eliminated by edge filters, and to achieve nearly confocal configuration the entrance slit was closed down to 10-15 µm. The signal was finally dispersed using a 1800 gr/mm grating and analyzed by a Peltier cooled RENCAM CCD detector. Before each session, the spectrometer was calibrated with a silicon standard. Because Raman spectroscopy of CM can be affected by several analytical mismatches,

we followed closely the analytical and fitting procedures described by Beyssac *et al.* (2002, 2003). CM was systematically analyzed below a transparent adjacent mineral, generally quartz. 10-15 spectra were recorded for each sample in the extended scanning mode (1000-2000 cm-1) with acquisition times from 30 to 60 s. Spectra were then processed using the software Peakfit (Beyssac *et al.* 2003).

Determination of parameters and temperature

The Raman spectrum of CM can be divided in first- and second-order regions (Fig. 5).

In the first-order region (1100-1800 cm-1), there are two vibration modes (E2g mode) of graphite; the first one (E2g1 mode) is attributed to the vibration of carbons within the polyaromatic structure and occurs at very low frequency (~ 42 cm-1), however, it is very difficult to separate practically this mode from the Rayleigh band and it is therefore rarely studied.

The second mode (E2g2 mode) corresponds to the stretching vibration in the aromatic layers. Because the aromatic bond involves very high energy, this mode occurs at an unusually high frequency (1580 cm-1) and can be easily studied; this mode is called the G band (Fig. 5a). In perfect crystalline CM (graphite s.s.), there is only the G band in the first order region (Fig. 5a); for poorly organized CM or very small crystallite dimensions,

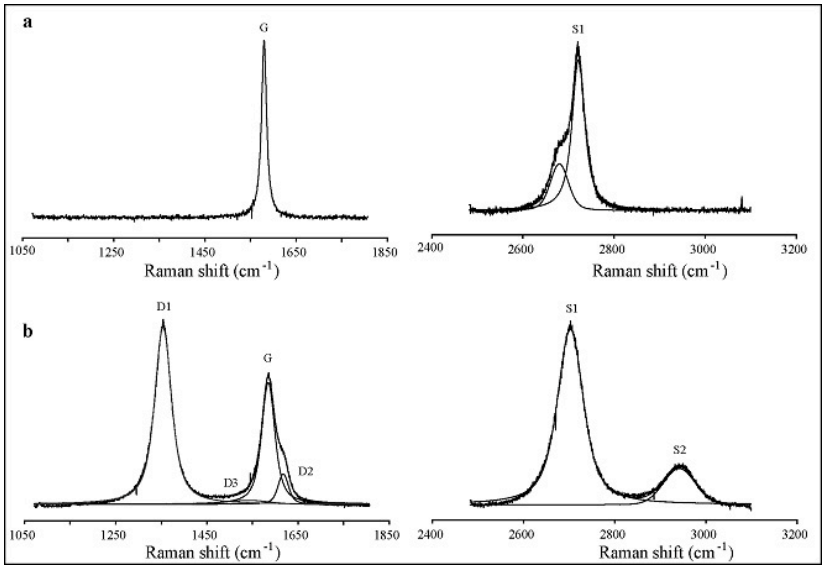

Figura 5. (a) first- and corresponding second-order regions of the Raman spectrum of perfect graphite. (b) first- and corresponding second-order regions of the Raman spectrum of disordered CM (Beyssac *et al.* 2003).

additional bands appear in the first-order region around 1150 (D4 band), 1350 (D1 band), 1500 (D3 band) and 1620 (D2 band) cm-1 (Fig. 5b). The second-order region (2200-3400

cm-1) shows several features about 2400, 2700, 2900 and 3300 cm-1 (Fig. 5a,b), attributed to overtone or combination scattering. The most important one, near 2700 cm-1 (S1 band), splits into two bands in well crystallized graphite.

In this work spectra acquisition is focused on the 1100-1800 cm-1 region which includes all first-order bands.

Different parameters are then useful to estimate the CM degree of organization. Bands position, bands FWHM (full width at half band maximum intensity), D1 / G intensity ratio (R1 ratio), and D1 / (G+D1+D2) area ratio (R2 ratio). Peak position, band area (integrated area), and band width (full width at half maximum FWHM) are determined using the computer program PeakFit 3.0 (Jandel Scientific) with a Voigt function. A linear correlation between this R2 parameter and metamorphic temperature (T(°C)= - 445R2 + 641) is calibrated by Beyssac *et al.* (2002a) using samples from different regional metamorphic belts with well-known P-T conditions in the range 350°C-650°C (Fig. 6).

For samples with temperatures lower than 350°C peak temperatures are referred to a good qualitative approach developed by Lahfid A. (2008).

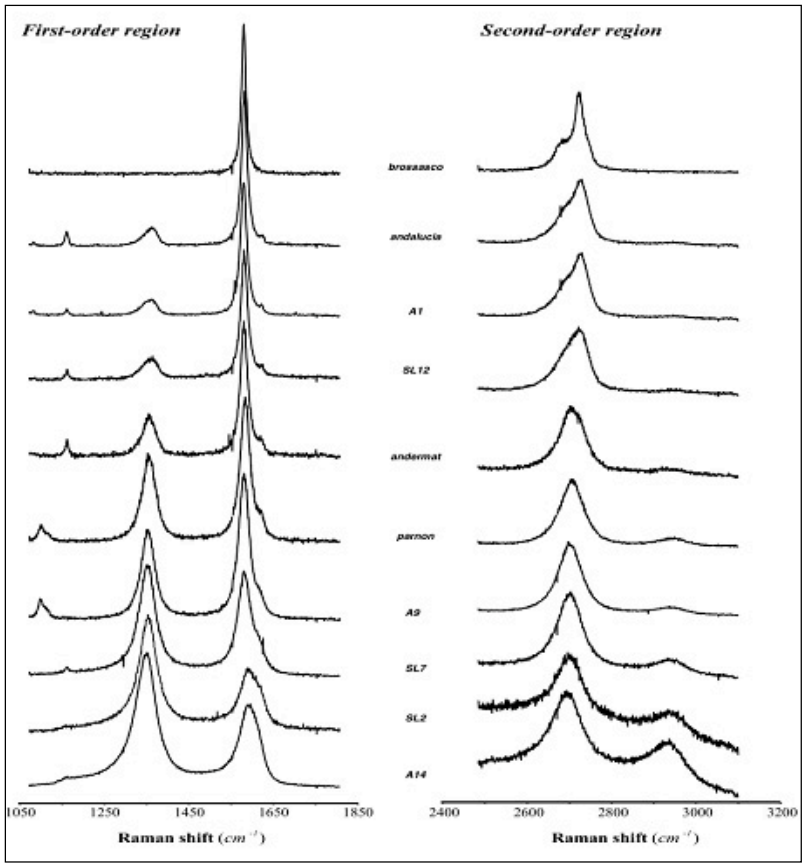

Figura 6. Selection of representative first-order and corresponding second-order regions of Raman spectra from various samples in order of increasing metamorphic grade, the temperature range for these sample is 350°C - 650°C (Beyssac et al. 2002).

APPENDIX 4

Apatite fission track (AFT) analysis

Separation of apatite

Apatite grain were separated from about 5 kg bulk rock. Samples were first washed and dried, then split and crushed using a jaw crusher and a disc mill to obtain sand-grain fragments. The heavy mineral fraction that include both apatite and zircon grains was then separated using a Gemeni shaking table. Minerals with magnetic characteristics were removed using a Franz magnetic separator. To separate any remaining quartzo-feldspathic mineral, the <250 micron fraction of heavy mineral separates was passed through different heavy liquids. For this step Tetrabromoethane (density 2.96 g/cm^3) is used. Apatite (density 3.1-3.35 g/cm^3) is then separated from zircon (density 4.6-4.7 g/cm^3) using the liquid methylene iodide (density 3.3 g/cm^3). The mineral were finally washed with acetone and dried.

Mounting in epoxy resin and polishing

A mixture of resin and hardener is prepared just before the mounting procedure. Each sample number is then engraved on microscope slides, previously cleaned with acetone. The slide is then put on a hot plate and some drops of the resin are put in the middle of the glass. The resin is carefully mix to eliminate possible bubble of air, and the mineral concentrate can then be mixed with the resin on an area of about 1 x 1.5 cm. The ideal mounting consists in a single layer of crystal not too close each other. The resin is then hardened leaving the mounting on the hot plate for some minutes. Apatite mounts are first hand-ground using wet grinding paper to exposed planar surfaces within the grains and then polished using a polishing machine, using first 1 μm diamond paste and then 0.3 μm diamond paste.

Chemical etching of Apatites

To reveal the spontaneous tracks, single mounts are put in 5N HNO_3 at 20°C for 20 seconds and immediately washed for some minutes (any residual nitric acid can be eliminated leaving for an hour or more the mounts in simple water).

Irradiation

Samples are cut according the dimensions of the mounts a corner of the obtained glass is slightly rounded and the surface is cleaned with the acetone. A piece of muscovite is split along cleavage, to obtain a layer of about 1 mm thick. The mica can be cut according the dimension of the mount. It is important that the surface of the muscovite which will be in contact with the mount is perfectly clean and without grazes. On its external side the sample number is engraved with a diamond pen and the corner corresponding to the rounded corner in the mount is cut. Samples, dosimeter and standards are put in a holder. The samples are then irradiated with thermal neutrons in the DR3 reactor at the Radiation Center of the Oregon State University with a nominal neutron fluence of 9×10^{15} n cm^{-2}. The standard glass CN5 was used as a dosimeter to measure the neutron fluence.

Procedures after the irradiation

The holder is put in a special container and left there until the radioactivity decreases down to 10 times the natural level (about 100 μR/h or 10 μ/Sh).

Induced fission tracks in the low-U muscovite that covered apatite grain mounts and glass dosimeter are etched in 40% HF at 20°C for 45 minutes.

The mounts and the mica can be fixed to the microscope slide with resin or, better with nail varnish. A label with the indication of sample and irradiation number is glued along a side.

The microscope analysis

AFT ages are measured and calculated using the external-detector (EDM) (Fig 7) and the zeta-calibration methods (Hurford & Green, 1983). Zeta-calibration is performed following the procedure recommended by Hurford (1990). Neutron fluences is measured counting neutron-induced tracks in the Corning glass dosimeter CN-5 (Uranium concentration: 2.17± 0.62 ppm, ^{235}U atom %: 0.720; Hurford, 1990; Bellemans *et al.* 1995). Age standard used are Durango and Fish Canyon apatites (IUGS age standards). The mean value obtained (332.54±5.55) is in a good agreement with values obtained by other analyst working with similar techniques and criteria (Hurford, 1998).

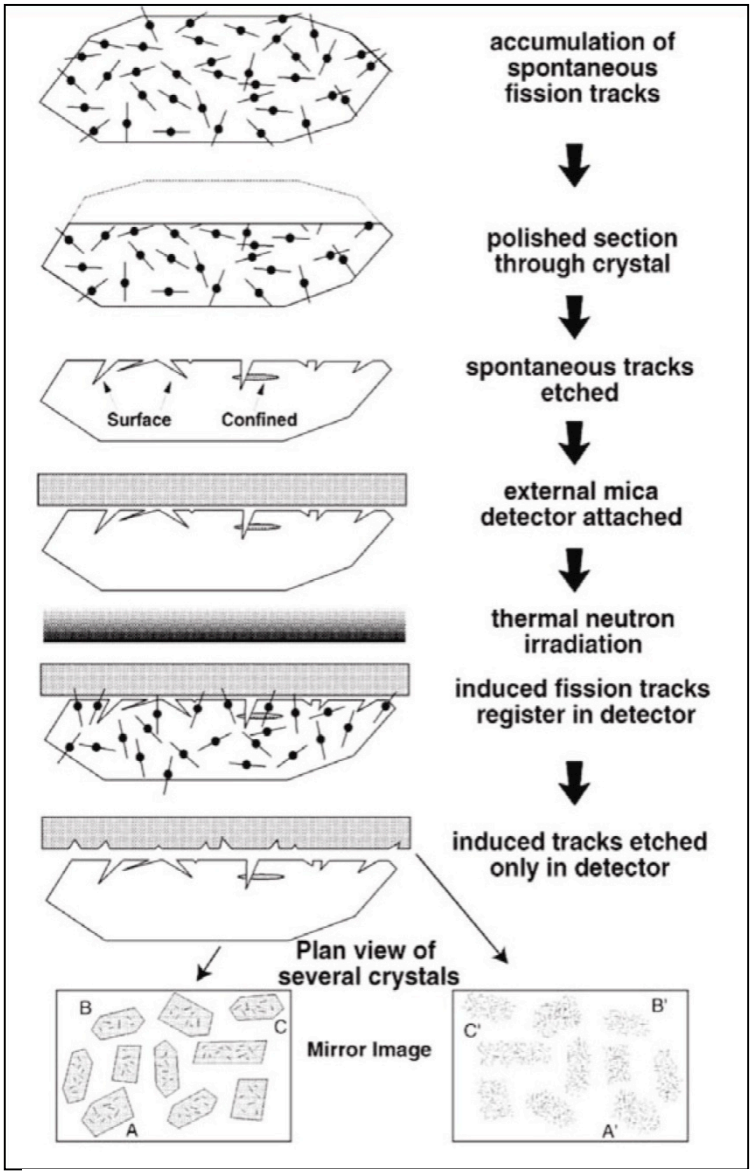

Figure 7. External detector method (EDM). From Gallagher et al. 1998.

The analyses were subject to the χ^2 test (Gailbraith, 1981) to detect whether the data sets were normally or overall dispersed. A probability of less than 5% denotes a mixed distribution.

According to EDM, the spontaneous (ρ_s) and the induced (ρ_i) tracks densities are calculated on the mount and the mica respectively. Counting of tracks has been carried out using a microscope Zeiss Axioscope (Fig. 8), equipped with motorized stage, transmitted and reflected lights and at a total magnification of x1250 (ocular x10 + additional lens Optovar x 1.25 + objective x100).

Before counting, the stage is calibrated to automatically pass from the apatite to the corresponding image on the mica. Where possible, at least twenty crystal with the proper

characteristics (section parallel to the c axis; no fractures or inclusion, no zoning) are selected. The recognition of the proper section is facilitated by the reflected light since the etch pit are all parallel. The number of selected crystal can increase in specific case (low density of tracks, provenance studies etc.).

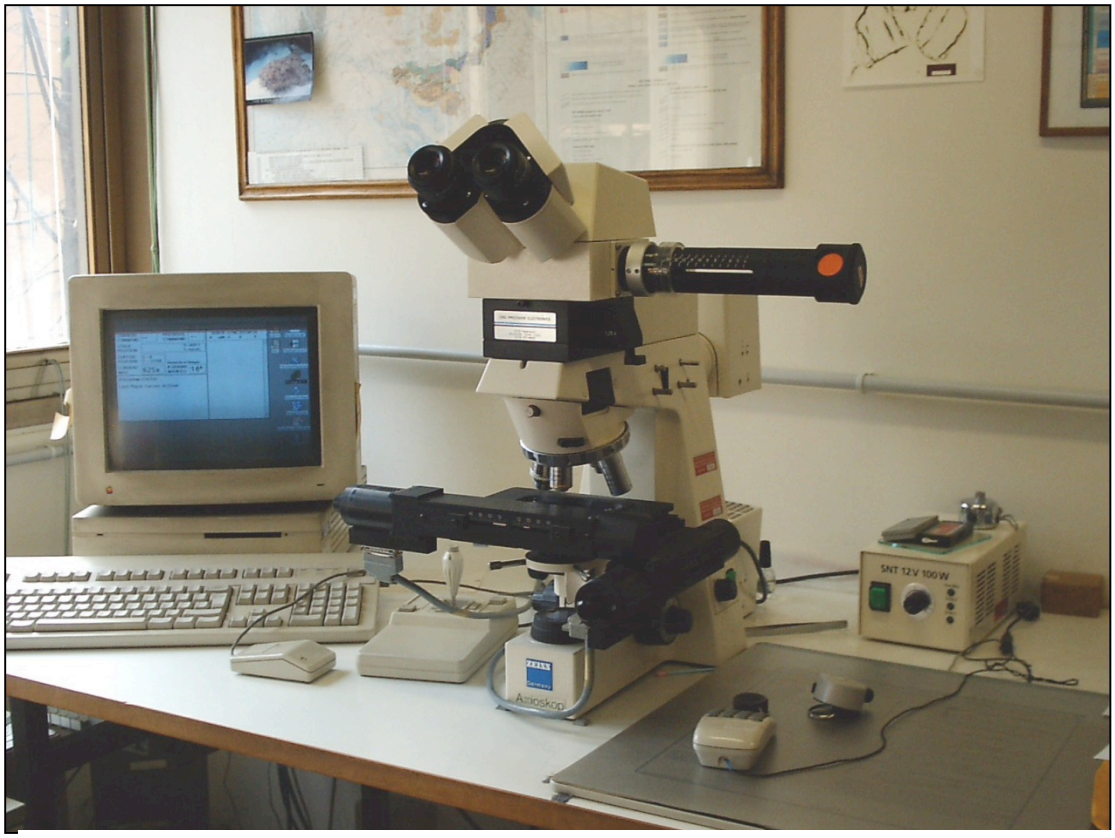

Figura 8. Microscope Zeiss Axioscope, equipped with motorized stage.

Track lengths are measured using digitizing table connected to a computer. A led is fixed to a cursor and its light is projected on the slide across a drawing tube. The led is used to determine the coordinates of the ends of the tracks; the computer then automatically calculates the length. Only the horizontal confined tracks on the section parallel to the c-axis can be measured. About 100 tracks should be measured to have a statistically significant distribution.

Modelling

Inverse modelling of track length data are performed using HeFTy program (Ehlers *et al*. 2005). The programme generates the possible T-t paths by a Monte Carlo algorithm. Predicted FT data were calculated according to the Ketcham *et al.* (1999) annealing model. In figure 9 the modelling of sample TU 116 is reported as example.

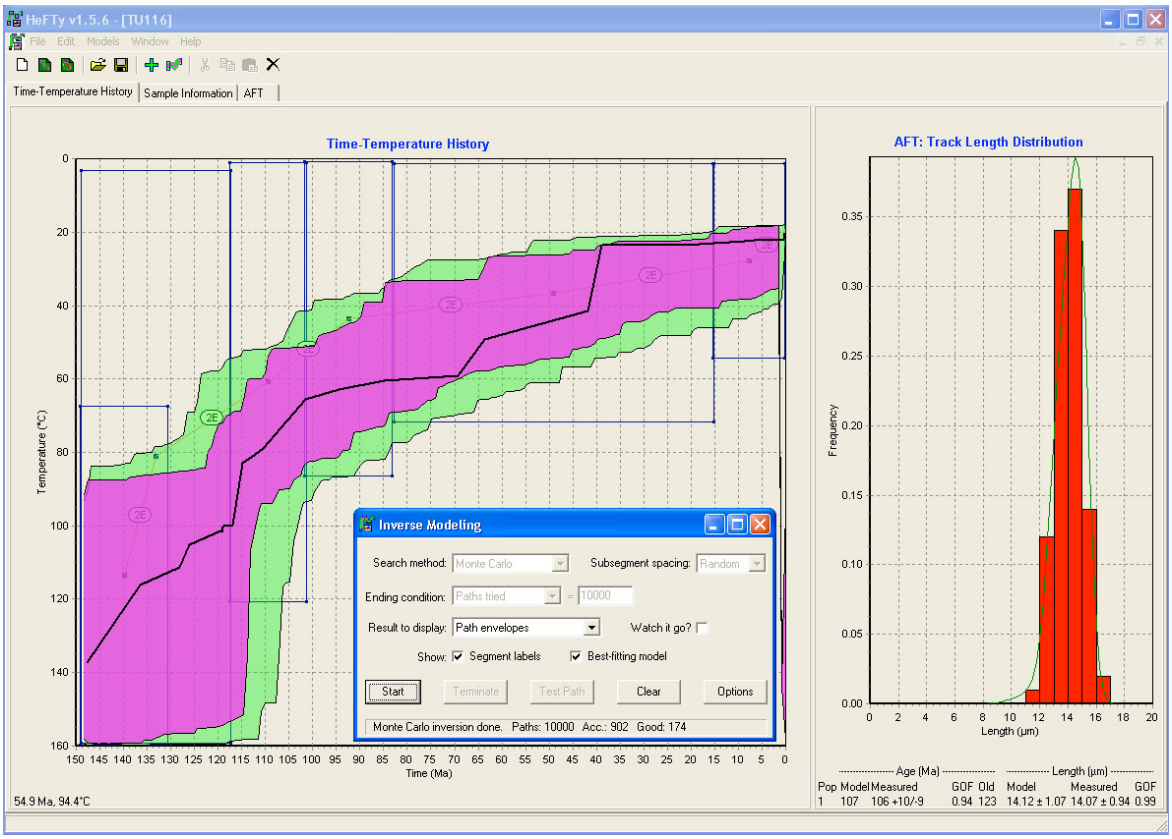

Figura 9. Inverse modeling for sample TU 116 using HeFTy program.